Confinement effects in nanopores: Elastic properties, phase transitions, and sorption-induced deformation

Dissertation

zur Erlangung des Grades

des Doktors der Naturwissenschaften

der Naturwissenschaftlich-Technischen Fakultät II

- Physik und Mechatronik -

der Universität des Saarlandes

von

Klaus Bernhard Schappert

Saarbrücken
2014

Tag des Kolloquiums: 21.07.2014

Dekan: Univ.-Prof. Dr. rer. nat. Christian Wagner

Mitglieder des Prüfungsausschusses:
Vorsitzender: Univ.-Prof. Dr. rer. nat. Helmut Seidel
1. Gutachter: Univ.-Prof. Dr. rer. nat. Rolf Pelster
2. Gutachter: Prof. Dr. rer. nat. Patrick Huber (TU Hamburg-Harburg)
3. Gutachter: Prof. Dr. rer. nat. habil. Andreas Schönhals (TU Berlin)
Akademischer Mitarbeiter: Dr. rer. nat. Herbert Wolf

Eidesstattliche Versicherung

Hiermit versichere ich an Eides statt, dass ich die vorliegende Arbeit selbstständig und ohne Benutzung anderer als der angegebenen Hilfsmittel angefertigt habe. Die aus anderen Quellen oder indirekt übernommenen Daten und Konzepte sind unter Angabe der Quelle gekennzeichnet. Die Arbeit wurde bisher weder im In- noch im Ausland in gleicher oder ähnlicher Form in einem Verfahren zur Erlangung eines akademischen Grades vorgelegt.

Saarbrücken, 11.03.2014 Klaus Bernhard Schappert

Copyright notice and publications

Some chapters in this dissertation contain material that was originally published in my papers in different journals and the corresponding contents are subject to the following copyrights.

Chapter 2 (parts of section 2.1 and section 2.2.1):

[1] Elastic properties and freezing of argon confined in mesoporous glass
Klaus Schappert and Rolf Pelster
Physical Review B, 78, 174108 (2008)
Copyright 2008 by the American Physical Society

Chapter 2 (parts of section 2.1 and section 2.2.2) and chapter 3:

[2] Freezing behavior of argon layers confined in mesopores
Klaus Schappert and Rolf Pelster
Physical Review B, 83, 184110 (2011)
Copyright 2011 by the American Physical Society

Chapter 4

[3] Continuous Freezing of Argon in Completely Filled Mesopores
Klaus Schappert and Rolf Pelster
Physical Review Letters, 110, 135701 (2013)
Copyright 2013 by the American Physical Society

Chapters 5 and 6:

[4] Elastic properties of liquid and solid argon in nanopores
Klaus Schappert and Rolf Pelster
Journal of Physics: Condensed Matter, 25, 415302 (2013)
Copyright 2013 IOP Publishing Ltd

Chapter 7:

[5] Influence of the Laplace pressure on the elasticity of argon in nanopores
Klaus Schappert and Rolf Pelster
Europhysics Letters (EPL), 105, 56001 (2014) Editor's choice
Copyright 2014 by the Europhysics Letters Association

Chapter 9:

[6] Strongly enhanced elastic modulus of solid nitrogen in nanopores
Klaus Schappert and Rolf Pelster
Physical Review B, 88, 245443 (2013)
Copyright 2013 by the American Physical Society

The publication of the results presented in chapter 8 is currently in preparation:

The influence of the geometrical arrangement of adsorbate
on the deformation of nanoporous glass
Klaus Schappert and Rolf Pelster

Abstract

This dissertation addresses in particular the phase behaviour and the elastic properties of adsorbate in nanoporous glass. Ultrasonic measurements permit the determination of the effective elastic moduli of the heterogeneous system consisting of matrix and pore filling. These effective moduli and notably the moduli of the adsorbate that are deduced via an effective medium analysis yield information on the state of the adsorbate. Both isothermal measurements and temperature cycles with different constant fillings of argon evidence a broad continuous liquid-solid phase transition of the adsorbate. The interaction between argon atoms in the pore centre and in the surface layers influences the freezing behaviour of these layers. The elastic moduli of adsorbed argon are basically the same as for bulk argon. The curvature of menisci of the adsorbate and the related Laplace pressure causes only a small change of the elastic properties of argon. The replacement of the spherical argon by the diatomic nitrogen reveals the importance of interactions: The stronger binding between nitrogen and pore wall results in a strong enhancement of the shear modulus of adsorbed nitrogen layers.

The curvature of adsorbate and changes of the surface free energy during sorption of argon result in a deformation of the porous matrix. An analysis shows that from the deformation behaviour conclusions on the geometrical arrangement of the adsorbate can be drawn.

Kurzzusammenfassung

Diese Dissertation befasst sich insbesondere mit dem Phasenverhalten und der Elastizität von Adsorbat in nanoporösem Glas. Ultraschallmessungen erlauben die Bestimmung der effektiven Elastizitätsmodule des heterogenen Systems aus Matrix und Porenfüllung. Diese effektiven Module und vor allem die daraus abgeleiteten Module des Adsorbates liefern Informationen über den Zustand des Adsorbates. Isotherme Messungen und Temperaturgänge mit verschiedenen konstanten Argon-Füllungen zeigen einen breiten flüssig-fest Phasenübergang des Adsorbates. Die Wechselwirkung zwischen Argon-Atomen im Porenzentrum und in den Wandlagen beeinflussen das Gefrierverhalten dieser Argon-Lagen. Die Elastizitätsmodule von adsorbiertem Argon entsprechen im Wesentlichen den Modulen für “normales” Argon. Die Krümmung von Menisken des Adsorbates und der damit verbundene Laplace-Druck verursacht nur eine kleine Änderung der elastischen Eigenschaften von Argon. Bei Verwendung von diatomarem Stickstoff als Adsorbat (anstelle von sphärischem Argon) zeigt sich die Bedeutung von Wechselwirkungen: Die stärkere Bindung zwischen Stickstoff und Porenwänden verursacht eine starke Erhöhung des Schermoduls der adsorbierten Wandlagen.

Die Krümmung des Adsorbates und Änderungen der freien Oberflächenenergie während der Sorption von Argon führen zu einer Deformation der porösen Matrix. Eine Analyse zeigt, dass aus dem Deformationsverhalten Rückschlüsse auf die geometrische Anordnung des Adsorbates gezogen werden können.

Contents

Frequently used symbols

β	effective longitudinal modulus of the heterogeneous system of porous sample and pore filling
β_0	longitudinal modulus of the empty porous sample
$\beta_{Ar,ads}$	longitudinal modulus of the adsorbed argon pore filling
β_{pore}	longitudinal modulus of the pores
β_Q	longitudinal modulus of quartz glass (i.e. the material of the porous sample)
c	ultrasonic velocity
E	effective Young modulus of the heterogeneous system of porous sample and pore filling
E_S	Young's modulus of the material of the porous sample
ε	scaled volume change ($\varepsilon = \Delta V/V_0$)
f	volume filling fraction ($f = n/n_0 = V_{ads}/V_{pores}$)
$\tilde{f}$	filling fraction of frozen argon ($\tilde{f} = f - f_1$)
f_1	filling fraction for the onset of freezing during isothermal adsorption
f_2	filling fraction for the onset of the formation of capillary sublimate during isothermal adsorption
f_c	filling fraction above which capillary bridges exist
G	effective shear modulus of the heterogeneous system of porous sample and pore filling
G_0	shear modulus of the empty porous sample
$G_{Ar,ads}$	shear modulus of adsorbed argon
$G_{Ar,bulk}$	shear modulus of bulk argon
$G_{Ar,SL}$	shear modulus of adsorbed argon surface layers
$G_{filling}$	shear modulus of the adsorbed pore filling
G_{pore}	shear modulus of the pores
G_Q	shear modulus of quartz glass (i.e. the material of the porous sample)

γ	surface tension
γ_{lv}	liquid-vapour surface tension
γ_{sl}	solid-liquid surface tension
γ_{wl}	pore wall-liquid surface tension
K	effective bulk modulus of the heterogeneous system of porous matrix and pore filling
K_0	bulk modulus of the empty porous sample (i.e. the material of the porous sample)
K_{pore}	bulk modulus of the pores
K_Q	bulk modulus of quartz glass
K_S	bulk modulus of the material of the porous sample
l	length of the porous sample
l_0	initial length of the sample at $f = 0$ and $p/p_0 = 0$
Δl	length change of the sample ($\Delta l = l - l_0$)
Δl_{max}	maximum length change at $p/p_0 = 1$
λ	ultrasonic wavelength
m_M	molar mass of the adsorbate
m_0	mass of the empty sample
M	effective modulus
M_0	modulus of the empty porous sample
M_{pore}	modulus of the pores
M_Q	modulus of the material of the porous sample
n	molar amount of adsorbate
n_0	molar amount of adsorbate necessary for complete filling of the pores
N_A	Avogadro constant
ν	Poisson's ratio
p	(external) pressure
p_0	bulk vapour pressure
p_L	Laplace pressure
p_s	solvation pressure (causing a deformation of the porous sample)
p_s^c	solvation pressure for pores filled with capillary bridges
p_s^f	solvation pressure for pores filled with adsorbed layers
p_s^{f+c}	solvation pressure for pores filled with both adsorbed layers and capillary bridges

ϕ	porosity [$\phi = n_0 m_M / (\rho_{ads} V_{sample})$]
Π	disjoining pressure
r_K	Kelvin radius or radius of curvature (negative for concave menisci)
r_P	pore radius
r_1,r_2	radii of curvature
R	gas constant
ρ_0	density of the empty porous sample
ρ_{ads}	density of the adsorbate
ρ_S	density of the material of the porous sample
t	thickness of an adsorbed layer ($t = zu$)
t_0	thickness of the adsorbed surface layer above f_c
T	(absolute) temperature
$T_{fr,Ar,bulk}$	freezing temperature of bulk argon
$T_{fr,Ar,pore}$	freezing temperature of confined argon
T_m	melting temperature
θ	contact angle
u	thickness of one adsorbed monolayer
V_0	volume of the empty sample
V_{ads}	volume of the adsorbate
$V_{Ar,ads}$	volume of the adsorbed argon
V_m	molar volume of the adsorbate
V_{pores}	volume of the pores
V_{sample}	volume of the sample
ΔV	volume change of the sample during sorption
x	fraction of solid adsorbate ($x = \tilde{f}/f$)
ξ	fraction of pores with capillary bridges
z	number of adsorbed monolayers/surface layers

Introduction

The possibility to build nanostructures has resulted in a continuing research of the physical properties on the nanoscale. Confinement on the nanoscale can also be achieved with objects of macroscopic dimensions like filled nanoporous samples. With such porous materials it is possible to prepare nanoconfined substances and to study nanoeffects.

Nanomaterials and nanoconfined substances may exhibit physical properties that differ substantially from the properties of “normal” bulk materials; e.g. viscosity, stiffness, strength, mechanical toughness, elastic moduli, crystalline structure, the order of adsorbate and also its density can be influenced [7–27].

Elasticity is a fundamental and important property of a substance. There is no general rule that nanoobjects are elastically stronger or weaker than the corresponding bulk counterparts, but nanoeffects can lead to interestingly different elastic properties. The knowledge of the elastic properties of nanoconfined material, the possibility to calculate the effective properties from the intrinsic properties of the components of a composite, and the understanding of deviations from bulk are essential; amongst others for the development of nanoscale materials, and in geophysics.

The investigation of the temperature-dependence of the elastic properties of a filled porous material can in turn shed light on the phase transition of a substance. The study of the freezing and melting behaviour is an important field of reasearch also because liquid-solid phase transitions are ubiquitous in nature, both in macroscopic geometries and in confined geometries like porous stone. The restriction of a substance to nanopores changes the phase behaviour considerably [25, 28–41]. In general, the freezing and melting temperatures are reduced in pores in consequence of the curvature of the pore wall [28]. This phenomenon and possible further factors influencing freezing and melting in confinement are a topic of ongoing research. Amongst others the degree of curvature, the structure of the pore surface, impurities, nucleation rates, and the adsorbate itself change in different ways the freezing and melting [7, 25, 28–43].

The elastic properties are related to an effect that is well-known for porous materials: Adsorption of a substance in pores results in a deformation of the porous matrix because of changes of the surface free energy and of the Laplace pressure due to the curvature of the adsorbate [44]. The understanding of the adsorption-induced deformation is important for the description of any porous system. This swelling of porous materials has a particular relevance because of its influence on the geological storage of CO_2 and the methane production [45–47]. Deformation measurements during isothermal sorption have often been used to estimate the elastic moduli of porous samples [48–55]. Recently, it has been suggested that differences between theoretical calculations of the deformation of porous samples and the measured deformation behaviour might be related to changes of the elastic properties during sorption [56].

To achieve an understanding of the fundamental influences of the confinement of a substance on the nanometre-scale, it is necessary to study a simple system. Therefore, the use of the noble gas argon as the filling in a porous sample seems a suitable model system to study phase transitions and elastic properties in nanoconfinement. Already the substitution of argon (with its spherical structure that simplifies the interactions between adsorbate and pore wall) by nitrogen shows strong differences of the confinement effects.

Chapter 1

Fundamental knowledge

1.1 Porous matrix and adsorbates

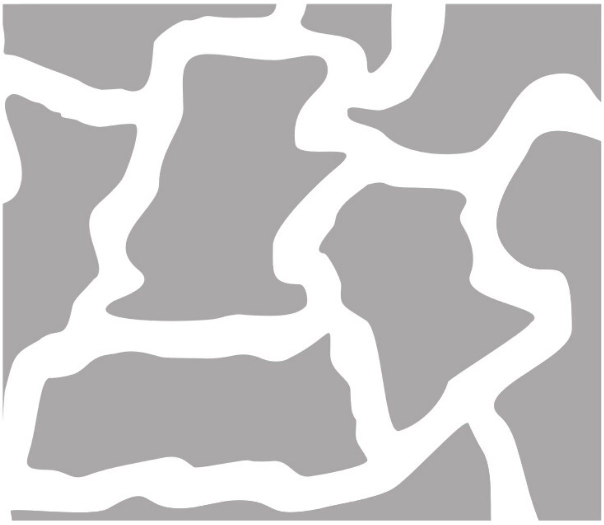

FIGURE 1.1 – *Schematic sketch of the structure of the porous Vycor® glass sample. It possesses a spongy three-dimensional structure of interconnected pores. The average pore radius* r_p *of the Vycor® glass samples used for this dissertation is typically* $\approx 3.8 - 4.0$ *nm and the porosity* ϕ *is* $\approx 25 - 28$*%. Figure from [2] (Copyright © 2011 by the American Physical Society).*

For the research of the phase behaviour and the elastic properties on the nanometre scale the well-known nanoporous Vycor® glass (Corning, Inc.) is used in this dissertation. The pores of this matrix are for that purpose (partly) filled, which also influences the porous matrix itself (cp. section 1.4). The porous glass consists of a three-dimensional spongy network of almost pure silicon dioxide (cp. figure 1.1) [57,58]. The pores possess a certain pore size distribution around the average pore radius $r_P \approx 3.8 - 4.0$ nm. A typical example of such a size distribution for a sample with an average pore radius of ≈ 3.8 nm is shown in figure 1.2.[1] With such an average pore radius, the nanoporous Vycor® glass belongs to

---

[1] The standard method for the calculation of the pore size distribution from the desorption branch of a sorption isotherm may give a distorted impression of the actual size distribution. The fraction of

the subcategory of mesoporous materials [59, 60]. The porosity ϕ of the samples used in this dissertation differs slightly for different samples in a range of $\phi \approx 25 - 28\%$.

For most of the experiments in this dissertation, the pores of the samples were filled with the adsorbate argon. Because of the simple, globular structure of the noble gas argon, van der Waals interactions predominate. Therefore the system of porous matrix and adsorbate can be regarded as a sort of model system to study influences of nanoconfinement on liquid-solid phase transitions. In chapter 9 nitrogen was used as an adsorbate. In contrast to argon, this diatomic molecule possesses a quadrupole moment. With those measurements it will be shown which change this quadrupole moment provokes for the binding of the adsorbate and its elastic properties.

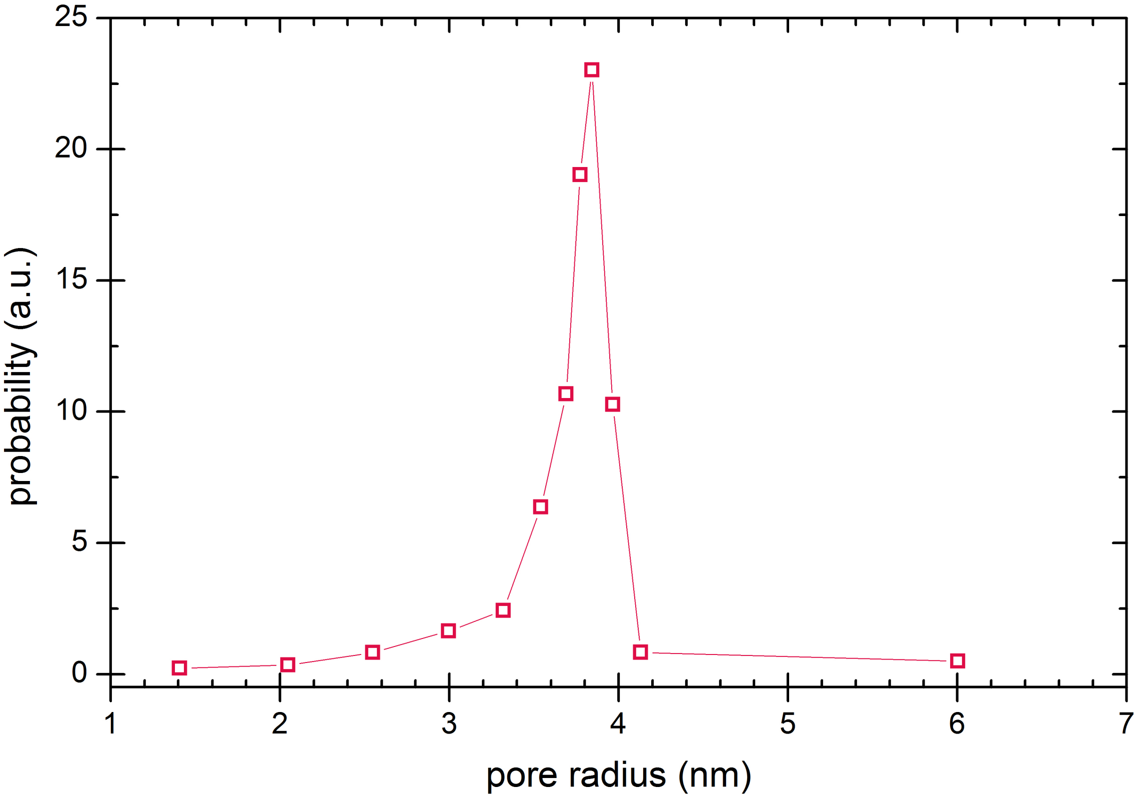

FIGURE 1.2 – *The porous Vycor® glass exhibits a certain pore size distribution. The average pore radius of the sample with the shown size distribution amounts to* $r_P \approx 3.8$ *nm.*

1.2 Sorption isotherms

If a porous sample is exposed to an external vapour pressure, atoms or molecules from the vapour will be adsorbed in the pores [59]. The amount of the adsorbed substance

---

bigger pores is possibly underestimated and the fraction of smaller pores overestimated because of the pore-blocking effect (see section 1.2 and reference [59]).

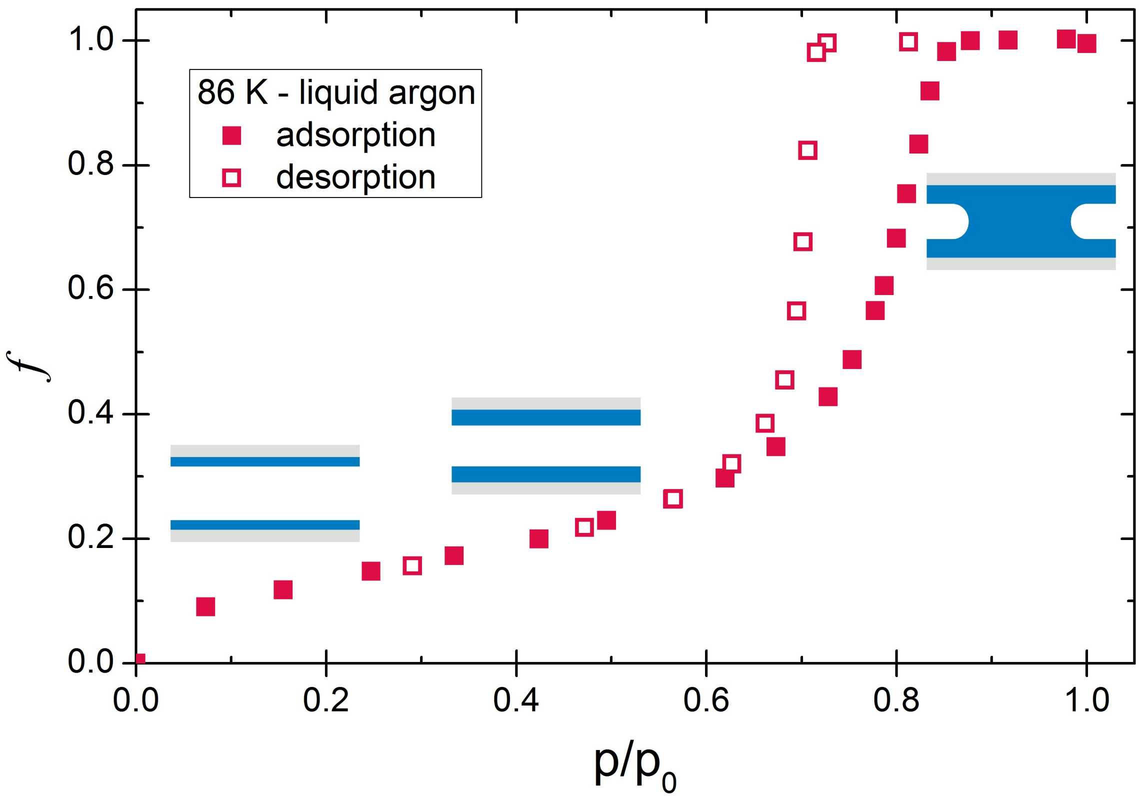

FIGURE 1.3 – *The nanoporous glass sample is gradually filled with liquid argon (at* 86 *K) by the successive increase of the external pressure* p *up to the vapour pressure* p_0 *of bulk argon at the corresponding temperature. At lower values for the reduced pressure* p/p_0 *the adsorbate forms surface layers on the pore walls. The thickness of these layers increases at a further rise of the pressure until the formation of capillary bridges (capillary condensate) becomes energetically more favourable. In this pressure range the filling fraction* $f = n/n_0$ *depends strongly on* p/p_0*. During the desorption porocess (as usually) a hysteresis, caused by the draining mechanism, is observed until all capillary bridges have disappeared (for details see text).*

depends decisively on the external pressure p (see figure 1.3). A complete filling of the pores of the sample (with the maximum molar amount of adsorbate, n_0) is achieved at the vapour pressure p_0 of the adsorbate in the normal bulk state. For reduced pressures $p/p_0 < 1$ the sample is only partly filled (with a molar amount $n < n_0$). Starting at low values for p/p_0, only a film is adsorbed on the pore walls [59]. The thickness of this surface layer increases when the reduced pressure rises to higher values [61]. During the further course of the adsorption process at a higher reduced pressure, a critical film thickness is reached and the adsorbate forms capillary bridges because this becomes energetically more favourable [60]. This capillary condensation occurs in the steep range of the adsorption branch (cp. figure 1.3) [61]. A further increase of p/p_0 results in a filling of all pores with capillary condensate and finally the remaining concave menisci at the pore ends flatten and the pores of the sample are completely filled [61].

During the desorption process the reduction of the pressure leads initially to a reversible

FIGURE 1.4 – *During the desorption process smaller pores can block the emptying of bigger pores (schematic sketch, blue: adsorbate, grey: quartz glass matrix).*

formation of concave menisci at the pore ends and no appreciable change of the filling fraction of the sample, $f = n/n_0 \approx 1$ (cp. reference [61]). At a critical pressure p_c the pores start to empty. According to the Kelvin equation [61] capillary bridges with a radius

$$r_K = -\frac{2\,\gamma_{lv}\,V_m \cos(\theta)}{R\;T\;\ln(p/p_0)} \tag{1.1}$$

are removed at a pressure p. Here γ_{lv} denotes the liquid-vapour surface tension of the adsorbate, V_m the molar volume of the adsorbate, θ the contact angle, R the gas constant, and T the absolute temperature.[2] Generally, it is presumed that a thin adsorbed film (typically with a thickness of about two surface layers) remains on the pore walls during the removal of the capillary bridges [59] (see also section A.2).

The hysteretic range of the sorption isotherm ends when all capillary bridges have disappeared and then the course of the desorption branch is identic with the adsorption branch [61].

The observation that the pressure at which the capillary bridges are removed is lower than the pressure at which they are formed has been much discussed in previous studies [60]. Sometimes, the pore size distribution was given as the origin of the hysteretic behaviour [60]. As mentioned above, the nanoporous Vycor® glass possesses pores of different radii (see figure 1.2). During the desorption process smaller pores can block the emptying of bigger pores that are further inside (see equation 1.1: the smaller r_K the lower the pressure p/p_0 at which the pore filling is removed) [59]. Figure 1.4 shows a schematic sketch of this pore-blocking effect for a small part of a sample. The pore blocking effect can be connected to the formation of inhomogeneities (empty and filled regions in the sample) on a length scale considerably bigger than the pores [e.g. inhomogeneities in the range of the wavelength of light (see references [62–66]) or the ultrasonic wavelength (see reference [1])].

The existance of a hysteresis in pores with a constant pore diameter, puts this explanation in question at least as the sole reason for the hysteresis. The possibility of the occurance

---

[2] For the calculation of r_K usually a complete wetting is assumed, i.e. a contact angle of $\theta = 0°$ [59]. In this dissertation that assumption was adopted.

of a hysteresis during sorption in such pores was shown by Saam and Cole [67]. Here the formation of a metastable state (a metastable film) during adsorption forms the reason for the hysteresis [67]. Hence the desorption branch corresponds in this model by Saam and Cole to the state in thermodynamic equilibrium [67]. A possible coppling between pores as a result of the deformation of the pore walls was also given as a mechanism that can explain the filling and emptying behaviour during sorption [68]. This explanation supposes that the filling or emptying of a pore depends decisively on the filling of neighbouring pores, independently from a direct connection of the pores [68]. This work by Grosman and Ortega contrasts to the model by Saam and Cole, especially in the assumption, that the adsorption branch corresponds to the stable state of the adsorbate [68]. During desorption certainly also the possibility of cavitation, i.e. the formation of vapour bubbles in the pores, when the stability of the adsorbate is exceeded during the reduction of the external pressure p, plays a decisive role [69–71].

For a simple porous system without any pore size distribution it is possible to construct the sorption isotherm approximately [44, 67] (for more details see also section 8.2). The influence of the pore size distribution can also be included (if it is known) in the theoretical model by Saam and Cole [67].

1.3 Influences of confinement on phase transitions

If a substance is spatially confined to a few nanometres, its phase behaviour will be changed. Such a confinement of a substance is given by its adsorption in pores with a diameter of a few nanometres. The influence of the confinement on phase transitions is known for a multitude of systems [25, 28–42, 64, 65, 72–89].

A main part of this dissertation deals with the liquid-solid phase transition in nanopores. Because of the high ratio of pore surface to pore volume in comparison to bulk, the phase transition is in particular influenced and complicated by the curvature and by the structure of the pore walls (see below).

A thermodynamic approach of the phase transition from the solid to the liquid state demonstrates that the melting point is given by the intersection of the Gibbs free energy G_E of the solid state with the one of the liquid state [90], i.e. by the temperature T_m for which the difference between the Gibbs free energy of the solid and the liquid state vanishes: $\Delta G_E = 0$. Figure 1.5 schematically illustrates that above the melting point the temperature dependence of the Gibbs free energy is higher than in the solid state because of the higher entropy S ($dG_E/dT|_p = -S$) [90].

In a nanopore with capillary condensate (capillary bridges) the melting point is shifted in comparison to the bulk substance [28] and therefore also the intersection between the Gibbs free energy of the solid adsorbate and the liquid adsorbate is shifted. Usually, for capillary condensate in nanopores the shift is towards lower temperatures (cp. reference [28]).

From the validity of

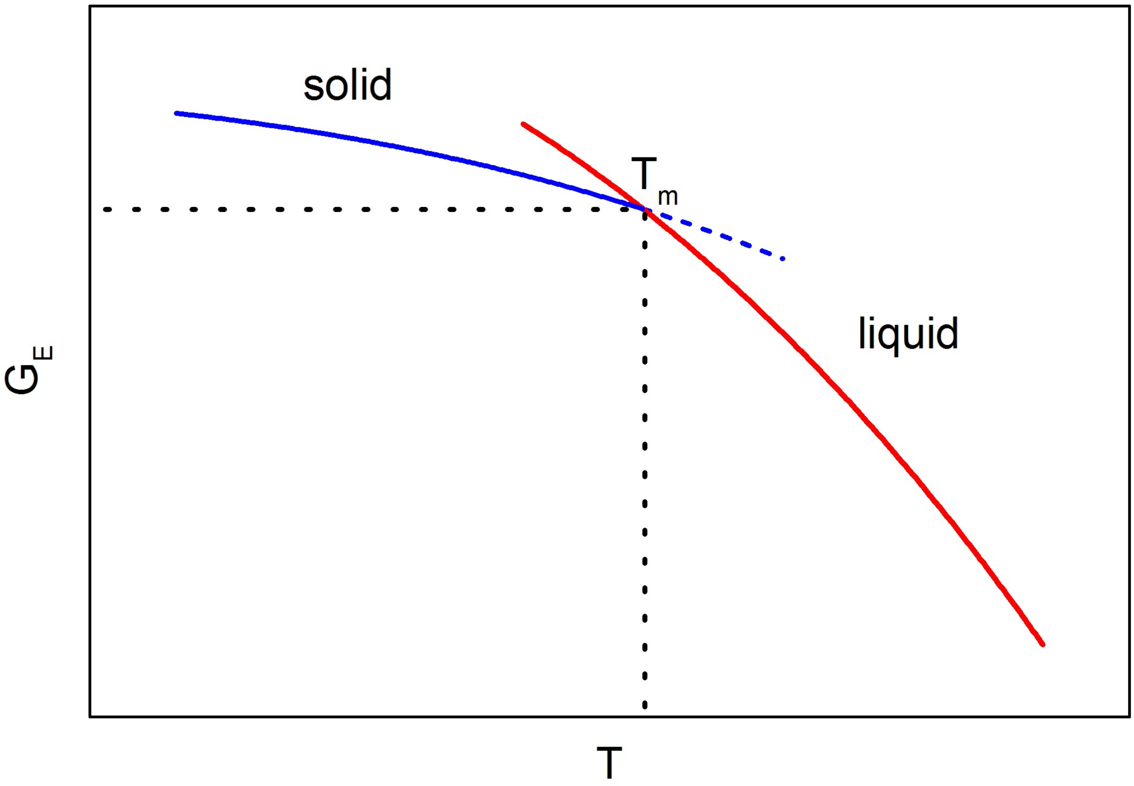

Figure 1.5 – *The melting point is located at the intersection of the Gibbs free energy of the solid state with the one of the liquid state. (Figure after [90]).*

$$\Delta G_E = 0 = A\left(\gamma_{li} - \gamma_{si}\right) + V\frac{\Delta T \Delta H_f}{V_m T_m} \tag{1.2}$$

at the melting temperature (with A: total surface of the pore; γ_{li}: substrate-liquid interfacial energy; γ_{si}: substrate-solid interfacial energy; V: total volume of the adsorbate; V_m: molar volume; ΔH_f: heat of fusion)[3] [28], an equation for the reduction of the melting temperature in cylindrical pores with radius r_P can be deduced [28]:

$$\Delta T = \frac{2T_m V_m \gamma_{sl}}{r_P \Delta H_f} \propto 1/r_P \tag{1.3}$$

In this equation ΔT denotes the reduction of the melting temperature T_m and γ_{sl} the solid-liquid surface tension. The deviation of the above equation requires the existance of a thin liquid layer between the solid crystal in the pore centre and the pore wall [28]. From experiments it is known that at least a few Kelvin below the melting point such a liquid (non-freezing) interfacial layer is often present on the pore wall, i.e. the solid phase is wetted by its own melt [25, 28, 29, 40, 41]. The analysis in section 3.1 shows, however, that at temperatures considerably lower than the melting point the assumption

---

[3] Differences of molar volume and heat capacity between liquid and solid are neglegted [28].

is wrong for argon in porous glass. For example for argon in nanoporous glass, it is known that the thickness of such a liquid layer increases with increasing temperature because of changes of the free energy of the filled pore [29]. This phenomenon is related to the so-called premelting and interfacial melting, which is also known for flat surfaces and especially for water [30, 35, 37, 43, 80, 91–96]. The model of reference [29] considers the first two adsorbed surface layers as so-called "dead" layers that do not at all participate in a liquid-solid phase transtion. The phase behaviour of these layers is throughly discussed in chapter 3.

Equation 1.3 is identic with the Gibbs-Thomson equation that can be derived from the Clausius-Clapeyron equation and the Kelvin equation [28]. According to equation 1.3, the melting point depression is inversely proportional to the pore radius for a certain adsorbate, i.e. in small pores the shift of T_m should be especially distinct.

Between melting and freezing mostly a hysteresis is observed; its origin is much discussed [28]. A homogeneous nucleation in the pore centre can explain a reduction of the freezing point that is by a factor of 3/2 bigger than the melting point reduction in equation 1.3 (freezing of a minimum-size stable spherical nucleus vs. melting of a cylindrical pore filling) [28]. Effects because of the pore geometry and the pore size distribution are also possible [28].

Due to the simplifying approach the Gibbs-Thomson equation (equation 1.3) can only by regarded as a first explanation of the melting and freezing behaviour of adsorbates in nanoporous systems. A great number of experiments with different adsorbates and porous systems showed nevertheless an agreement with this equation [28, 30, 38, 39, 83]. In some cases, however, the pore radius r_P in equation 1.3 had to be reduced by the thickness t of a non-freezing surface layer [28,30,38,83]. Other measurements revealed that equation 1.3 is not always observed. This was for example shown for krypton in crystalline carbon pores, which does not adhere to the Gibbs-Thomson equation [32]. As a possible reason for the differences, the crystalline surface of the pore walls of that carbon sample and differences in the interaction energy between krypton and such a crystalline surface respectively an amorphous pore wall were given [32]. Also not always a reduction of the melting point is observed. The properties of the pore surface can even induce a shift of the melting point to higher temperatures than in bulk [76].

1.4 Deformation of porous samples during sorption

Porous samples deform during the sorption of an adsorbate [97]. Among the first observations of a macroscopic deformation during adsorption are measurements with porous charcoal [98–105]. In these early studies always a continuous increase of the macroscopic length l of the sample was observed (see e.g. references [98, 100]). The relative length changes during those measurements are typically a few tenths of a per cent of the length of the porous matrix.

As the reason for the appearance, the pressure exerted by the adsorbed but mobile[4] molecules on the pore walls was given [100–102]. The observed relative expansion $\chi = \Delta l / l_0$ of a sample with the initial length l_0 was found to be proportional to the so-called surface pressure F [101]:

$$\chi = \frac{\Delta l}{l_0} = \Lambda F \tag{1.4}$$

The constant Λ depends considerably on the sample and the adsorbate (cp. also reference [106]). Assuming that the adsorbate behaves like a two-dimensional gas, the surface pressure F is equal to the reduction of the surface free energy as well as of the surface tension [101, 103, 107].[5] The surface free energy and the surface tension are equal for a one-component liquid [108, 109]. This signifies that the observed continuous expansion of the sample during adsorption has to be ascribed to the reduction of the surface free energy (see e.g. reference [108]). The reduction of the surface free energy can be determined with the aid of Gibbs's adsorption equation from the adsorption isotherm [105, 107, 110–112].

From the initial part of an adsorption isotherm which often shows a linear relation between the length change of the sample and the surface pressure, elastic properties of the porous sample were estimated. Bangham and Maggs [52] set up a formula for the correlation between the Young modulus E_S of the material of the matrix (not the effective modulus of the porous matrix) and the deformation behaviour:

$$E_S = \frac{\Sigma \rho_S}{\Lambda}, \tag{1.5}$$

here ρ_S denotes the density of the matrix material and Σ is the specific surface. The derivation of the equation requires considerable simplifications of the actual conditions.[6] For porous samples (like porous Vycor®) with a three-dimensional network of disordered pores, Amberg and McIntosh considered the measured length change of a porous sample to correspond to only one third of the expansion along the pore axis [50]. Accordingly, the modulus determined with equation 1.5 would be to high by a factor of three [50].

Yates improved the above formula and established a connection between Λ and the bulk modulus K_S. The deformation for samples with an isotropic arrangement of the pores is also isotropic [98]. For Young's modulus E_S, an expansion in one direction of the sample is connected with a contraction in the other two directions, whereas for the bulk modulus the length changes are all isotropic [108]. The model by Yates [53, 54, 108] is based on a system of slightly sintered spheres. A reduction of the surface tension γ increases the radius r of the spheres (and the sample expands) [53]. Therewith the following relation for the bulk modulus of the matrix material (again not the effective modulus) was derived [53, 108]:

---

[4] parallel to the pore surface

[5] Note that the units of the surface pressure N/m, surface tension N/m, and surface energy J/m^2 are equivalent.

[6] The sample was regarded as a thin cylinder with a surface equal to the specific surface of the porous sample. The reduction of the surface free energy results in an increase of the length of the rod [52, 108].

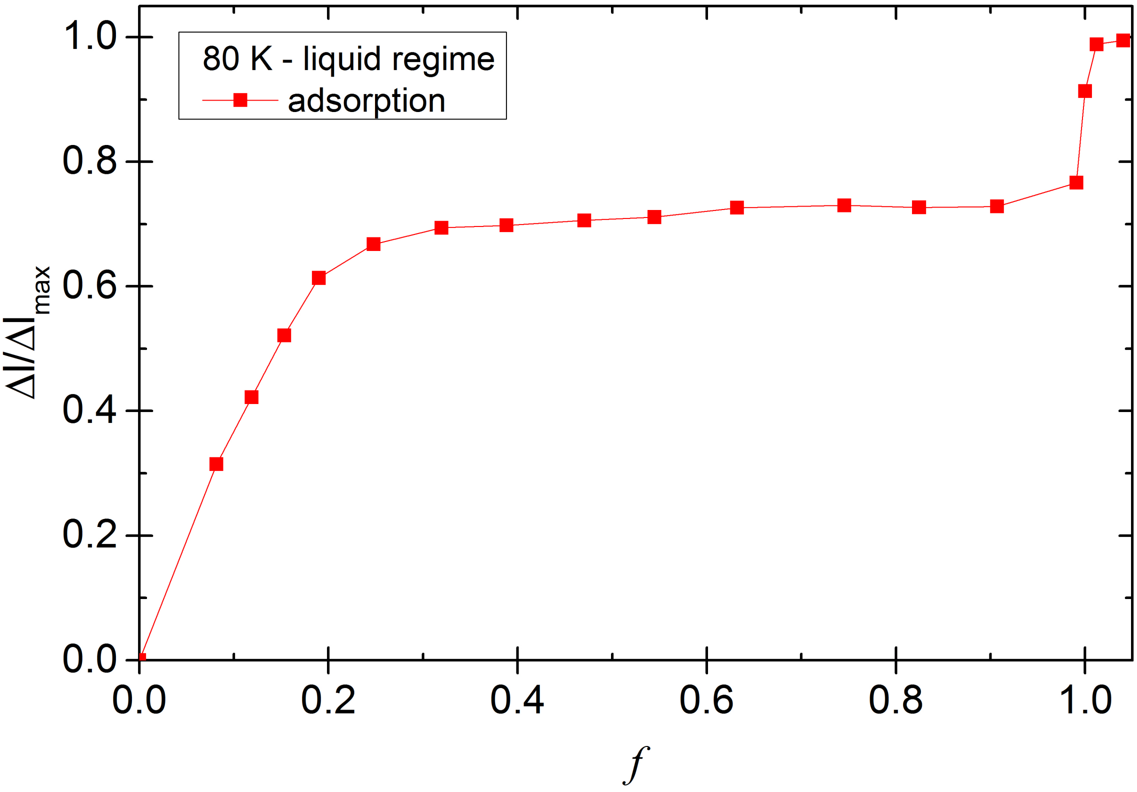

FIGURE 1.6 – *The adsorption of liquid argon (at* 80 *K) causes a marked expansion up to a filling fraction of* $f \approx 0.2-0.3$*. A further increase of the filling exhibits almost no influence on the length of the nanoporous glass sample. Only when the pores are almost completely filled the flattening of the concave menisci of capillary condensate (at the pores ends) results in an expansion. This measured adsorption-induced deformation closely resembles the behaviour during adsorption of water observed by Amberg and McIntosh [50]. The length change* Δl *is scaled to the maxium length change* $\Delta l_{max} = 1.2$ *µm at complete filling (initial sample length at* $f = 0$*:* $l_0 = 2.4$ *mm).*

$$K_S = \frac{2}{9}\frac{\Sigma\rho_S}{\Lambda} \tag{1.6}$$

A comparison between the elastic moduli determined with those equations from deformation measurements and the literature values of the corresponding material shows that both equations yield values in the right order of magnitude [53]. Though the equation by Yates results in better values, the determined moduli are still far to high [53]. From energetical considerations Scherer [54] arrived at a similar result as Bangham and Maggs (cp. equation 1.5). In his equation Young's modulus differs only by a factor $(1-\nu)$, with the Poisson ratio ν. The equations 1.5 and 1.6 relating the deformation with the Young modulus E_S or the bulk modulus K_S, however, do not yield the correct relation between E_S and K_S [54]. Scherer set up a model for a factor in equation 1.6 that depends on the pore structure and the Poisson ratio [54]. With this additional factor a better agreement with the experiments could be achieved [54].

The measurements of the deformation of porous Vycor® glass during sorption of water by Amberg and McIntosh [50] showed that adsorption does not simply result in a continuous expansion of the porous sample. Figure 1.6 shows the behaviour during adsorption of liquid argon (own measurement), which is very similar to the observations for the adsorbate water in reference [50]. The deformation of porous materials during sorption is not only caused by changes of the surface free energy discussed above (see e.g. reference [44]). An important contribution to the pressure exerted by the adsorbate on the pore walls is the Laplace pressure due to curved interfaces of the adsorbate [44, 113]. The Laplace pressure is related to the radii of curvature, r_1 and r_2, and the surface tension γ [114]:

$$p_L = \gamma(1/r_1 + 1/r_2) \tag{1.7}$$

This equation simplifies for capillary bridges to $p_L = 2\gamma/r_K$ (with $r_1 = r_2 = r_K$). Thus the formation of capillary bridges during adsorption results in a contracting effect because of their hemispherical menisci at both sides ($r_K < 0$) [44, 50]. Therefore, Amberg and McIntosh hold the formation of capillary bridges responsible for the very small increase of the length of the sample at higher fillings and $f < 1$ (cp. figure 1.6 for $0.3 \lesssim f < 1$) [50]. The formation of capillary bridges can counteract the reduction of the surface free energy and such a plateau value would be possible [50]. But for adsorbed surface layers in a cylindrical pore the Laplace pressure also contributes to the pressure on the pore walls [44]. For thin surface layers its contribution is small compared to the pressure as a result of the reduction of the surface free energy [44]. With increasing thickness of the surface layers the contracting effect of the negative Laplace pressure grows and it can cause a relative reduction of the length of the sample because the radius of curvature becomes smaller (cp. equation 1.7 and reference [44]). Thus not only the formation of capillary bridges but also the formation of thick surface layers tends to a contraction and the sort of plateau observed for fillings above $f \approx 0.2 - 0.3$ (cp. figure 1.6) does not (necessarily) indicate the formation of capillary bridges (in contrast to the assumption in reference [50]).

When all pores are filled with capillary bridges, only concave menisci remain at the pore ends. The flattening of these menisci induces a further expansion of the sample because the absolute value of the contracting Laplace pressure decreases (cp. figure 1.6 for $f \approx 1$).

The possibility to calculate the deformation for different reduced pressures was shown by Gor and Neimark [44, 113]. Because of the importance of their thermodynamic model for the discussion in chapter 8, its fundamentals will be explained at the appropriate place (see section 8.2).

During the initial desorption process a reduction of the reduced pressure is accompanied by a virtual constant filling fraction $f \approx 1$ (see figure 1.3). The corresponding part of the sorption isotherm was also used in several studies to estimate the elastic properties of the porous sample from the measured deformation [48–50, 115]. In that part a reduction of the reduced pressure causes the formation of concave mensici at the interface of the pore condensate at the pore ends. As discussed above, these concave menisci are related to a negative Laplace pressure and cause a contraction. The determination of the Laplace pressure forms the basis for these estimates of the elastic properties of the porous matrix [48–50, 115]. According to the Kelvin equation [61] the Laplace pressure p_L in the adsorbate amounts to [48, 116]

$$p_L = \ln\left(\frac{p}{p_0}\right)\frac{RT}{V_m} \tag{1.8}$$

A simple estimate of the Young modulus of the matrix material, E_S, of SBA-15 (a porous sample with a hexagonal arrangement of parallel pores) from the measured lattice deformation $\varepsilon = \Delta V/V_0$ (ΔV: volume change, V_0: initial volume) was indicated by Zickler et al. [55]. These authors presumed the validity of the mechanical behaviour of a honeycomb structure [55]:

$$\varepsilon = \frac{p_L\left(1-2\nu\right)}{E_S\left(1-\phi\right)^3} \tag{1.9}$$

The deformation ε determined with this equation using the literature value for E_S differs by a factor of two from the measured deformation [55]. This might originate in the simplifying assumptions for the structure of the porous sample [55].

Prass et al. [48] calculated from the ratio of this Laplace pressure p_L to the measured lattice deformation ε of two ordered nanoporous pulvers (MCM-41 and SBA-15) a so-called pore-load modulus M_{PL} [48, 51]:

$$M_{PL} = \frac{p_L}{\varepsilon} = \frac{1}{\varepsilon}\frac{RT}{V_m}\ln\left(\frac{p}{p_0}\right) \tag{1.10}$$

It appears from this equation that no knowledge of the surface tension or the wetting angle is necessary for the determination of this modulus [48]. The measurements and calculations by Prass et al. showed that this modulus is independent of the used adsorbate (valid at least for three adsorbates with considerable different chemical and physical properties) [48]. On the other hand it depends on the porous sample and the porosity and it represents an elastic constant of the porous matrix [48]. A comparison of the pore-load modulus with the Young modulus and the Poisson ratio was accomplished in reference [48] via the stress σ_{PL} in the silica matrix (perpendicular to the cylindrical and parallel pores of their samples). This stress $\sigma_{PL} = \varepsilon E_S/\left(1+\nu\right)$ was approximated by “the hoop stress in a thin-walled cylinder with internal pressure” p_L [48]: $\sigma_{PL} = p_L r_P/t_w$, with the pore radius r_P and the thickness $2t_w$ of the wall. Thus an estimate of the Young modulus is possible [48]:[7]

$$M_{PL} = \frac{p_L}{\varepsilon} \approx \frac{t}{r_P}\frac{\sigma_{PL}}{\varepsilon} \approx \frac{\pi/\left(2\sqrt{3}\right)-\phi}{2\phi}\frac{E_S}{1+\nu} \tag{1.11}$$

---

[7] For the hexagonal lattice of pores of their sample (with the lattice parameter a_l) the porosity ϕ is given by $\phi = 2\pi r_P^2/\left(\sqrt{3}a_l^2\right)$ [48]. For the deduction of equation 1.11 this relation is necessary together with the approximations $a \approx 2\left(r_P + t_w\right)$ and $t_w \ll r_P$ [48].

The values determined with this approximation from the elastic properties of fused silica (the material of the matrix) show a good agreement with the experimentally determined pore-load modulus M_{PL} [48]. Consequently, equation 1.11 can be used to estimate the Young modulus of the material of the porous matrix [48].

Balzer et al. [49] deduced a possibility to approximate the effective bulk modulus of their porous carbon matrix by the following equation:

$$\frac{\Delta l}{l_0} \approx \frac{1}{3}\frac{\Delta V}{V_0} \approx \frac{\varphi \phi_{meso}}{3K} \frac{RT}{V_m} \ln\left(\frac{p}{p_0}\right), \tag{1.12}$$

with the so-called mesoporosity ϕ_{meso} and the filling fraction of the mesopores, φ, i.e. the total filling fraction less the surface layers [49]. With this relation between the deformation and the general correlation $E = 3K(1 - 2\nu)$ between the Young modulus and the bulk modulus, Balzer et al. [49] achieved an estimate of the effective bulk modulus and Young's modulus of their porous carbons from the measured macroscopic deformation. Thus, it is not only possible to approximate the elastic properties of the matrix material (e.g. via the equation 1.5 by Bangham and Maggs). The estimates of the effective moduli in reference [49] show an agreement with the elastic moduli determined from ultrasonic measurements on the empty sample (deviations $\approx 20 - 50\%$).

Depending on the system of porous sample and adsorbate, the deformation exhibits a very complex behaviour during sorption. Measurements by Haines and McIntosh [110] on activated carbon showed a marked contraction below the length of the empty sample during the initial desorption of water (still before the steep part of the desorption branch is reached). They considered this as an evidence that concave menisci form in the desorption branch [110]. In contrast to measurements on charcoal or porous Vycor® (see above), for the adsorption of surface layers no noticable deformation was measured for the activated carbon [110]. In addition, a deviation from the Bangham equation (cp. equation 1.4) was observed for low fillings [110].

As mentioned above, the effect of adsorption-induced deformation of porous samples was not only observed for samples with an unordered arrangement of pores, but also for samples with parallel pores [48, 88, 89, 117–120]. Thus Dolino et al. [117] detected the deformation of the pores in porous silicon via x-ray diffraction. Especially for samples with a small pore diameter (of about 3 nm) a marked contraction was observed during adsorption of pentane at low pressure (i.e. at low filling) [117]. This effect was partly attributed to the impact of attractive van der Waals forces in small nanometre-sized cavities in accordance with considerations by Ash et al. [117, 121]. Prior to this, Ash et al. [121] set up the thermodynamic energy for a liquid between two parallel walls considering the influence of the distance on the attractive or repulsice forces. Günther et al. [119, 120] also studied the pore deformation of SBA-15 and MCM-41 with small angle x-ray diffraction and performed Monte Carlo simulations. Both methods provided very similar results [119]. Because of a considerable difference between the measured deformation and the deformation expected as a result of the Laplace pressure, Günther et al. [119] concluded that the curved surface of the menisci and the Laplace pressure cannot be the sole explanation for the deformation. Also because of the simulations, these authors consider dispersion forces as an essential reason for the deformation [119]. As mentioned above, dispersion forces were also used to explain a contraction of samples at low fillings [117, 121]. For these samples with parallel pores (including SBA-15 [48], MCM-41 [119], porous silicon [117], and another thin porous silica film [115]), the first adsorbed surface layers cause a significantly smaller deformation than capillary bridges at high filling (cp. e.g. figure 1 in reference [48]), similar to the behaviour mentioned above for activated charcoal [110]. This contrast e.g. to the observations for porous Vycor® (cp. figure 1.6).

The adsorbate and its properties directly influence the deformation behaviour. Yates evidenced that polar adsorbate causes a contraction of a porous glass sample at the beginning of the filling process, in contrast to non-polar gases [53, 122]. He assumed that this behaviour is related to the electrical properties of the adsorbate and possibly to the dipole and quadrupole moment of polar adsorbates [123]. The gases that cause a contraction possess both a dipole and a quadrupole moment [123]. Also a hydrogen bonding between the adsorbate and the porous sample (for the corresponding adsorbates, e.g. ammonia) were named as a possible origin [123]. The observed contraction of the sample is related to properties of the hydrogen bonding between adsorbed molecules and pore surface [124], which in turn influences the effective Young modulus of the porous sample [125].

Chapter 2

Sorption of liquid and solid argon in nanopores

The previous knowledge of the physical behaviour of argon in the nanopores of porous Vycor® glass, i.e. in particular the existance of both liquid and solid argon below the actual freezing point of confined argon, are sketched in the first part of section 2.1 (own work, diploma thesis [126]). The second part (starting from page 21) as well as the results presented in section 2.2 are already part of this dissertation. Ultrasonic measurements supply information on the phase state of the adsorbed argon on the basis of the effective shear modulus of the porous matrix and the pore filling. Isothermal measurements between 50 *K and* 75 *K (freezing point of confined argon* $T_{fr,Ar,pore} \approx 76$ *K [85]) reveal that the fraction of liquid argon decreases with decreasing temperature. The ultrasonic measurements on the heterogeneous system of pores and porous matrix do not directly supply the intrinsic elastic properties of each constituent. For the determination of the intrinsic shear modulus* $G_{Ar,ads}$ *of adsorbed argon from the effective shear modulus* G *some efforts are necessary. Possibilities and requirements for the extraction of the intrinsic shear modulus are presented. The development of an effective medium analysis permits the determination of the intrinsic shear modulus of adsorbed surface layers (and for adsorbate in completely filled pores). This analysis reveals the formation of solid argon layers on top of liquid-like surface layers during isothermal filling at low temperatures (*$T < T_{fr,Ar,pore} \approx 76$ *K). These frozen and solid argon layers are bulk-like, i.e. their shear modulus* $G_{Ar,SL}$ *is about equal to the shear modulus* $G_{Ar,bulk}$ *of crystalline bulk argon at the corresponding temperature.*

2.1 Effective shear modulus during isothermal sorption of liquid and solid argon

At the beginning of this dissertation some information of the influence of adsorbed argon in the nanopores of porous Vycor® glass on the effective shear modulus G of the porous sample were known from my previous studies [126]. Liquid adsorbed argon does not contribute to the effective shear modulus of the porous sample independently from the filling fraction $f = n/n_0 = V_{Ar,ads}/V_{pores}$ (see figure 2.1);[1] The deviations are smaller than

---

[1] n: molar amount of pore filling; n_0: molar amount of adsorbate necessary for complete filling of the pores; $V_{Ar,ads}$: volume of the adsorbed argon; V_{pores}: volume of the pores

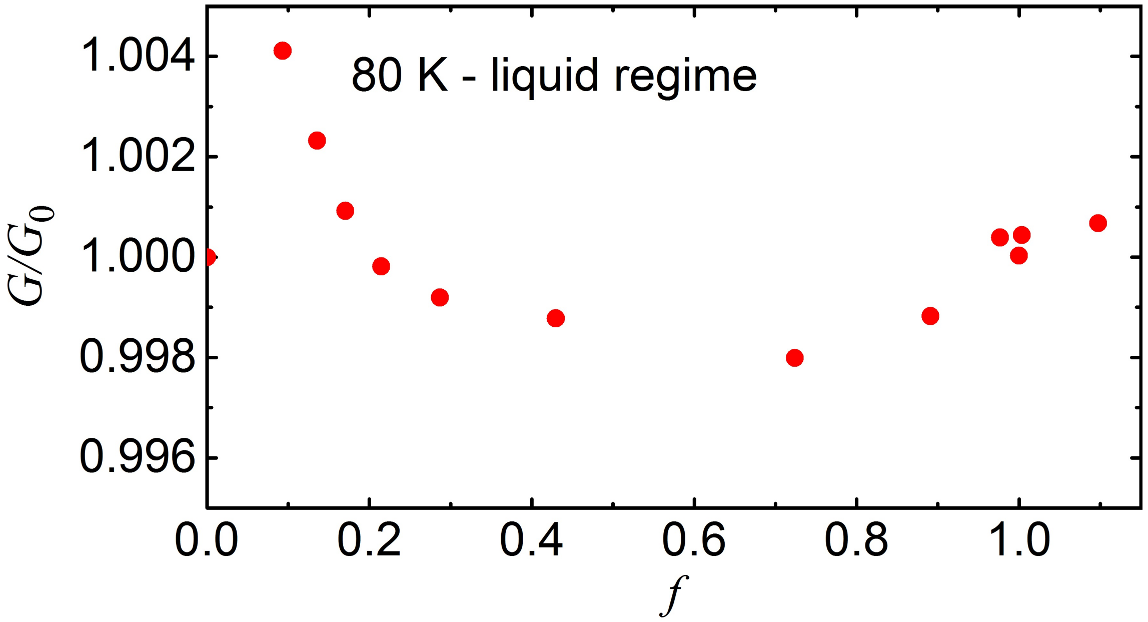

FIGURE 2.1 – *Effective shear modulus of a porous glass sample (scaled with the shear modulus* $G_0 = 6.86$ *GPa of the empty sample) during adsorption of liquid argon at* 80 *K as a function of the filling* $f = V_{Ar,ads}/V_{pores}$. *The effective shear modulus remains essentially unchanged by the adsorbate and the deviations are smaller than* 0.5%, *which reflects the accuracy of the method. Figure from [1] (Copyright © 2008 by the American Physical Society).*

0.5%. This behaviour is not particularly astonishing, as (inviscid) liquids cannot sustain shear stress.

During the successive isothermal filling of the porous glass sample with argon below its freezing point ($T_{fr,Ar,pore} \approx 76$ K for completely filled pores with a pore radius of $r_P \approx 3.9$ nm [85]), the effective shear modulus features three characteristic ranges (see figure 2.2) for a measurement at 72 K. Below a filling fraction $f_1 \approx 0.53$ the adsorbed argon does not change the effective shear modulus. This shows directly that the adsorbate behaves liquid-like though the measurement was performed below the freezing point of confined argon. It appears clear that at such low filling fractions (region I up to f_1) the liquid-like argon consists of adsorbed surface layers (cp. section 1.2). The existance of such liquid-like, non-freezing or amorphous surface layers below the actual freezing point of argon is also known from other measurements [29]. The average number z of adsorbed argon monolayers at f_1 can be estimated with the relation

$$f = \frac{V_{Ar,ads}}{V_{pores}} = \frac{r_P^2 - (r_P - zu)^2}{r_P^2}, \tag{2.1}$$

with the average pore radius $r_P = 4.0$ nm and the thickness $u \approx 0.34$ nm of one adsorbed

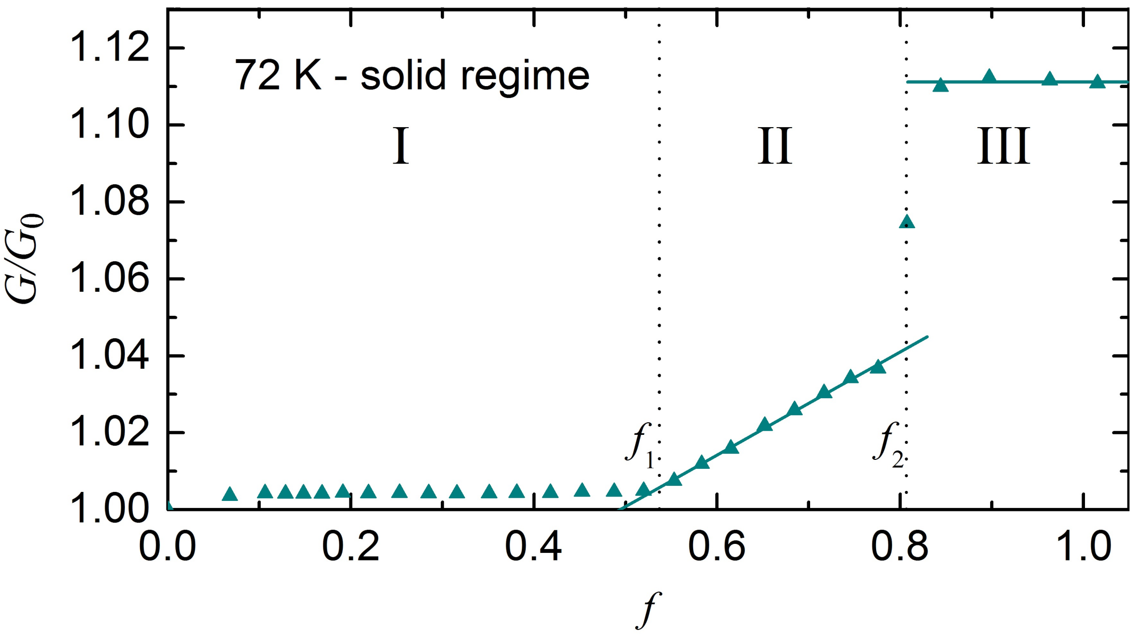

FIGURE 2.2 – *At 72 K, i.e. below the freezing point of argon the scaled effective shear modulus exhibits three characteristic ranges during filling ($G_0 = 6.88$ GPa). The process of freezing starts only at a filling fraction of $f_1 \approx 0.53$ and the effective shear modulus increases linearly with increasing filling. Above a higher filling $f_2 \approx 0.81$ the effective shear modulus remains at a plateau value. Figure from [1] (Copyright © 2008 by the American Physical Society).*

layer.[2] Thus, the filling fraction $f_1 \approx 0.53$ at a temperature of 72 K corresponds on average to three or four adsorbed surface layers on the pore wall that do not freeze ($z \approx 3.7$).

The (linear) increase of the shear modulus above f_1 indicates the presence of frozen adsorbate, since liquids cannot sustain shear stress or contribute to the shear modulus. At this point the spatial arrangement of the pore filling above f_1 cannot be determined. The intuitive assumption that solid capillary bridges form in region II (which corresponds to the steep part of the adsorption isotherm) will prove as erroneous (see section 2.2.2). Above f_2 a plateau values is observed for the effective shear modulus (region III). At f_2 beside changes of the spatial arrangement also changes of the intrinsic properties of the adsorbed argon (amorphous ⇒ crystalline) would be possible. At this state of the research interpretations regarding the different properties and spatial structures of the adsorbed argon in these three ranges were somewhat speculative. The meaning and origin of the special behaviour of the effective shear modulus will be elucidated in section 2.2.2.

My previous measurements at 70 K, 72 K, and 74 K also showed that the filling fractions f_1 and f_2 are shifted to lower values when the temperature is reduced (see figure 2.3 for 72 K and 74 K). The reduction of f_1 by ≈ 20% as a consequence of a temperature change of 2 K evidenced that at lower temperatures the process of freezing starts already at lower

---

[2] The thickness u of one adsorbed argon layer can be estimated with the density of argon, $\rho_{Ar} \approx 1.66\ \mathrm{g/cm^3}$ (at 72 K) [127], the molar mass $m_M = 39.948$ g/mol and the Avogadro constant N_A: $u \approx [m_M/(\rho N_A)]^{1/3} = 0.34$ nm.

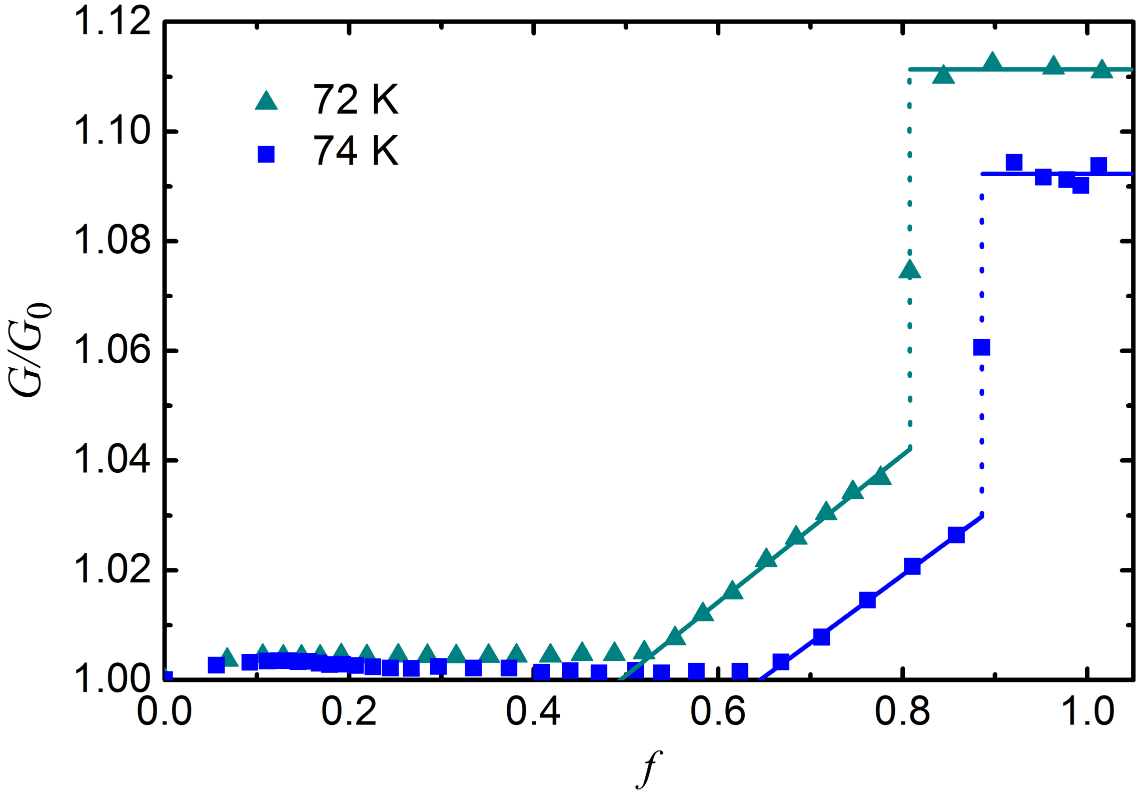

FIGURE 2.3 – *Scaled effective shear modulus during adsorption of argon at* 72 *K and* 74 *K as a function of the filling fraction* f*. A reduction of the temperature results in a shift of the curves for the effective shear modulus to lower filling fractions. Consequently, the process of freezing starts at lower filling fractions* f_1 *when the temperature is reduced. Figure from [1] (Copyright © 2008 by the American Physical Society).*

filling fractions.

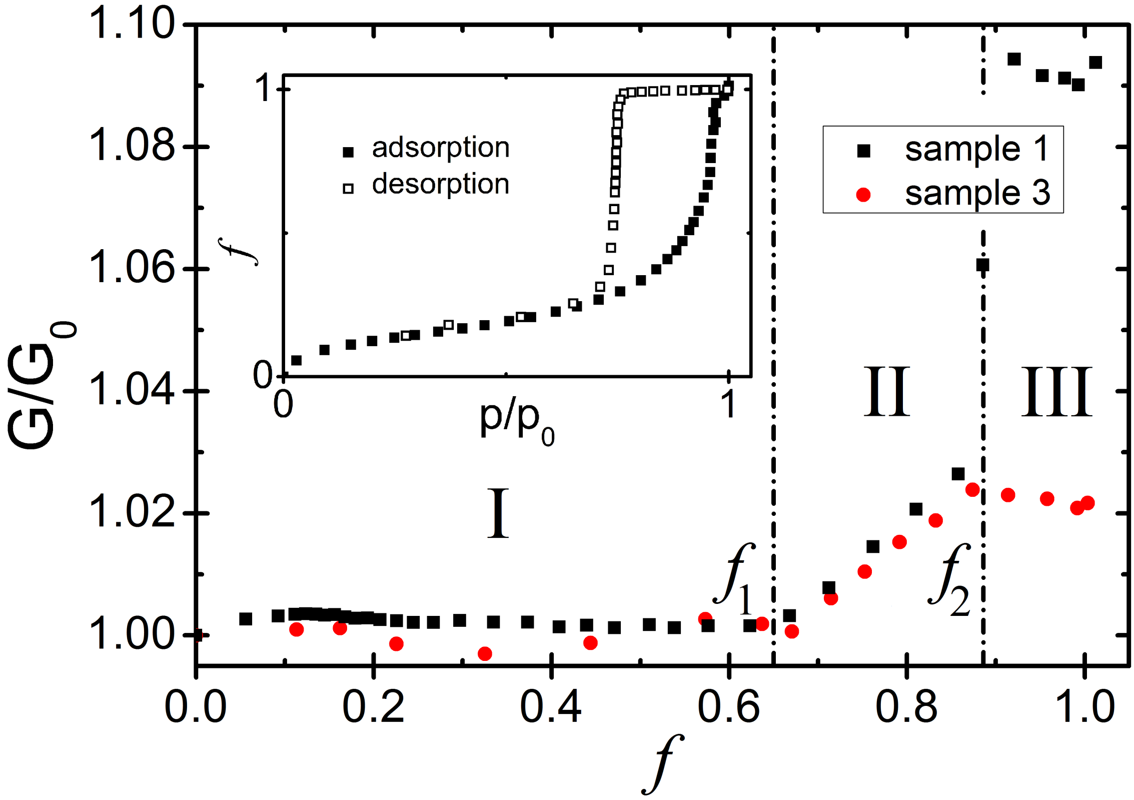

Figure 2.4 – *Effective shear modulus G (scaled) for two Vycor® samples (each $r_P \approx 4.0$ nm) during filling with argon at 74 K. Both samples show three regions for the effective shear modulus, however, only for one sample the transition from region II to III at f_2 is connected with an abrupt jump to a higher plateau value. This could be related to strains or distortions in the porous matrix because of the formation of solid capillary bridges (cp. section 2.2.2). The inset shows the filling fraction f as a function of the reduced vapour pressure for adsorption and desorption (sample 1). Figure from [2] (Copyright © 2011 by the American Physical Society).*

For this dissertation, initially, additional sorption isotherms at other temperatures and with other porous Vycor® samples were performed. All these measurements show a behaviour similar to that described above. Always the effective shear modulus G starts to increase at a certain filling fraction $f_1 > 0$ and this increase of G is essentially proportional to the filling fraction $(f - f_1)$ up to f_2. The transition from the region of the linear increase $(f_1 \leq f \leq f_2)$ to the region with the plateau value for G is, however, not always connected with an abrupt jump to higher values for the effective shear modulus G (see figure 2.4).

Even at temperatures as low as 50 K still a small filling fraction of $f_1 \approx 0.2$ (corresponding to a bit more than one monolayer) behaves liquid-like. The amount of liquid-like argon during isothermal adsorption measurements, i.e. f_1, is shown in figure 2.5 for different temperatures. The dependence of f_1 is particularly strong just below the freezing point $T_{fr,Ar,pore} \approx 76$ K [85]. A reduction of the temperature from 75 K by only 5 K reduces f_1 by about 50%. But at lower temperatures the reduction of f_1 with decreasing tempera-

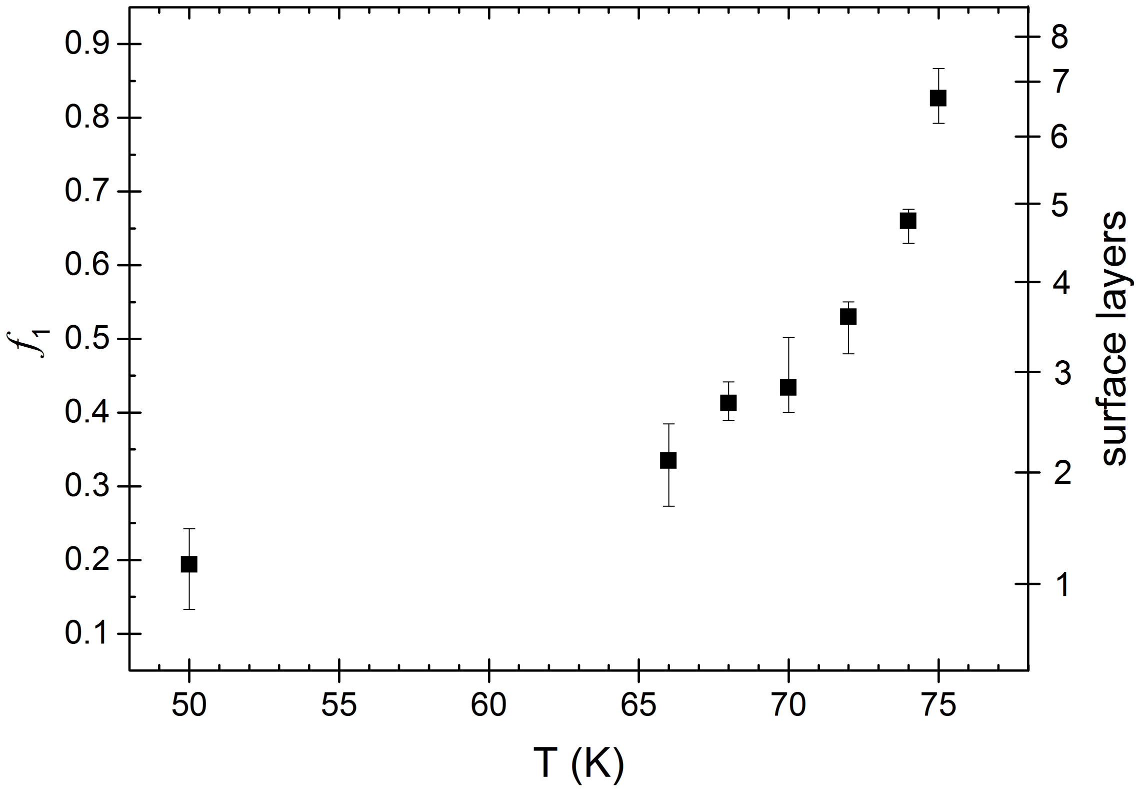

FIGURE 2.5 – *Temperature dependence of the filling fraction f_1 [and of the corresponding number of surface layers (with the thickness $u \approx 0.35$ nm for one monolayer)]. A reduction of the temperature results in a shift of the filling fraction f_1, i.e. of the onset of freezing during isothermal adsorption, to lower values. At 50 K still a bit more than one surface layer remains liquid-like.*

ture lessens considerably and the fraction of liquid-like argon seems to approach a final minimum value of $f_1 \approx 0.2$. This would suggest that the first adsorbed surface layer does not participate in a liquid-solid phase transition and remains even at low temperatures in a liquid-like state corresponding to the model of “dead” surface layers near the pore wall (see below). A close study of the phase transition behaviour of the first few surface layers during temperature cycles in chapter 3 will show, however, that also these surface layers crystallize completely at very low temperatures.

Wallacher and Knorr have proposed a simple model describing thermal equilibrium in completely filled pores (see reference [29]), where the pore walls are at first covered by “dead” layers (two monolayers) and then by a liquid shell. The latter one serves as a buffer between the frozen capillary sublimate in the pore centre and the “dead” layers that do not undergo a liquid-solid phase transition reducing the free energy of the system [29]. There is an interplay between volume and interfacial energies and with decreasing temperature the thickness of the liquid shell decreases [29]. Taking their model, the amount f_1 of liquid-like argon would correspond to the sum of “dead” layers and liquid shell, which are indistinguishable in the ultrasonic measurements. The first two “dead” layers represent a filling fraction of $f_{dl} \approx 0.31$ [cf. equation 2.1]. Thus, for example at 72 K the liquid

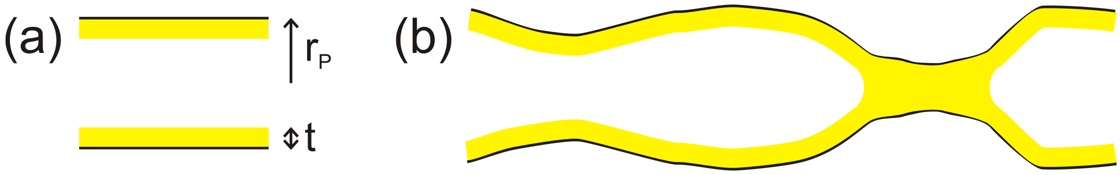

Figure 2.6 – *(a) Idealized pore with constant radius r_P. The pore wall is covered with an argon layer of the thickness t. There are not yet any capillary bridges. (b) Because of a certain pore size distribution possibly there are a few pore sections with capillary bridges already at low filling fractions (see text). Figure (b) from [2] (Copyright © 2011 by the American Physical Society).*

shell corresponds to $f_1 - f_{dl} \approx 0.22$. This value is larger than the one predicted by the model of Wallacher and Knorr (at 72 K they obtain $f \approx 0.05 - 0.10$ for a pore radius of 5 nm) [29], but it must be kept in mind that the total free energy they calculate depends on interfacial energies and on a coherence length, the values of which have to be estimated. Therefore, at least a qualitative agreement can be stated. In the above model, the existence of liquid-like argon is an inherent thermodynamical feature of pore confined argon, i.e., it is not related to the pore size distribution of the Vycor® glass.

Because of a certain pore size distribution of the porous Vycor® glass (see figure 1.2 in section 1.1 and figure 2.6) possibly already at low fillings capillary bridges form in a few very small pores or pore sections [(cp. figure 2.6(b)]. Assuming the validity of the Gibbs-Thomson equation, adsorbed argon will only freeze in these pore sections during sorption measurements at lower temperatures, as the reduction of the freezing point is especially big in the smallest pores ($\Delta T_{fr} \propto 1/r_p$, cp. equation 1.3 in section 1.3). Thus, it would be difficult to differentiate clearly between capillary bridges in these small pores and liquid-like surface layers.

2.2 Intrinsic shear modulus of adsorbate $G_{Ar,ads}$

2.2.1 Estimate of the intrinsic shear modulus $G_{Ar,ads}$ for $f = 1$

According to the effective medium theory, the effective elastic moduli of a heterogeneous material depend on both the material parameters as well as on the spatial distribution, i. e. on the microstructure. This makes it difficult to evaluate precisely the shear modulus of the confined frozen argon from the measured effective shear modulus G. It is possible to get an estimate since there are lower and upper bounds for G corresponding to the principles of least work and of minimum potential energy, respectively [128]. For a two-phase system of arbitrary microstructure the upper bound is given by $G \leq \sum_i (V_i/V)G_i$, i.e., each component i contributes at maximum with its volume fraction [128]. For the lower bound the volume-weighted reciprocal values are to be taken, i.e., $G \geq 1/\{\sum_i (V_i/V)/G_i\}$ holds [128]. At complete filling ($f = 1$) only the shear modulus of quartz glass, $G_Q = 27.95$ GPa [129], and that of the pore filling has to be considered for the lower bound. A rearrangement of the above equation for the lower bound results in an upper bound for the shear modulus of the adsorbed argon:

$$G_{Ar,ads}|_{f=1} \leq \frac{\phi}{\frac{1}{G} - \frac{1-\phi}{G_Q}} \tag{2.2}$$

Here $G_{Ar,ads}$ denotes the shear modulus of the whole pore filling, i. e. of pore condensate and surface layers. For example for a measurement with sample 1 at 72 K (cp. figure 2.2), equation 2.2 gives an upper bound of $G_{Ar,ads} = 2.4$ GPa.[3] Equation 2.2 disregards that the surface layers do not contribute at low filling fractions $f \leq f_1$ (see section 2.1), where they have a free surface facing the empty core volume. But when pore sublimate forms they become interfacial layers between two solids, i. e. between matrix and frozen argon, and thus their properties could change (at least they are able to transmit elastic vibrations). Therefore, equation 2.2 only yields an upper bound for the shear modulus of the pore filling as a whole but it supplies no possibility to separate contributions from pore sublimate and surface layers. The values for the shear modulus of (poly-)crystalline bulk argon are at a temperature of 72 K in a range of $\approx 0.8 - 1.2$ GPa (see also figure 2.8) [130–132]. Thus the effective medium analysis is in good agreement with this data showing that the confined frozen argon can be in a crystalline or in a poly-crystalline state.

---

[3] There are small differences between different Vycor® samples ($r_P \approx 4.0$ nm) for the upper bound of the shear modulus of the pore filling $G_{Ar,ads}$ (changes in the first decimal place). Reasons for that are slight differences for G_0 and the appearance of an abrupt increase of G at f_2 for one sample.

2.2.2 Quantitative determination of the intrinsic shear modulus $G_{Ar,ads}$ and implications for the geometrical configuration of the adsorbate

In the following the linear increase of the effective shear modulus in region II of the sorption isotherms (i.e., a common feature of all samples studied, see e.g. figure 2.4) is analyzed. This region II corresponds to a range where a considerable increment of the pore filling barely alters the reduced vapour pressure p/p_0 (see the steep increase of the adsorption branch in the inset of figure 2.4). The onset of capillary condensation or sublimation is expected somewhere in this range [60]. But its exact location is difficult to predict: Geometrical instabilities and fluctuations may be less important on a solid phase at low temperatures, so that capillary sublimation might occur only at rather high fillings.

The scope of the following effective medium analysis is thus twofold: First the analysis will show that the geometrical arrangement of the adsorbed frozen argon in region II mainly corresponds to that of surface layers, i.e., that capillary sublimate only forms at higher fillings. Second the analysis will permit the evaluation of the intrinsic shear modulus of the adsorbed frozen argon.

The unfilled Vycor® glass has a complicated network-like microstructure consisting of quartz glass and empty pores [see schematic sketch in figure 2.7]. For this reason its shear modulus, G_0, is smaller than that of bulk quartz glass, G_Q. Up to a porosity of $\phi \approx 0.25 - 0.3$ for many materials the elastic moduli depend approximately linearly on the porosity [133, 134]. Thus for a given porosity ϕ the shear modulus G_0 can be written as

$$G_0 = G_Q \cdot (1 - a \cdot \phi), \tag{2.3}$$

where a is a factor that depends on the microstructure, i.e., on the spatial arrangement of the pores (connectivity, shape, size distribution, etc.).

Supposing that one would start to refill the pores of a sample (at $\phi \approx 0.25$) by adding a small amount of quartz glass, the material can be deposited at different places creating various geometrical arrangements [compare figure 2.7(b)+(c)].

The corresponding increase of the shear modulus is given by

$$\frac{dG_0}{G_Q} = -(a \cdot d\phi + \phi \cdot da). \tag{2.4}$$

Only when the microstructure of the existing porous network is preserved, $da = 0$ holds and this change is solely proportional to $d\phi$, i.e., to the amount of added material.

A preservation of the microstructure can for example be achieved by changing slightly the local pore radius [adding surface layers, see figure 2.7(b)] and in the following this

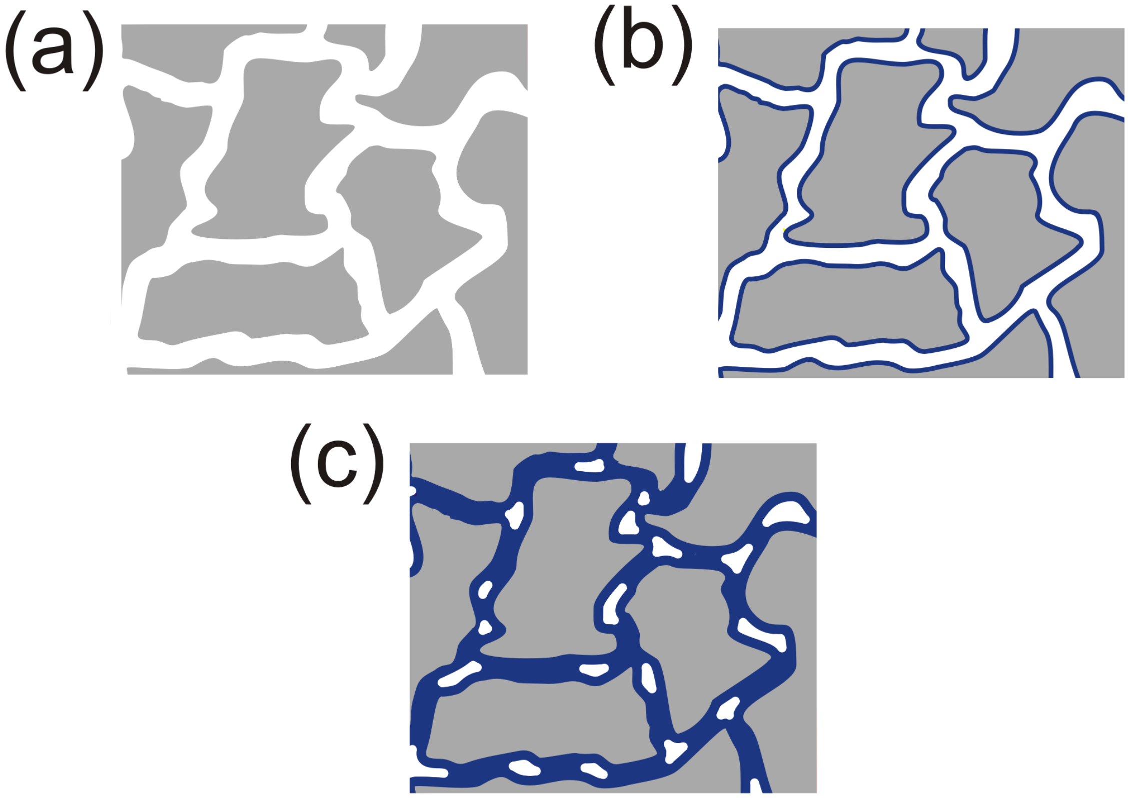

FIGURE 2.7 – *Schematic sketch of the structure of porous Vycor® glass. (a) Unfilled sample. Additional material can be deposited as surface layers preserving the microstructure of the empty network (b) or in the centre of the pores as it is the case for capillary sublimate (c). In the latter case the microstructure is changed. Figure from [2] (Copyright © 2011 by the American Physical Society).*

case will be considered in more detail. Let f be the filling fraction of the pores so that $d\phi = -f\phi$ holds. Adding surface layers of quartz would thus lead to a change,

$$dG_0 = a \cdot \phi \cdot f \cdot G_Q. \tag{2.5}$$

It is proportional to the known factors a and ϕ characterizing microstructure and porosity of the unfilled sample as well as to the filling fraction f of the pores and to the surface layers' shear modulus. Analogously, adding adsorbed layers of frozen argon yields an effective shear modulus of

$$G = G_0 + a \cdot \phi \cdot \tilde{f} \cdot G_{Ar,SL}. \tag{2.6}$$

Here, the total filling fraction f had to be replaced by the filling fraction of frozen argon $\tilde{f}$ because only frozen and solid adsorbate leads to a change in G. Before proceeding with the analysis of the data and a test of the above model, the assumptions that are connected with equation 2.6 are now recapitulated. The constancy of the geometry of the frozen argon upon filling is required in order to explain the observed linear increase of the shear modulus. But the validity of equation 2.6 requires even more: the preservation of the porous microstructure of empty Vycor® upon filling with frozen argon. Only in this case the geometrical factor a in equation 2.6 equals that in equation 2.3 and is experimentally accessible via the characterization of the unfilled sample. Combining equations 2.3 and 2.6 yields

$$G = G_0 + (1 - \frac{G_0}{G_Q}) \cdot \tilde{f} \cdot G_{Ar,SL}. \tag{2.7}$$

First a test of the model will be performed by an application of equation 2.7 to the experimental data. From the measurements both the filling fraction of frozen argon, $\tilde{f} = f - f_1$, as well as G_0 can be deduced. With the aid of the shear modulus of quartz glass, $G_Q = 27.95\ GPa$ [129], the shear modulus of the frozen argon, $G_{Ar,SL}$, is evaluated from the measured slope in region II (see figure 2.4). These values for the shear modulus of adsorbed argon (for several isothermal measurements with different samples at various temperatures) show a good agreement with values for bulk argon, i.e.,

$$G_{Ar,SL} \approx G_{Ar,bulk} \tag{2.8}$$

holds (see figure 2.8).

This result assesses the validity of the above effective medium analysis, especially the requisite that the microstructure is not altered. But is the associated geometrical picture sound for a network of rather uneven pores? In other words, is a simple polylayer growth of a frozen argon film a realistic scenario and to what extend does it preserve the microstructure of the porous Vycor® matrix? The situation is illustrated in figure 2.9 showing irregular pores of varying diameter (as a part of the network-like microstructure having a certain pore size distribution; cp. figure 2.7).

At low pore fillings the adsorbed argon is liquid-like, so that it does not contribute to the shear modulus ($G = G_0$; region I in figure 2.4). The first atoms will adsorb in surface layers, but pores or pore sections with small diameters may fill completely [see figure 2.9(I)]. Such capillary condensed argon would not freeze during a sorption isotherm, since the smallest pores exhibit the largest freezing point depression ($\Delta T \propto 1/r_P$; cp. equation 1.3 in section 1.3, section 2.1 and reference [28]). It is thus not distinguishable from liquid-like surface layers.

The observed linear increase of the shear modulus in a large filling range (region II in figure 2.4) and the fact that the quantitative effective medium analysis via equation 2.7 yields bulk-like mechanical properties for the frozen argon, $G_{Ar,SL} \approx G_{Ar,bulk}$, are not casual but distinct features reflecting that adsorbed layers of frozen argon form, probably on top of the previously deposited liquid layers [see figure 2.9(II)]. The microstructure of the frozen layers essentially reproduces the form of the pore walls (i.e., only a negligible amount of argon is deposited in a different geometrical configuration, for example, as capillary sublimate in the centre of pores). Otherwise, the factor a in equation 2.6 would

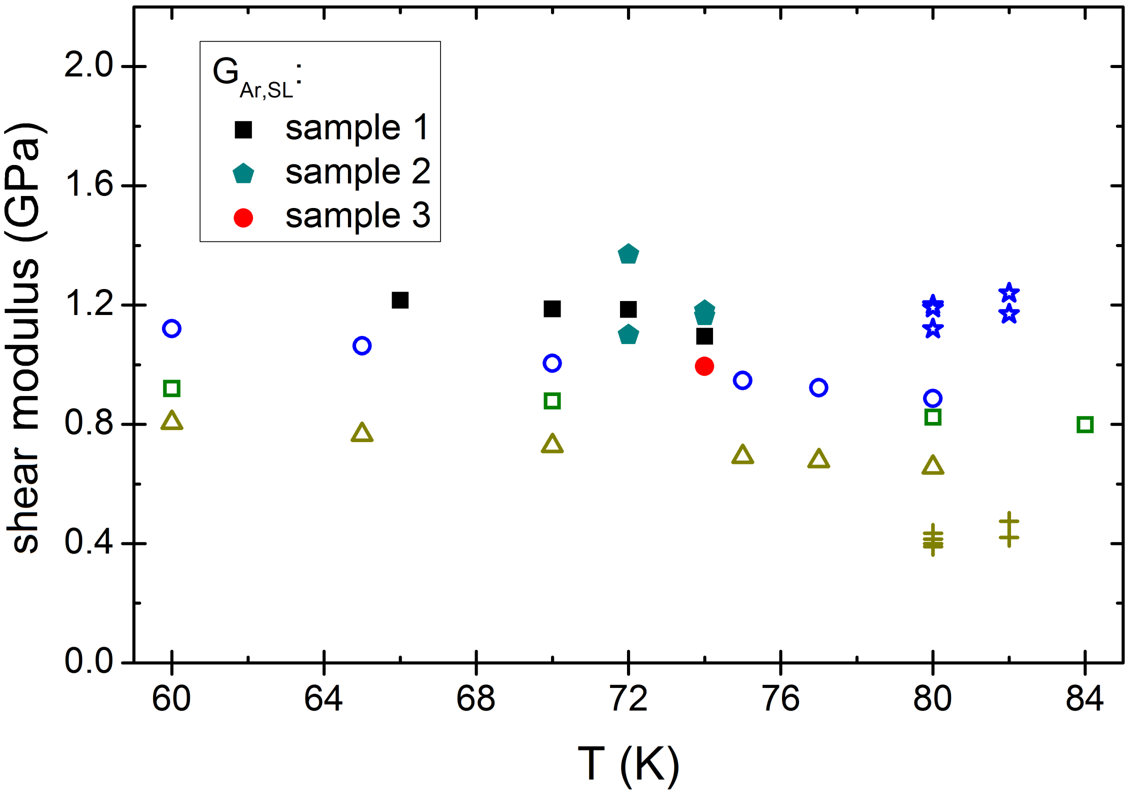

Figure 2.8 – *The intrinsic shear modulus of frozen argon confined to nanopores as a function of the temperature as well as values for bulk argon. The values for confined argon (solid symbols) are calculated from isothermal measurements on three samples using equation 2.7 (sample 1, measurements at four temperatures; sample 2, four measurements at two temperatures; sample 3, one adsorption isotherm). The data for bulk argon are taken from literature: The open squares are values for poly-crystalline argon [131], the open circles [130] and stars [132] for the shear modulus C_{44}, and the triangles [130] and crosses [132] for a different propagation direction ($(C_{11} - C_{12})/2$). Figure from [2] (Copyright © 2011 by the American Physical Society).*

change and the quantitative effective medium analysis would not yield the bulk properties of argon. Liquid capillary condensate that already formed at lower fillings (region I) remains in its state and does not affect the measured shear modulus. The characteristic range $[f_1(T), f_2(T)]$ in which polylayer growth occurs (i.e., width and position of region II) depends on temperature: the lower the temperature, the lower the characteristic filling fractions f_1 and f_2 (see figure 2.3 showing data for $T = 72$ K and $T = 74$ K).

The deviation of the linear increase observed at higher fillings (region III above $f_2 \approx 0.89$ at 74 K in figure 2.4) reflects a change of microstructure of the frozen adsorbate [i.e., now a considerable amount of capillary sublimate has formed; see figures 2.7(c) and 2.9(III)]. The measurements of a volume averaged quantity, the effective shear modulus, provide no possibility to distinguish whether only the new adsorbate that is added in region III forms capillary sublimate or whether also the previously deposited argon undergoes a structural change, for example, a spatial redistribution via a partial delayering of the frozen argon

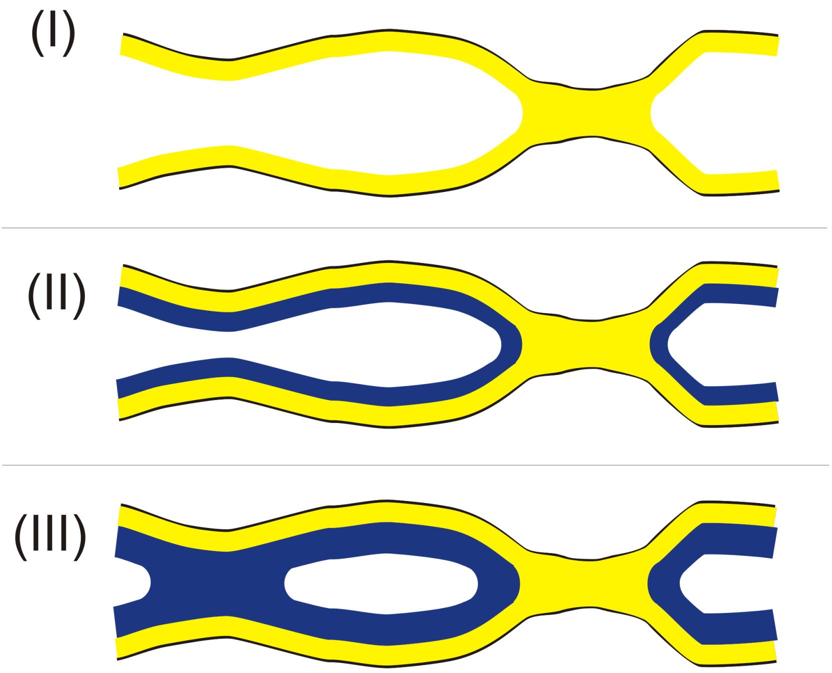

FIGURE 2.9 – *Schematic sketch of pore sections during isothermal filling for different regions. Due to the pore size distribution of porous Vycor® glass there are bigger and smaller pores. In region (I) smaller pores can possibly be filled with liquid pore condensate; in bigger pores there are only liquid-like adsorbed layers. In region (II), i.e., at higher fillings, there are frozen layers formed on top of the liquid-like layers. Finally, in region (III) a further filling of the sample leads to the formation of solid capillary condensate. Figure from [2] (Copyright © 2011 by the American Physical Society).*

film. (The delayering of surface layers will be discussed in section 3.2.) Although the real microstructure is rather complex, the dimension of the surface layers can be estimated (with equation 2.1): The thickness of an adsorbed layer is approximately 0.34 nm, so that at maximum ≈ 12 layers would fit into a pore with a pore radius of 4 nm. At 74 K, region III corresponds to fillings $f > f_2 \approx 0.89$, that is, on average there are more than eight surface layers (the lower the temperature, the lower f_2; cp. figure 2.3). Due to the pore size distribution there are many bottlenecks where capillary sublimate can form. Note that all samples exhibit a saturation of the effective shear modulus, i.e., a plateau in region III (figure 2.4): sample 1 after a step-like increase of G, the other samples without any discontinuity. The actual value for G in region III (plateau) might be caused by internal mechanical tensions or distortions as a result of the abrupt formation of solid capillary bridges during adsorption at f_2. Also a possibly different microstructure of sample 1 may account for the peculiar behaviour at f_2. The formation of a plateau in G can be understood by a simple comparison: Capillary sublimate acts like rivets stabilizing a mechanical construction. When a certain stability is achieved, new fixings have only a small impact.

Conclusions

The first few adsorbed layers do not freeze during isothermal sorption cycles, at least not in the temperature range of the sorption measurements ($50 - 74$ K). The reason for this behaviour might be seen in the difficulty of the argon atoms to accommodate to the structure of the SiO_2 pore surface. But lowering the temperature leads to a decrease in the number of liquid-like layers: from ≈ 4.9 layers at $T = 74$ K ($f_1 \approx 0.66$) to $\approx$ 1 layer at $T = 50$ K ($f_1 \approx 0.2$); cp. figure 2.5. This is an indication of a stronger increase of the interaction between the argon atoms compared to the interaction of argon atoms with the SiO_2 wall.

The wetting of the solid phase by its own melt, i.e. the appearance of liquid-like interfacial or surface layers below the bulk melting temperature (so-called interfacial premelting), is known for many substances including solid rare gases [25,29,34,35,37,40,41,43,80,81,91–96]. For example, ice on a planar SiO_2 surface as well as in porous Vycor® glass exhibits liquid-like interfacial layers, the thickness of which grows with increasing temperature [35, 96]. At a given temperature the layers' thickness is given by the state of the minimal interfacial free energy [29]. Likewise the existence of liquid interfacial layers of argon in pores has been explained as a result of the interplay between volume and interfacial energies; the liquid layers reduce the free energy of the system (see section 2.1) [29].

The effective medium analysis evidences a particular feature: Solid surface layers form on top of the first liquid-like layers during isothermal filling below $T \approx 76$ K. The derived effective medium analysis provides the possibility to determine the shear modulus of these adsorbed surface layers in the nanoporous glass sample. The frozen adsorbed argon layers behave bulk-like and exhibit a shear modulus about equal to the shear modulus of bulk argon, i.e., there are no size or surface effects that alter their shear modulus notably.

Chapter 3

Behaviour of surface layers of argon

The observation that the shear modulus of confined solid argon is about equal to the shear modulus of bulk argon (see section 2.2.2) forms the starting point for a thorough research of the liquid-solid phase transition of argon in nanopores. This finding and the effective medium analysis pave the way for the investigation of the phase behaviour of adsorbed surface layers during temperature cycles via ultrasonic measurements. Adsorbed layers of argon in nanoporous Vycor® glass exhibit a peculiar phase behaviour. In this chapter it will be shown that both the first and the second layer undergo a continuous phase transition in a broad temperature range of at least 40 K. The analysis of the ultrasonic measurements reveals that the fraction of frozen argon increases with decreasing temperature. A complete freezing is only achieved at very low temperatures of approximately 20 K (i.e., far below the bulk freezing temperature $T_{fr,Ar,bulk} = 84$ *K [85]). Whereas those two adsorbed layers remain stable during cooling, the third one becomes unstable around 66 K, rearranges, and solid capillary condensate is formed (delayering transition).*

3.1 First and second adsorbed surface layer

In order to find out whether all liquid layers (cp. figure 2.5) solidify at sufficiently low temperatures or whether there is a minimum number of interfacial layers that always remain liquid, measurements at lower temperatures are required. Since isothermal measurements below 70 K or 60 K are too time-consuming (waiting for an equilibrium distribution after each filling step; see note in section A.1), temperature cycles with nearly constant fillings were conducted (see figure 3.1). Argon gas in the dead volume of the sample cell successively condensates into the sample when the temperature is lowered and thus increases the filling fraction. But this change is negligible below ≈ 60 K, due to the low vapour pressure of argon in that temperature range. Then the filling fraction is constant and the quantity of adsorbed argon corresponds to 1, 2, or 3 surface layers (SL); see figure 3.1.

This specification is used to label the curves of the simultaneously measured effective shear modulus displayed in figure 3.2. To be as near to equilibrium as possible, mostly not more than two or three measurements were made a day for temperature steps of 1 K. The shear modulus of the empty porous glass sample increases almost linearly with decreasing temperature. Adsorbed layers lead to a significant increase of the effective

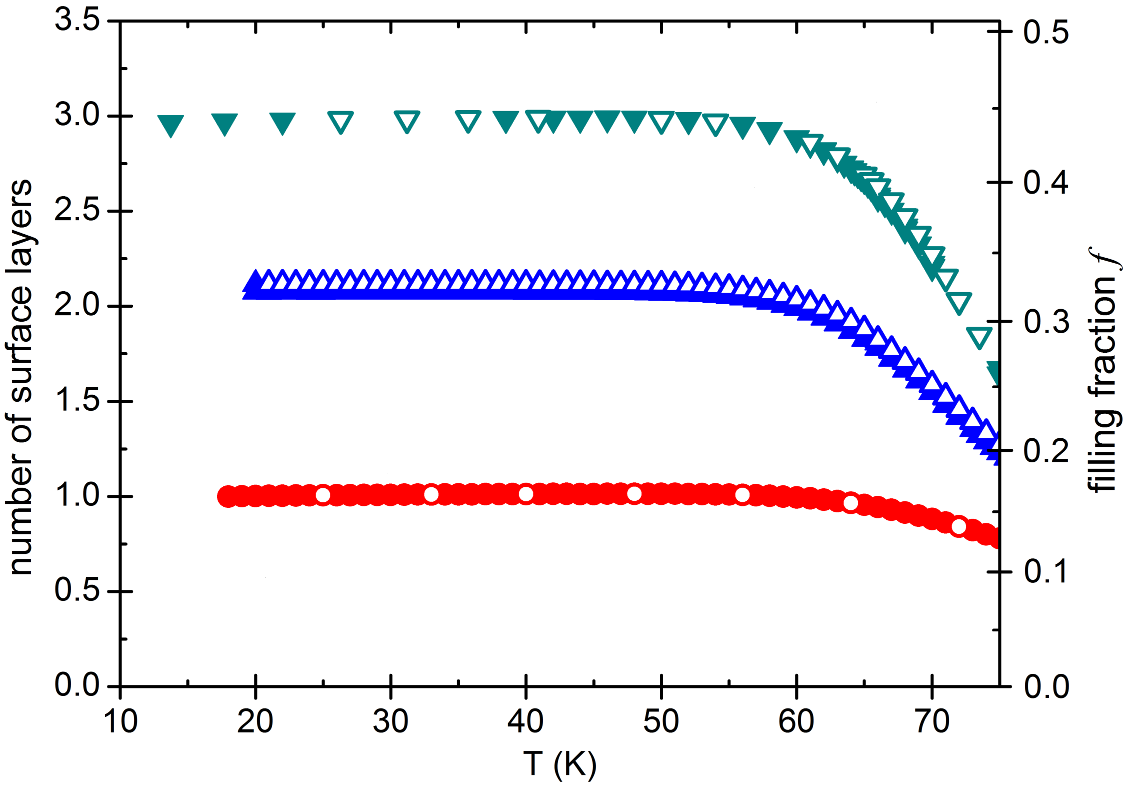

Figure 3.1 – *Number of adsorbed layers, z, during cooling (solid symbols) and heating (open symbols). The number was calculated from the measured filling fraction f using equation 2.1. Argon gas in the dead volume of the sample cell successively condensates into the sample when the temperature is lowered and thus increases the filling fraction. Due to the low vapour pressure of argon below 60 K the change in the number of layers is negligible in that temperature range. Figure from [2] (Copyright © 2011 by the American Physical Society).*

shear modulus at low temperatures.

At first the results for fillings corresponding to one or two adsorbed layers will be discussed. There is no hysteresis between cooling and heating and no abrupt freezing transition upon cooling (i.e., the layers seem to undergo a continuous stiffening). But the picture described in section 2.1 – a lowering of temperature yields to a continuous decrease in the number of liquid-like layers – is no longer physically sound when all in all only one or two adsorbed layers are present. But there are two possible hypotheses. One might assume that the adsorbate makes some kind of glass transition, where the shear modulus of the surface layers increases continuously with decreasing temperature. The other possibility is a continuous freezing and melting of the adsorbate, i.e., depending on the local interaction the adsorbed film consists of liquid-like and of crystalline parts: the lower the temperature, the higher the fraction of frozen argon. The effective medium analysis can give more clues, since it allows to perform a quantitative test of the second hypothesis by calculating the fraction of frozen argon. Equation 2.7 (in section 2.2.2) is valid, presupposing that there are only adsorbed layers that do not change the microstructure of the nanoporous system.

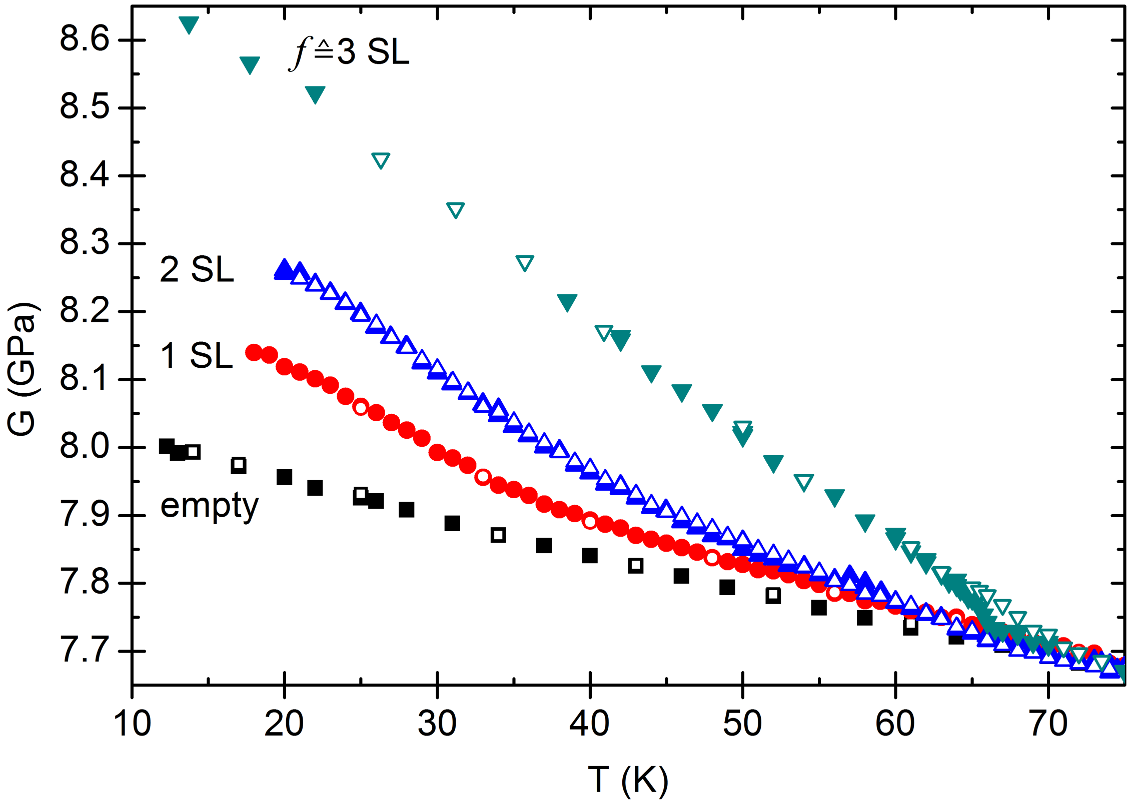

FIGURE 3.2 – *Effective shear modulus of the porous sample for different fillings as a function of the temperature during cooling (solid symbols) and heating (open symbols). The modulus increases continuously for both one and two adsorbed layers and shows no hysteresis between cooling and heating. For a filling that corresponds to three adsorbed layers the effective shear modulus increases sharply upon cooling between* 66 *and* 65 *K and there is a hysteresis between freezing and melting (see also figure 3.4). Figure from [2] (Copyright © 2011 by the American Physical Society).*

From the sorption isotherms it is already know that for the shear modulus of frozen adsorbed argon layers $G_{Ar,SL} \approx G_{Ar,bulk}$ holds (see section 2.2.2; figure 2.8). Therefore, at low temperatures the literature values for crystalline bulk argon from reference [130][1] can be used. For the determination of the fraction of frozen adsorbate $x = \tilde{f}/f$, equation 2.7 is solved for the amount of frozen argon, $\tilde{f}$. With this relation and the values for the measured shear modulus, the fraction x of frozen argon is calculated as a function of temperature (see figure 3.3).

First the observed behaviour of x indicates that the percentage of frozen argon is almost the same for one and for two adsorbed layers and that there is no thermal hysteresis between melting and freezing. Upon cooling down to 20 K almost all argon freezes continuously ($x \to 1$). Thus the above picture – the assumption that there is only liquid and frozen bulk-like argon, the percentage of which increases with decreasing temperature – is

---

[1] They measured the transversal ultrasonic velocity in crystalline bulk argon at various temperatures between 3 K and 77 K and determined the shear modulus (C_{44}). From a polynomial fit of those values the shear modulus $G_{Ar,bulk} \approx G_{Ar,SL}$ was calculated.

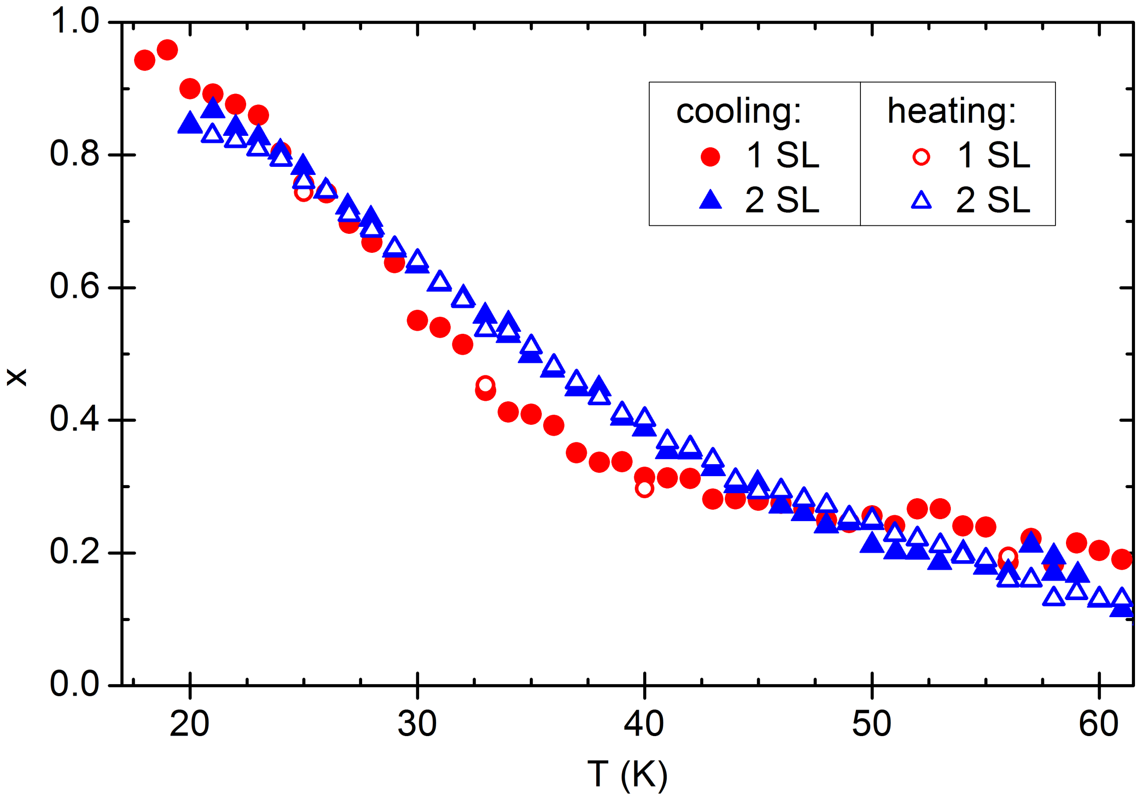

Figure 3.3 – *Fraction of frozen adsorbed argon,* $x = \tilde{f}/f$*, as a function of the temperature for both one adsorbed layer (circles) and two adsorbed layers (triangles) during cooling (solid symbols) and heating (open symbols). The values are calculated with equation 2.7 using the experimental data of the temperature cycles. By lowering the temperature successively to about* 20 *K almost all argon freezes continuously and there is no hysteresis between freezing and melting. Figure from [2] (Copyright © 2011 by the American Physical Society).*

consistent. If one assumed instead of that a homogeneous layer undergoing a glass transition [i.e., a constant $\tilde{f} = f$ in equation 2.7 and a change of the layers' shear modulus], the modulus would increase from $G_{Ar,SL} \approx 0$ at high temperatures to $G_{Ar,SL} \approx G_{Ar,bulk}$ at 20 K. That means that by coincidence at the lowest temperature the adsorbed argon would have the properties of crystalline argon. For this reason this scenario is less plausible. The results of the effective medium analysis clearly favour the first picture, i.e., a continuous freezing and melting of the first two surface layers (see figure 3.3).

Interfacial premelting that reflects in a gradual phase transition has also been observed in other systems: for mesoporous and macroporous samples containing octamethylcylotetrasiloxane, an only weakly polar molecule with a close to spherical shape [37], but also for polar molecules such as water in controlled pore glass [35, 80] or in siliceous MCM-41 with a pore radius of 1.2 nm [30]. In addition, computer simulations point to a continuous phase transition of water in a nanopore slit [42] and in carbon nanotubes [135].

3.2 Delayering of the third layer

The temperature cycle with a quantity of argon that corresponds to up to three layers features a peculiar behaviour (see figures 3.2 and 3.4). Between 66 K and 65 K the measured effective shear modulus increases markedly on cooling. In that temperature range the filling fraction increases only slightly: The average number of adsorbed layers is equivalent to 2.58 at 66 K and to 2.66 at 65 K (see figure 3.4(b)). This small change can neither explain the steep increase of the effective shear modulus between 66 K and 65 K nor the observed hysteresis between cooling and heating. If the same effective medium analysis as before were used – assuming bulk-like adsorbed layers and calculating the fraction of frozen adsorbate, $x = \tilde{f}/f$, via equation 2.7 – this quantity would show a step at 66 K and then an almost linear increase up to a value of 127% at the lowest temperature. This contradiction shows that the specific assumptions of equation 2.7 are not correct for this measurement. In order to maintain $x \leq 1$ the artificial assumption of $G_{Ar,SL} > G_{Ar,bulk}$ would be necessary, which contradicts the previous results of the isothermal measurements (see figure 2.8) as well as the observations for the first two surface layers (see section 3.1) [and for completely filled pores (see chapter 4)]. In addition, the abrupt freezing step at 66 K would have to be explained. Therefore, it appears much more consistent to abandon the basic assumption of equation 2.7, i.e., that of a constant microstructure consisting solely of adsorbed layers: A spatial rearrangement of the adsorbate at the steep increase of G around 66 K (e.g., as sketched in figure 3.4) would lead to a sudden change of the effective shear modulus, even when the intrinsic shear modulus of the adsorbate remains unchanged. This also explains the observed hysteresis, the formed solid capillary condensate melts only at a higher temperature (completely filled nanopores as well as partial fillings in the regime of capillary bridges usually show a freezing and melting hysteresis; see e.g. references [28–30, 33, 38, 39, 64, 72, 74, 76, 85, 136–139]. In addition, a spatial rearrangement of a partial pore filling during cooling can be expected from the isothermal measurements. At 74 K all fillings $f \leq 0.66$ form liquid surface layers (see region I in figure 2.4). But the maximum number of liquid-like layers decreases with temperature and at 66 K the fractional filling of $f \approx 0.4$ [see figure 3.4(b)] already lies in region II [$f > f_1(66\ K) \approx 0.33$, cp. figure 2.5], so that frozen layers exist on top of liquid-like layers [see figure 2.9(II)]. But also the characteristic filling fraction f_2 at which a transition from region II to III occurs depends on the temperature (cp. figure 2.3). Thus a further cooling can finally yield to $f > f_2$, so that the geometrical configuration becomes that of region III and capillary sublimate forms. Of course, the comparison of isothermal measurements and of temperature cycles is only correct assuming equilibrium states, which are entirely characterized by filling fraction and temperature (metastable states would depend, e.g., on thermal history). But it is obvious that a constant filling fraction does not necessarily imply a constant microstructure during cooling. Such a change of the pore condensates' geometrical arrangement has been previously assumed for argon in Vycor® [29, 64] and for water in parallel arranged pores [76]. The calorimetric measurements in reference [29] showed a freezing anomaly around 66 K that the authors interpreted as a delayering transition: The third liquid argon layer becomes unstable during cooling and converts into solid capillary condensate. The above analysis of the ultrasonic data supports this

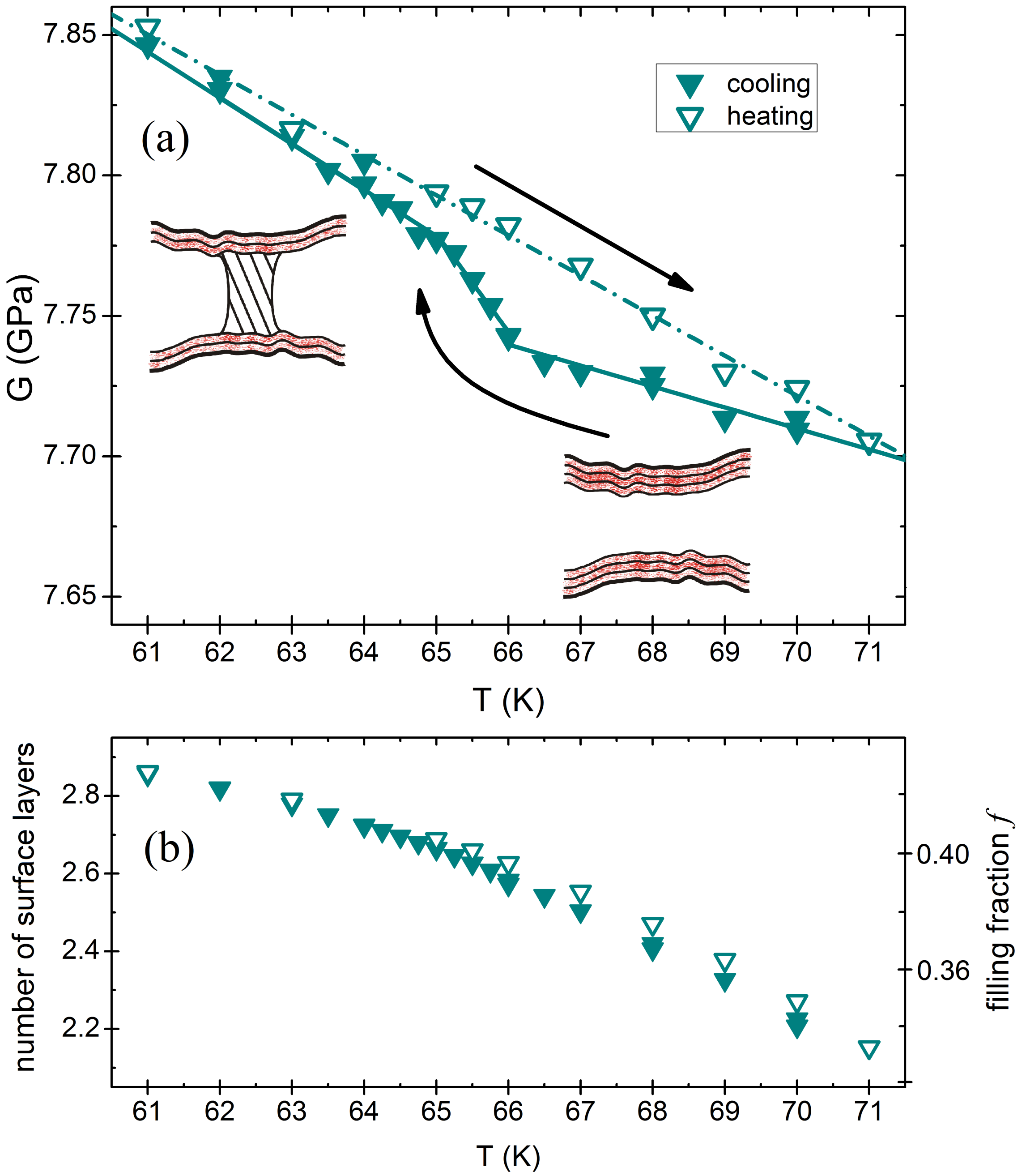

Figure 3.4 – *(a) During the cooling (solid symbols) with a filling that corresponds to up to three adsorbed layers the effective shear modulus increases sharply between* 66 *K and* 65 *K due to a change of the adsorbates' microstructure (surface layers → frozen capillary condensate). On heating (open symbols) the formed solid capillary condensate melts only at a higher temperature and a hysteresis is observed. (b) During cooling the number of pores or, respectively, of pore sections with a filling that is equivalent to three adsorbed layers increases. The increase in the average number of adsorbed layers on cooling (solid symbols) due to the vapour in the sample cell is, however, continuous and gets smaller the lower the temperature. Open symbols are for heating. Figure from [2] (Copyright © 2011 by the American Physical Society).*

picture, giving a strong direct indication for such a geometric change.

Conclusion

The measurements of temperature cycles with (almost) constant fillings of the pores of porous Vycor® glass reveal a pronounced confinement effect. The first two adsorbed surface layers of argon freeze and melt continuously over a very broad temperature range of about 40 K. But the elastic properties of bulk argon are preserved for solid parts of the adsorbed argon. For a filling corresponding to three adsorbed layers, the analysis clearly indicates during cooling a delayering process at a temperature of $65 - 66$ K, i.e. the formation of solid capillary bridges.

Chapter 4

Continuous freezing of argon in completely filled nanopores

The analysis of the ultrasonic measurements presented in section 3.1 revealed that both one and two adsorbed surface layers of argon freeze and melt continuously over a broad temperature range. For completely filled pores, on the other hand, the known Gibbs-Thomson equation (see section 1.3) hypothesizes a reduction of the melting (and freezing) temperature but no continuous phase transition. From previous ultrasonic measurements, Molz et al. [85] concluded that argon in nanopores freezes within a narrow temperature range of a few Kelvin. They also interpreted their results as originating from differences between the shear modulus of confined solid argon and bulk argon that are especially strong at temperatures near $T_{fr,Ar,pore}$ *because of a thermally activated diffusion of vacancies [85]. The results of section 2.2.2 disproved the latter assumption as the solid surface layers exhibit a shear modulus about equal to the shear modulus of bulk argon (even just below the freezing temperature). In this chapter it is furthermore shown that argon undergoes a continuous liquid-solid phase transion over about* $45\ K$ *also for completely filled pores. The fraction of solid argon increases with decreasing temperature. The presence of solid argon in the pore centre results in an increase of the freezing temperature of the first two surface layer by about* $10\ K$.

As a consequence of a decrease of the temperature, a continuous increase of the effective shear modulus in comparison to the empty sample was observed for the first and the second surface layer (see figure 4.1, for more details see section 3.1). This is a clear evidence that these layers freeze. When the pores are completely filled the effective shear modulus also exhibits an increase that is related to the process of freezing of the pore condensate (see figure 4.1). Due to the greater amount of adsorbate the increase is of course more pronounced than in the case of single surface layers.

From the increase of the effective shear modulus during temperature cycles with one or two adsorbed surface layers (shown in figure 4.1) the fraction $x = \tilde{f}/f$ of frozen argon was calculated using equation 2.7 of the effective medium analysis discussed in section 2.2.2.[1] As noted in section 2.2.2, this equation is only valid if the microstructure

---

[1] For the shear modulus of crystalline bulk argon ($G_{Ar,SL}$) the literature values from reference [130] are used (cp. chapter 3).

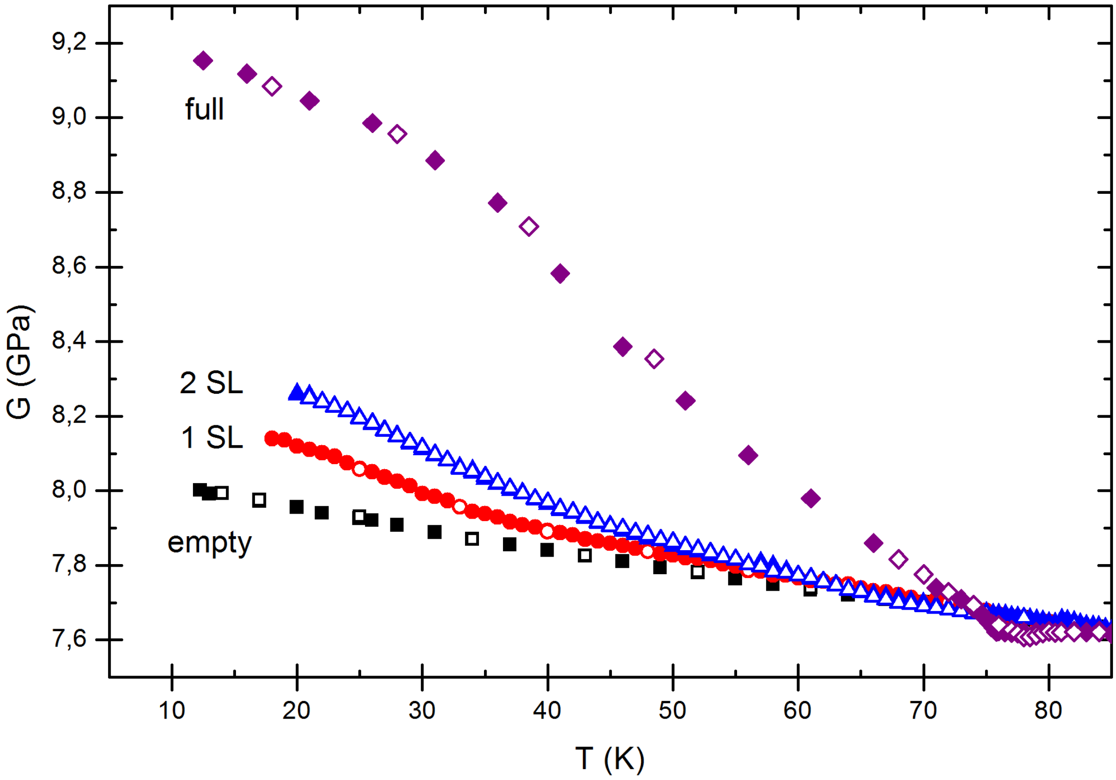

FIGURE 4.1 – *Effective shear modulus during temperature cycles for different fillings of the porous sample. During cooling (closed symbols) the first two surface layers (1 SL or 2 SL) are stiffened and the effective shear modulus is higher than for the empty sample. This indicates that the argon layers solidify. Also the effective shear modulus of the completely filled sample (i.e. for $f = 1$) increases markedly on cooling. In this case the value of the slope of the increase, however, is considerably smaller for temperatures below about 30 K. Between cooling (closed symbols) and heating (open symbols) only with complete filling a small hysteresis is observed (between ca. 76-80 K). Figure from [3] (Copyright © 2013 by the American Physical Society).*

of the existing porous network is maintained. When the microstructure of the porous network [see figure 4.2(a)] is altered by capillary bridges [see figure 4.2(c)] this equation no longer holds (cp. sections 2.2.2 and 3.2).

For completely filled pores the microstructure of the adsorbate is essentially the same as for surface layers [see figures 4.2(b) and (d)]. In this case the microstructure is not a composition of layers and capillary bridges [see Fig. 4.2(c)], but the adsorbate can be regarded as being composed of single layers. So, the factor a in the effective medium equation should be equal to the factor used for surface layers. Consequently, equation 2.7 can also be used to calculate the fraction of frozen argon during cooling and heating for the case of complete filling.

This fraction of frozen argon is shown in figure 4.3. Below 75.8 K the process of freezing starts and the fraction of frozen argon increases continuously over a rather broad tem-

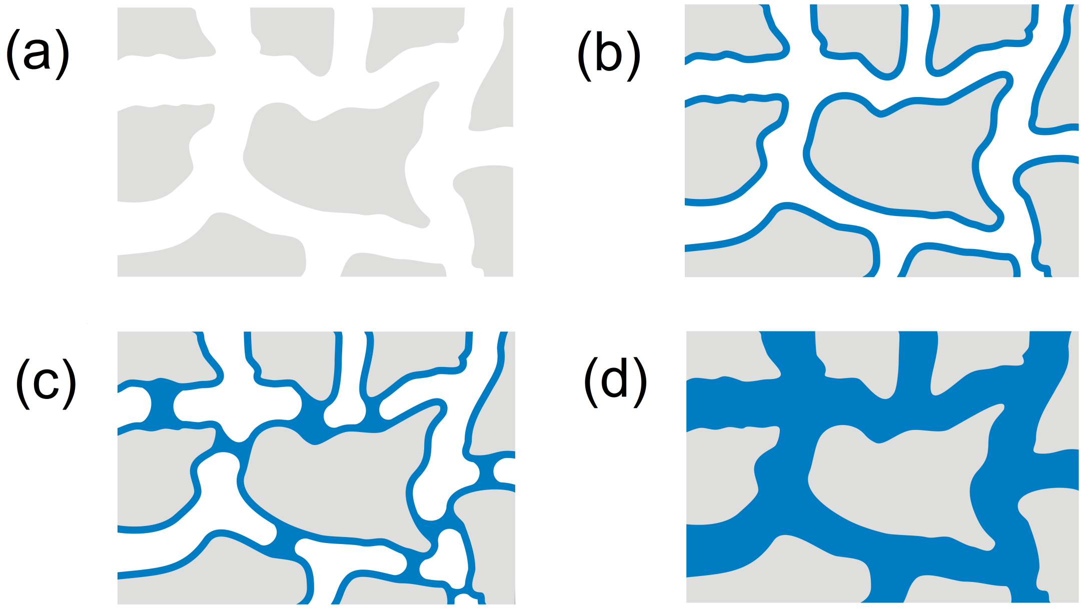

Figure 4.2 – *(a) Schematic sketch of the spongy structure of the empty porous Vycor® glass. (b) At low filling the pore walls are only covered with surface layers of argon. This structure maintains the microstructure of the porous network. (c) At higher fillings capillary bridges are formed and lead therewith to a change of microstructure. (d) In the case of complete filling the initial microstructure of the network is restored. Figure from [3] (Copyright © 2013 by the American Physical Society).*

perature range (about 45 K).[2] At a temperature of about 30 K all argon is frozen. The effective medium analysis yields at temperatures below 30 K a fraction of about 1. This means that below this temperature no non-freezing surface layer of argon remains; then the influence of the surface of the pore walls can no longer prevent a crystallization of the complete adsorbate. The result also further confirms the correctness of the effective medium analysis that was derived in section 2.2.2.

With the analysis only the fraction of frozen argon can be determined without resolving the spatial distribution of solid and liquid parts. The first and second surface layers freeze completely only at very low temperatures ($T \leq 20\ K$, see temperature cycles discussed in section 3.1). So it seems reasonable to assume that the freezing starts in the centre of the pores and with decreasing temperature the thickness of the liquid layer between the solid core in the centre of the pores and the pore walls decreases. This picture

---

[2] The origin of the slight decrease of G and x during cooling for 76 K $\lesssim f \lesssim$ 85 K (see figures 4.1 and 4.3) can be found in a slight error in the determined effective density of the sample. The density is necessary to calculate the effective shear modulus G from the measured ultrasonic transit time Δt, respective ultrasonic velocity c ($G = c^2 \cdot \rho$), and thereby also to calculate the fraction of frozen argon x. In the liquid regime, a rearrangement of adsorbate is still well possible, and during cooling additional argon can condense into the pores. In the solid regime, the time necessary for the system to reach equilibrium increases considerably, and consequently, the density can increase only very little. The effect of a minor change in the effective density was already noticed in reference [85] for the same system.

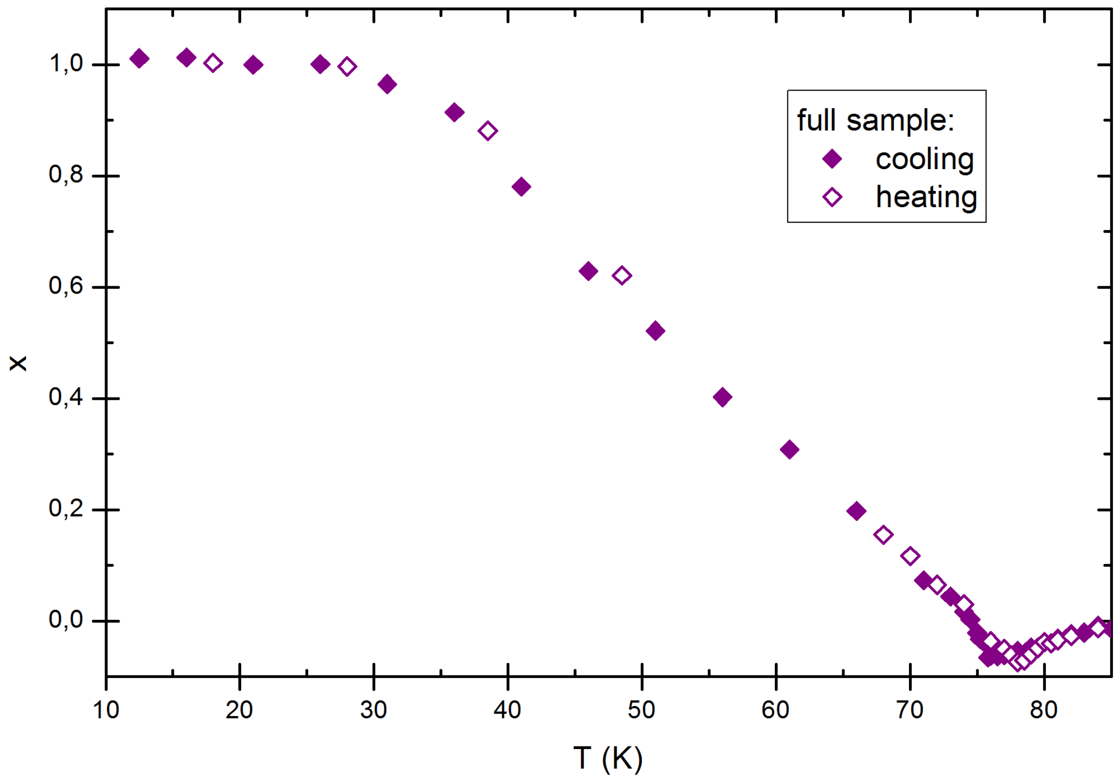

FIGURE 4.3 – *The fraction of frozen argon during cooling (solid symbols) and heating (open symbols) for completely filled pores. At temperatures below about 30 K the adsorbed argon is completely frozen and no non-freezing layer remains at these temperatures. The values calculated with equation 2.7 using the ultrasonic data result at low temperatures almost exactly in a fraction of 1. [The slight observed decrease during cooling in the liquid regime (between 85 K and 75.8 K) can be attributed to small density changes (see footnote 2).] Figure from [3] (Copyright © 2013 by the American Physical Society).*

essentially corresponds to the thermodynamic model used by Wallacher and Knorr in reference [29]. The model mentioned in the previous sections is related to the well-known effect of surface and interfacial melting [34, 35, 37, 43, 80, 81, 91, 93, 94, 96]. In interfacial melting experiments with flat substrates the thickness t of the liquid layer usually follows a power law ($t \propto (\Delta T)^{-1/3}$ with $\Delta T = T_{triple} - T$, [94]) or a logarithmic dependence ($t \propto |\ln(\Delta T)|$, [94, 96]) corresponding to van der Waals forces, respectively, short-range interactions. The peculiar, almost linear, increase of the volume fraction of solid argon over the very broad temperature range (see figure 4.3) does not follow these relations; a reason for this might be nanoconfinement and the related curvature of the substrate (pore surface).[3]

Molz et al. [85] interpret the measured increase of the ultrasonic velocity c with decreasing temperature as caused by “the diffusion of thermally activated vacancies” that result in

---

[3] On curved substrates for water and octamethylcyclotetrasiloxane, different deviations from these relations were observed [34, 35, 37, 81].

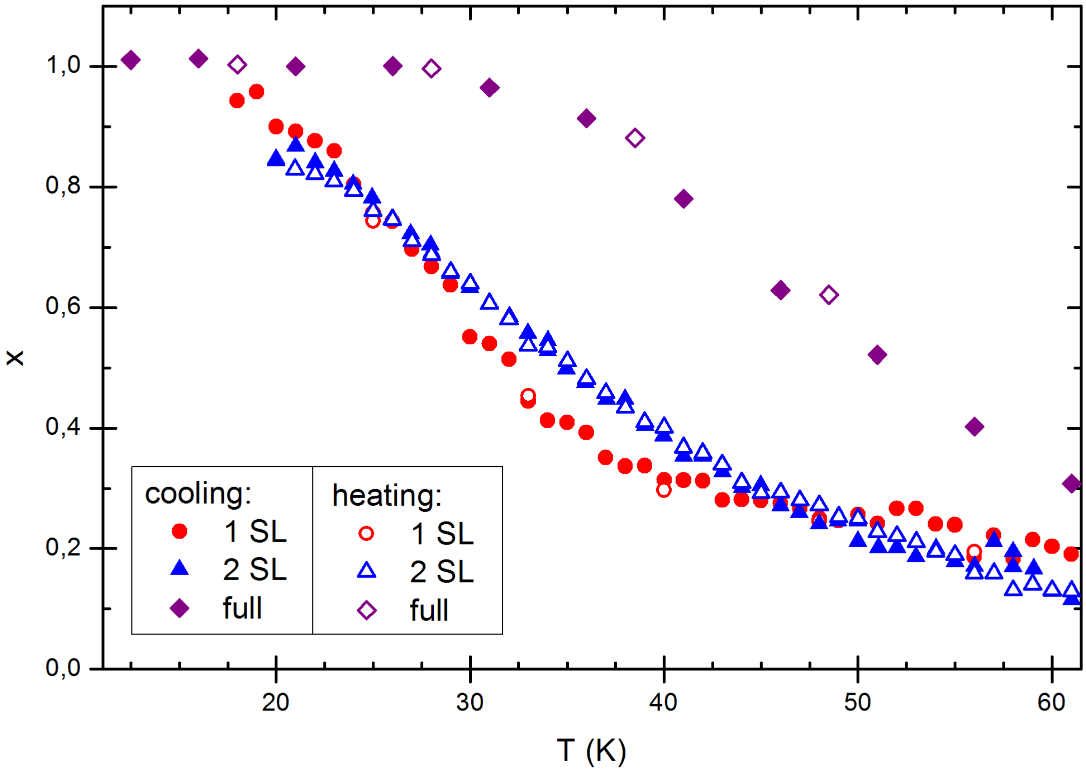

FIGURE 4.4 – *A comparison between the temperature-dependent fraction of frozen argon for one or two ardsorbed surface layers and completely filled pores. When the pores are completely filled the first few layers freeze already at a higher temperature. The solid argon in the centre of the pores obviously impresses its structure to the argon in the surface layers. Figure from [3] (Copyright © 2013 by the American Physical Society).*

a stress relaxation. But in the isothermal sorption measurements ($T = const.$, increase of the pore filling f) for all temperatures [$T = 74\ K - 50\ K$, cp. section 2.2.2] the shear modulus of solid adsorbed argon layers corresponds to the values for bulk argon. This clearly contradicts the argument forwarded in reference [85] that due to a stress relaxation the full modulus contribution can be observed only at very low temperatures. The isothermal sorption measurements showed also that the amount of solid argon increases with decreasing temperature (at least down to 50 K, see figure 2.5 in section 2.1). These observations are very convincing evidence for a continuous phase transition of argon in completely filled nanopores (cp. figure 4.3)

A comparison of the temperature dependence of the calculated fraction of frozen argon for complete filling and for the first two surface layers further enligthens the complex freezing behaviour in nanopores (see figure 4.4). The first and the second surface layers of argon are completely frozen around a temperature of 20 K. In the case of completely filled pores, however, already at a temperature of 30 K all argon is frozen. Thus, the crystalline structure of solid argon in the pore centre influences the surface layers near the wall, and this interaction of the argon atoms is stronger than the interaction of the argon atoms in the first layers with the amorphous pore walls.

Conclusion

The effective medium analysis of a temperature cycle with a completely filled sample shows that the confined argon undergoes a continuous liquid-solid phase transition over a broad range of 45 K. Below about 30 K all argon is frozen with a shear modulus that corresponds to the bulk shear modulus of argon, i.e., below that temperature the adsorbed argon does not perceive the confinement. The calculated continuous increase of the fraction of solid adsorbate during cooling corresponds to a continuous liquid-solid phase transition of the adsorbed argon.

Chapter 5

Generalization of the effective medium analysis

Non-local measurements on heterogeneous systems do not yield directly the intrinsic properties of a component, i.e. in this study those of the adsorbate (here mostly argon) in a nanoporous matrix (cp. section 2.2.2). An additional effort is required to obtain this information. For the determination of the intrinsic shear modulus of the adsorbate during sorption measurements in the solid regime an effective medium analysis was developed in section 2.2.2. With this analysis also the fraction of liquid or solid adsorbate during temperature cycles can be determined (when the pores are completely filled or only covered with surface layers; cp. section 3.1 and chapter 4). A more general derivation shows amongst others that also the intrinsic longitudinal modulus of adsorbate can be determined from ultrasonic measurements of the effective longitudinal modulus.

As long as the wavelength of an excitation A is large compared to the length scale of the structural inhomogeneities, a material is characterized by so-called effective quantities M, relating volume averaged excitation and response, $\langle B\rangle = M \cdot \langle A\rangle$ (here $\langle ...\rangle = 1/V \cdot \int ...dV$ denotes the volume average). Examples for effective elastic properties are the shear modulus G relating shear stress and strain, or the bulk modulus K relating changes of volume and pressure, $\langle -\Delta p\rangle = K \cdot \langle \Delta V/V\rangle$. In a porous system consisting of a quartz matrix (index Q) and pores (index pore) the volume average is simply given by the volume averages in the two components. Thus,

$$\langle A\rangle = \phi\langle A\rangle_{pore} + (1-\phi)\langle A\rangle_Q \tag{5.1}$$

holds (with a porosity $\phi = V_{pore}/V_{sample}$) as well as

$$\langle B\rangle = \phi M_{pore}\langle A\rangle_{pore} + (1-\phi)M_Q\langle A\rangle_Q, \tag{5.2}$$

with the modulus of the pores, M_{pore}, and the modulus of the material of the matrix, M_Q. By a combination of these two equations, the definition $\langle B\rangle = M \cdot \langle A\rangle$ can be rewritten as

$$M = (1 - a_M \cdot \phi) \cdot M_Q + a_M \cdot \phi \cdot M_{pore}, \tag{5.3}$$

with $a_M = \langle A\rangle_{pore}/\langle A\rangle$. The effective elastic properties are determined not only by the moduli of matrix material and pores, but also by its respective volume fractions, as well as by a factor $a_M = \langle A\rangle_{pore}/\langle A\rangle$. In general, the latter depends on ϕ, M_Q, M_{pore} as well as on the microstructure. For this reason a multitude of so-called mixing rules describing different microstructures may exist. However, for many porous materials the elastic moduli (inter alia G and K) show a linear dependence on ϕ for $\phi \lesssim 0.25 - 0.30$ [133, 134], i. e. the factor a_M is independent of ϕ (and as a consequence independent of the material properties). Hence the constant factor a_M can be determined from the measurement of the modulus of the empty sample, M_0, and the known modulus of quartz glass, M_Q: for $M_{pore} = 0$ equation 5.3 reads $M_0 = (1 - a_M \cdot \phi) \cdot M_Q$ (with $M = K$ or G). The term $a_M\phi = 1 - M_0/M_Q$ can thus be replaced in equation 5.3 and it can be rewritten as

$$M = M_0 + \left(1 - \frac{M_0}{M_Q}\right) \cdot M_{pore}. \tag{5.4}$$

If the pores are filled with capillary bridges the microstructure and the factor a_M is changed. Therefore, equation 5.4 can be used at partial fillings without capillary bridges (adsorbed surface layers) and for complete fillings: In section 2.2.2 the validity for the shear modulus ($M = G$) was shown setting $G_{pore} = \tilde{f} G_{Ar,bulk}$, where $\tilde{f}$ is the volume filling fraction of frozen argon.

The longitudinal modulus that can be determined from ultrasonic measurements is also an effective quantity (relating longitudinal strain and stress). Combining equation 5.4 for the shear modulus $M = G$ and the bulk modulus $M = K = \beta - 4/3 \cdot G$ (valid for isotropic materials, i.e. here for the properties of the heterogeneous sample as well as for its components) and solving for the effective longitudinal modulus β yields

$$\beta = \beta_0 + \left(1 - \frac{K_0}{K_Q}\right) \cdot \beta_{pore} + \frac{4}{3} G_{pore} \cdot \left(\frac{K_0}{K_Q} - \frac{G_0}{G_Q}\right). \tag{5.5}$$

In general, both bulk modulus and shear modulus are required to determine the intrinsic longitudinal modulus β_{pore}. Equation 5.5 is simplified for liquid adsorbate ($G_{pore} \approx 0$). But the properties of nanoporous Vycor® glass facilitate the analysis also for the case of liquid and solid adsorbate. For quartz glass $\beta_Q = 72.85$ GPa, $G_Q = 27.95$ GPa and thus $K_Q = 35.58$ GPa holds [129], while the measurements of the unfilled Vycor® sample at 80 K yield $\beta_0 = 16.88$ GPa, $G_0 = 6.75$ GPa and thus $K_0 = 7.88$ GPa (values for the sample used in chapter 6). Thus, $\beta_0/\beta_Q \approx G_0/G_Q \approx K_0/K_Q \approx 0.22 - 0.24$ and equation 5.5 reduces to

$$\beta = \beta_0 + \left(1 - \frac{\beta_0}{\beta_Q}\right) \cdot \beta_{pore}. \tag{5.6}$$

Conclusions

All three effective moduli G, K, and β are linear functions of the elastic modulus of the pore filling with identical microstructure factor a_M, as long as the microstructure is preserved (surface layers or complete pore filling). Consequently, equation 5.4 is valid for $M = K$, G, and β. For completely filled pores the above effective medium analysis gives a direct access to the intrinisic properties (M_{pore}). The remaining problem is to relate M_{pore} to the properties of the adsorbate in the case of a partial filling. In the discussion of the experimental data (see chapter 6) this will be done for the longitudinal modulus.

Chapter 6

Longitudinal elastic modulus of liquid and solid argon in nanopores

---

The analysis in chapter 5 revealed amongst others that it is possible to determine the intrinsic longitudinal moduli of the filling (β_{pore}) in nanporous glass. Ultrasonic measurements during isothermal sorption of argon show that in the liquid regime the adsorbate only contributes to the measured effective longitudinal modulus when the pores are completely filled and that it is bulk-like. At partial fillings its contribution is cancelled out by the high compressibility of the vapour phase. In contrast, at lower temperatures frozen argon as well as underlying liquid surface layers cause a linear increase of the effective longitudinal modulus upon filling. During sorption the contribution of the liquid surface layers near the pore wall $\beta_{Ar,SL}$ increases with the thickness of the solid layers reaching the bulk value $\beta_{Ar,liquid}$ only in the limit of complete pore filling. This effect is due to the gradual stiffening of the solid argon membrane.

In the liquid regime of the adsorbate the effective longitudinal modulus β remains unchanged during isothermal adsorption until the pores are almost completely filled (see figure 6.1). Only near this point the longitudinal modulus increases markedly and it remains approximately constant. At a temperature of 74 K, i.e. below the onset of freezing near 75.8 K[1] (see figure 6.2), the behaviour of the effective longitudinal modulus differs on first sight not significantly from the liquid regime [cp. figure 6.1(b)]. Due to the existence of solid adsorbate the increase at high reduced pressure is considerably higher than in the liquid regime.

The following discussion will show, however, that the liquid and solid regimes differ significantly and how much information both about the intrinsic elastic properties of the adsorbate and the physical processes happening during adsorption can be derived. First, the simple case where only liquid adsorbate exists is studied. In a second step the treatment of the more complicated situation at lower temperature, where solid and liquid argon coexist, shows how the intrinsic longitudinal moduli of both phases of the adsorbate can be determined.

---

[1] see section 4 and figure 4.1

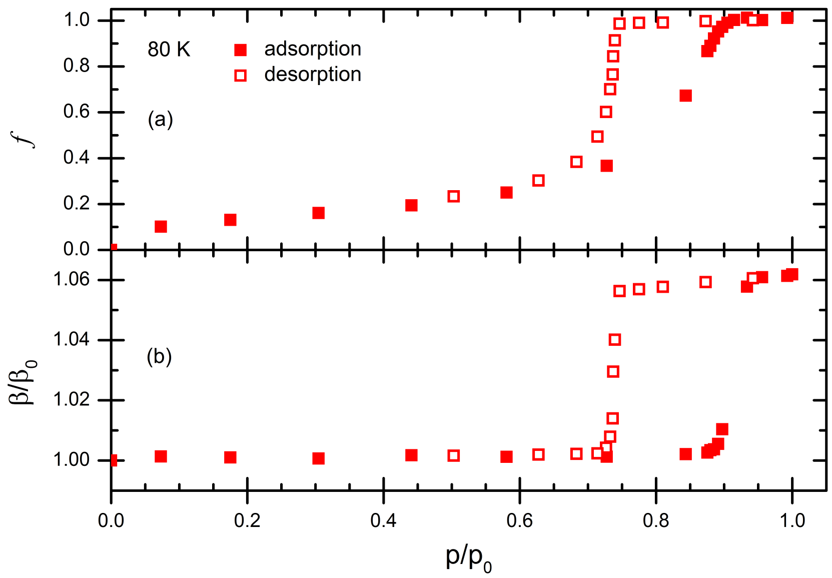

FIGURE 6.1 – *(a) Filling of the nanoporous Vycor® glass sample during adsorption (closed squares) and desorption (open squares) of argon in the liquid regime (at* $T = 80$ *K) as a function of the reduced pressure. (b) The effective longitudinal modulus* β *(scaled to the modulus of the empty sample,* $\beta_0 = 16.88$ *GPa) measured during the filling and emptying of the pores. Only when the pores are almost completely filled (*$f \to 1$ *at* $p/p_0 \approx 0.9$*) the adsorbate leads to an increase of the modulus. During desorption the modulus is again reduced to the initial value when the pores start to empty. Figure from [4] (Copyright © 2013 IOP Publishing Ltd).*

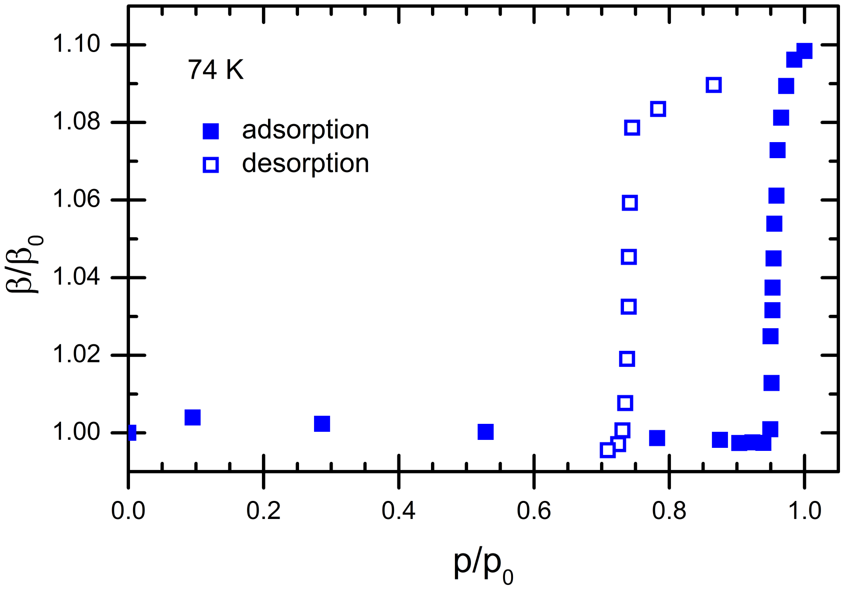

FIGURE 6.2 – *Effective longitudinal modulus during adsorption and desorption at 74 K, i.e. in the solid regime, as a function of the reduced vapour pressure (scaled to* $\beta_0 = 16.96$ *GPa at* $p/p_0 = 0$*). The general form seems to be comparable to the measurements with liquid adsorbate [cp. figure 6.1(b)]. The maximum increase of the modulus is considerably higher (due to the existence of solid argon). Figure from [4] (Copyright © 2013 IOP Publishing Ltd).*

6.1 Liquid regime

In the case of complete filling the longitudinal modulus of the pore filling is equal to the modulus of the adsorbed argon: $\beta_{pore} = \beta_{Ar,ads}$, i.e. the intrinsic longitudinal modulus of the adsorbed argon can be estimated from the ultrasonic measurements [see figure 6.1 at $p/p_0 = 1$ or figure 6.3(a) at $f = 1$]. With the aid of equation 5.6 the moduli $\beta_{Ar,ads} = 1.36$ GPa at 80 K and $\beta_{Ar,ads} = 1.1$ GPa at 86 K are determined. A comparison with the literature values for bulk argon shows a deviation of only $\approx 10 - 20\%$, i. e. $\beta_{Ar,bulk} = 1.12$ GPa for 80 K and $\beta_{Ar,bulk} = 1.0$ GPa for 86 K; the first value is extrapolated [140,141]. This agreement is quite good and reveals that the whole adsorbate including the first surface layers contributes at complete filling approximately with the longitudinal modulus of bulk argon.[2]

At partial fillings in the solid regime the increase of the effective shear modulus G is proportional to the fraction of adsorbed solid argon $\tilde{f}$ and its intrinsic shear modulus $G_{Ar,ads}$ ($G_{pore} = \tilde{f} \cdot G_{Ar,ads}$; see section 2.2.2). A transfer to the longitudinal modulus in the liquid regime is obviously not possible [see figure 6.3(a)]; there is no such linear relation between β_{pore} and $\beta_{Ar,ads}$. At low fillings $\beta = \beta_0$ holds, i.e. the effective modulus simply equals that of the empty porous matrix. The fact that the adsorbate's longitudinal modulus contribution can only be observed when the sample is almost completely filled was also observed for liquid nitrogen and hexane in porous glass [62,63,142]. Page et al. [62,63] explained, that vapour voids which exist in the pores until the pores are filled prevent the increase of the effective longitudinal modulus due to their high compressibilities ($1/\beta_{vapour}$). Actually, the compressibility κ is defined as the reciprocal value of the bulk modulus K ($\kappa = 1/K = -1/V \cdot \partial V/\partial p$), but for liquids and gases $K = \beta - 4/3G \approx \beta$, because $G \approx 0$. For a two-component system it follows directly from the definition of K (with $p_{av} = \langle p \rangle$):

$$\begin{aligned} \frac{V_{total}}{K_{eff}} &= -\frac{\partial V_{total}}{\partial p_{av}} = -\frac{\partial (V_1 + V_2)}{\partial p_{av}} \\ &= \underbrace{-\frac{\partial V_1}{\partial p_1}}_{=V_1/K_1} \cdot \left(\frac{\partial p_1}{\partial p_{av}}\right) \underbrace{-\frac{\partial V_2}{\partial p_2}}_{=V_2/K_2} \cdot \left(\frac{\partial p_2}{\partial p_{av}}\right) \end{aligned} \tag{6.1}$$

Usually, the pressure in component i can differ from the average pressure p_{av}. For the pore filling of liquid (component 1) and vapour (component 2), however, any change of exerted pressure results in the same change for each constituent, i.e. $\partial p_i/\partial p_{av} = 1$ in equation 6.1. The fundamental requirement for that behaviour is the unrestricted mobility of the components (this does not hold, e.g. in heterogeneous solid systems where the

---

[2] Page et al. [63] used Biot's theory to get some information on the elastic properties of the adsorbate hexane when the pores are completely filled. The values for $\beta_{Ar,ads}$ determined using their equation differ considerably from both the moduli determined with the above analysis as well as from the values for bulk argon (though for hexane a very good agreement was observed in reference [63]).

pressure distribution can be inhomogeneous). Dividing by V_{total} and using the definition of the filling fraction, $f = V_{liquid}/V_{pore}$, the above equation results for the system of liquid and vapour in a relation in the form of Wood's equation [63, 143]:

$$\frac{1}{K_{pore}} = \frac{f}{K_{liquid}} + \frac{1-f}{K_{vapour}} \tag{6.2}$$

The effective compressibility of a system of liquid and vapour is simply given by the volume-weighted sum of the compressibilities of each component (see also [63, 143]). Thus the effective compressibility of the pore filling is dominated by the high compressibility of the vapour (for an ideal gas $1/K_{vapour} = 1/p$ holds). Only when the voids disappear, which happens when reaching $f = 1$ during adsorption, the effective modulus can increase.[3]

Thus vapour being the third phase in partially filled pores prevents in the liquid regime the use of a linear relation between β_{pore} and $\beta_{Ar,ads}$ for the description of the behaviour of the effective longitudinal modulus at $f < 1$. But equation 5.6 can easily be used to determine the elastic properties of the confined adsorbate for completely filled pores, i.e. for $f = 1$.

6.2 Solid regime

The analysis in chapters 3 and 4 showed that ultrasonic shear waves are well suited to study the liquid-solid phase transition of argon in nanopores. The shear modulus of adsorbed solid argon corresponds to its bulk shear modulus. Between ultrasonic shear waves and longitudinal waves there is, however, one significant difference: Inviscid fluids cannot sustain shear stress and therefore do not cause an increase of the effective shear modulus during adsorption (see section 2.1). But usually adsorbed liquids are expected to increase the effective longitudinal modulus, though empty pore regions can prevent an increase (see section 6.1 and figure 6.1). Thus in the case of coexisting solid and liquid in the pores the intrinsic longitudinal modulus of the adsorbate is more complicated to be determined. The dependence of the modulus on the filling of the sample shows significant differences between the two regimes (see figure 6.3). In the liquid regime the modulus remains unchanged until the pores are almost completely filled. At a temperature of 74 K, i.e. below the onset of freezing, the effective longitudinal modulus remains unchanged by adsorbed argon up to a filling fraction $f_1 \approx 0.66$. Above this filling faction the modulus starts to increase linearly with increasing filling. Above the filling $f_2 \approx 0.89$ there is also a linear increase, but with a higher slope. The three regions observed during filling are partly similar to what was observed for the effective shear modulus at the same temperature (see inset in figure 6.3 and section 2.1). Analogously to the measurements of the effective shear modulus, f_1 corresponds to the onset of freezing. The value of f_1

---

[3] Note that equation 6.2 can also be deduced directly from the definition of effective quantities (cp. equation 5.3), choosing $M = 1/K$, $A = \Delta p$ (so that $-\Delta V/V = M \cdot A$), and setting $a_M = \langle \Delta p \rangle_{pore} / \langle \Delta p \rangle = 1$ for the liquid/vapour system.

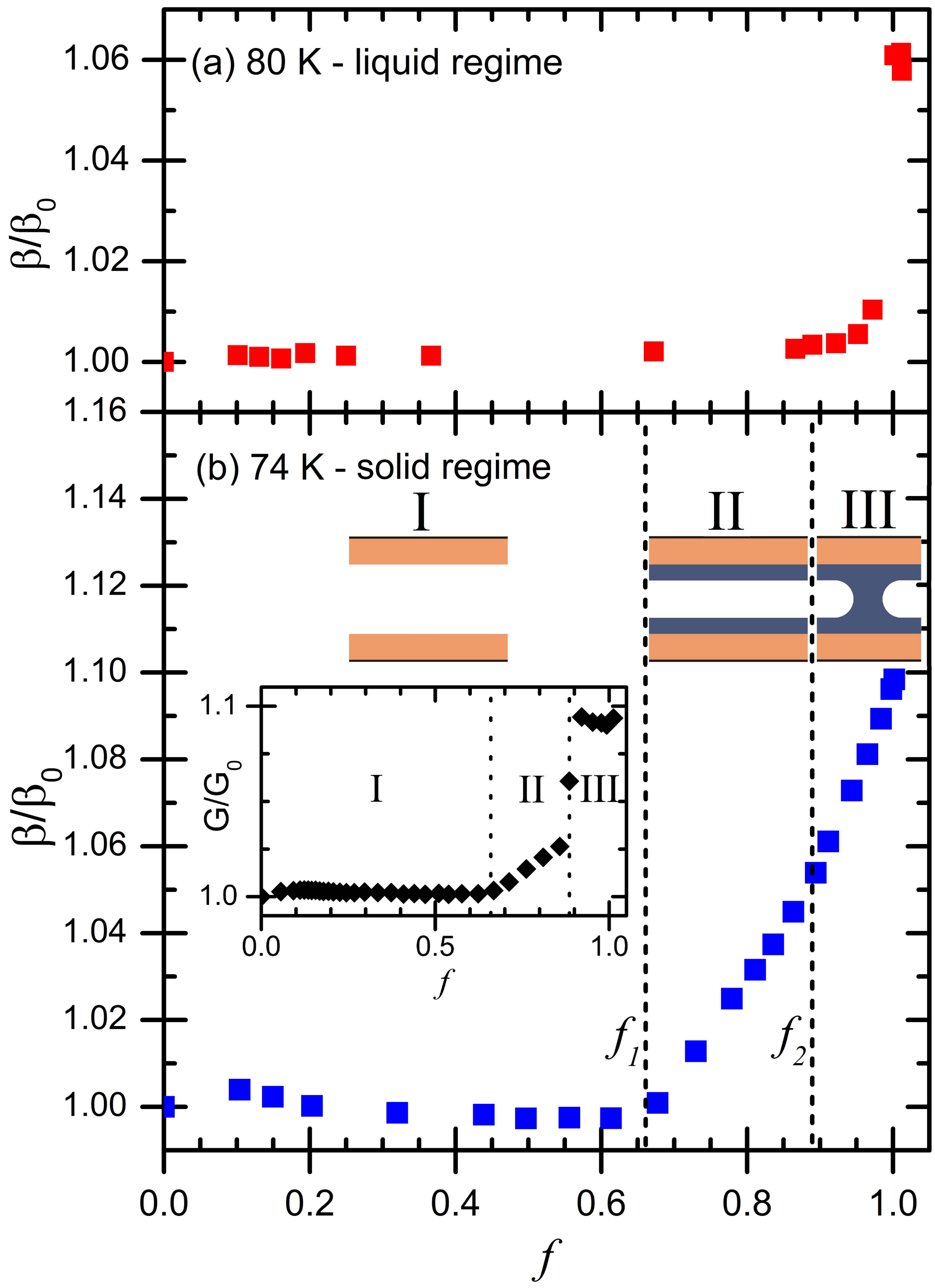

FIGURE 6.3 – *Effective longitudinal modulus during adsorption as a function of the filling of the pores in (a) the liquid regime (at* $80\ K$ *with* $\beta_0 = 16.88$ *GPa) and (b) the solid regime (at* $74\ K$ *with* $\beta_0 = 16.96$ *GPa). Here, a highly different behaviour is observed. In the solid regime there are three regions: Up to a filling* f_1 *the effective modulus remains unchanged by the adsorbate. At* f_1 *the process of freezing starts and results in a linear increase of the modulus. Above* f_2 *a different slope of the increase is observed. At and above* f_2 *solid capillary bridges are formed (see text). The inset shows the behaviour of the shear modulus* G *during filling for a similar sample. Figure from [4] (Copyright © 2013 IOP Publishing Ltd).*

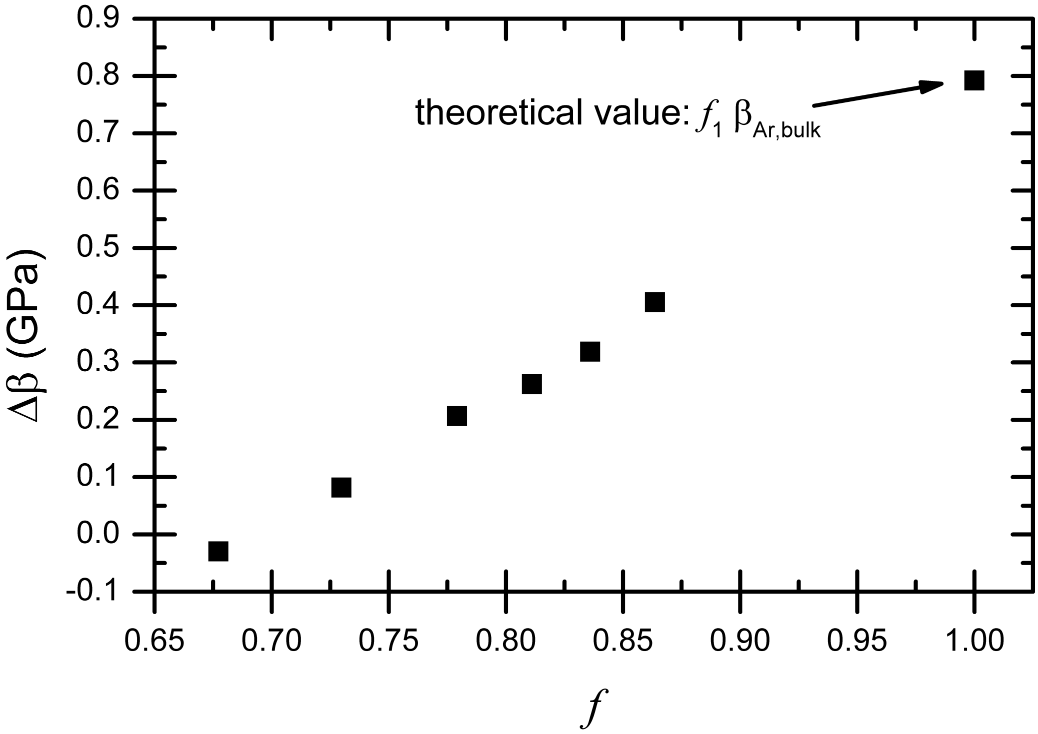

FIGURE 6.4 – *Contribution of the liquid adsorbate in region II of the sorption isotherm at 74 K as a function of the filling. As soon as solid adsorbate is formed on top of the liquid-like surface layers, these layers start to contribute to the effective longitudinal modulus. There is no abrupt increase in the contribution, but the contribution of the liquid below the solid layers increases continuously and linearly with the thickness of the solid layers. Only at complete filling ($f = 1$) all adsorbed liquid (f_1) contributes to the effective modulus with its intrinsic modulus $\beta_{Ar,bulk}$ (theoretical value shown for guidance). Figure from [4] (Copyright © 2013 IOP Publishing Ltd).*

is equal for both methods. Up to f_1 the adsorbate corresponds essentially to the liquid regime. In section 6.1 was already discussed why the effective longitudinal modulus does not increase below f_1. The behaviour of the shear modulus G in region II originates in the formation of frozen layers on top of liquid-like surface layers (see section 2.2.2). Therefore also here the adsorbate added in region II must correspond to solid surface layers. The effective shear modulus exhibits above f_2 a plateau value and no further increase in G, in contrast to the measurements of the effective longitudinal modulus.

As above f_1 a linear increase of the effective longitudinal modulus is observed, one might assume that equation 5.6 is valid in the solid regime with $\beta_{pore} = \tilde{f} \cdot \beta_{Ar,solid}$ (with $\tilde{f} = f - f_1$), just as for the shear modulus. But the longitudinal modulus of solid argon of 5.2 GPa calculated in that way from the slope of the increase above f_1 is considerably higher than the literature value for solid bulk argon ($\beta_{Ar,bulk} \approx 2.9$ GPa [130]). This would be very odd, also because the shear modulus of the adsorbed argon corresponds to the bulk values for argon (cp. section 2.2.2) and the longitudinal modulus of liquid argon is also about equal to the corresponding bulk values (see section 6.1). These observations are clear hints that the calculated modulus has a different origin than a confinement effect on the elastic moduli of argon. In the solid regime, β_{pore} in equation 5.6 has to be extended to account for the liquid adsorbate. Assuming that $\beta_{Ar,solid} \approx \beta_{Ar,bulk}$, the liquid adsorbate's contribution to the effective modulus can be calculated in region II (only surface layers): $\Delta\beta = \beta_{pore} - \tilde{f} \cdot \beta_{Ar,solid}$. This contribution $\Delta\beta$ (see figure 6.4) does not increase abruptly at the onset of freezing (f_1) but continuously, almost linearly. The liquid's contribution is thus proportional to the amount of solid adsorbate $\tilde{f} = f - f_1$ and can be well described by $\Delta\beta = \tilde{f} \cdot f_1/(1-f_1) \cdot \beta_{Ar,liquid}$, with the bulk value for $\beta_{Ar,liquid}$. Thus it depends both on the fraction of solid and of liquid adsorbate ($\tilde{f}$,f_1). Only in the limit of complete filling ($f = 1$) the full contribution of the liquid to the modulus is obtained ($f_1\beta_{Ar,bulk}$, see figure 6.4). Thus during adsorption, the total contribution of the pore to the modulus, β_{pore} in equation 5.6, must be expressed as the sum of the solid's and the liquid's contribution:

$$\beta_{pore} = \tilde{f}\left[\beta_{Ar,solid} + \beta_{Ar,liquid} \cdot \frac{f_1}{1-f_1}\right] \text{ for } \tilde{f} \geq 0 \tag{6.3}$$

How can the fact be interpreted that a constant volume fraction of liquid adsorbate (f_1) leads to a continuous increase of the effective modulus β? This can be explained in terms of the processes happening in the pores during adsorption. In region II solid surface layers are formed on top of liquid layers [see figure 6.5(b)]. The stiffness of this layer influences the liquid surface layers below and the liquid becomes noticable in the longitudinal modulus. The liquid layers have no longer a free surface in contact to the vapour in the pore centre and their mobility is reduced. There is no step in β and the range of the linear increase (region II) is very broad. Thus the solid layer in the pores can be regarded as a membrane which is still flexible just above f_1, but with increasing f this flexibility is lost and the liquid layers below become more and more perceptible. The increase in $\Delta\beta$ (see figure 6.4) is also a clear evidence that the liquid adsorbate consists of surface layers near the pore wall. If solid adsorbate formed at the surface of the pore walls and the liquid adsorbate were on top, these liquid layers would be unrestricted and not contribute to the effective modulus in region II.

At and above f_2 solid capillary bridges are formed in addition to solid surface layers (cp. section 2.2.2) and these might additonally reduce the mobility of the liquid surface layers. The formation of solid capillary bridges at and above f_2 can also distort the porous framework and hence result in the higher slope above f_2 [see figure 6.3(b)].

Conclusion

The determination of the longitudinal modulus of a (partially) filled nanoporous sample via ultrasonic measurements is a good method to study liquid-solid phase transitions. In contrast to shear waves, longitudinal ultrasonic waves offer the possibility to assess the elastic properties of liquid adsorbate. The longitudinal modulus of both liquid and solid adsorbed argon can be extracted from the measurement of the velocity of longitudinal waves propagating through a nanoporous sample. As during sorption experiments below the freezing point of the adsorbate usually some liquid remains in the form of surface layers

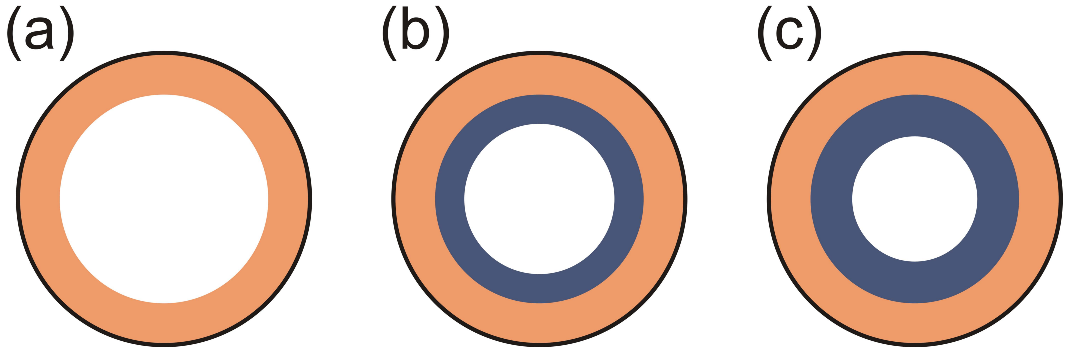

Figure 6.5 – *Schematic sketch of a partially filled pore. (a) Up to f_1 there are only liquid surface layers. (b) Above f_1 solid argon layers are formed on top of these layers. (c) With increasing thickness the solid layer becomes less flexible and the modulus contribution of the liquid layers is increased. Figure from [4] (Copyright © 2013 IOP Publishing Ltd).*

near the pore walls, it had to be regarded how this liquid contributes at different fillings to the effective modulus. Liquid surface layers adsorbed on the pore walls contribute to the longitudinal modulus only in consequence of the formation of solid argon layers on top of these layers and the related loss of mobility. The degree of the liquid layers' contribution increases with the thickness of the solid argon layer and thus depends on its flexibility. Only near the complete filling of the pores the full contribution of the adsorbed argon to the longitudinal modulus is observed. In the case of the adsorbate argon with its simple globular structure, the determined properties correspond to the bulk state. But nanoconfinement can lead to deviations in the properties of an adsorbed substance from its bulk state (see chapter 9). The possiblity to determine the elastic properties of liquid and solid adsorbate with this method might be of importance also in more complex systems.

Chapter 7

Influence of the Laplace pressure on the elasticity of argon in nanopores

---

In chapter 6 it was shown that at complete filling of the pores (for $p/p_0 = 1$) the longitudinal elastic modulus of liquid argon corresponds approximately to the value for bulk argon. At the beginning of an isothermal desorption process, the nanopores of the porous glass sample remain virtually completely filled over a certain pressure range. A reduction of the external pressure p below the bulk vapour pressure of argon, p_0, results, however, in the formation of concave menisci at the pore ends. The related decrease of the radius of curvature causes an increase of the negative Laplace pressure. This occurance is known to provoke a contraction of porous samples (cp. sections 1.4 and 8.1). In this chapter it is evidenced that the Laplace pressure also influences the elastic properties of the filled porous sample. A decrease of the radius of curvature at the pore ends becomes noticeable in a decrease of the effective longitudinal modulus. The analysis of the ultrasonic measurements reveals that this decrease originates in a reduction of the longitudinal modulus of the adsorbate. The proof of the influence of the Laplace pressure on the elastic properties is essential for the clarification of the correlation between the elastic moduli and the deformation behaviour.

For pressures below the steep part of the adsorption branch [see figure 7.1(a)] the adsorbate forms surface layers on the pore walls. The effective longitudinal modulus β of the porous Vycor® glass sample remains basically unaffected by the adsorption of these liquid argon layers on the pore walls (see figure 7.1(b) and section 6.1). In section 6.1 it was discussed that in the liquid regime the existance of argon vapour in the pore centre and the unrestricted mobility of the adsorbed atoms prevent an increase of the effective longitudinal modulus before a complete filling of the sample. Only just before the complete filling of the pores ($p/p_0 \approx 0.9$), when all pores are filled with capillary bridges, the effective longitudinal modulus is increased in comparison to the empty sample.

For high reduced pressures ($p/p_0 \geq 0.9$ during adsorption and $p/p_0 \geq 0.74$ during desorption) the pores are completely filled and an increased value for β/β_0 is observed. In those pressure ranges a decrease of the external pressure results in a decreasing radius of curvature r_K (cp. figure 7.2) at practically constant filling $f \approx 1$. The increasing curvature of these concave hemispherical menisci yields to an increase of the negative

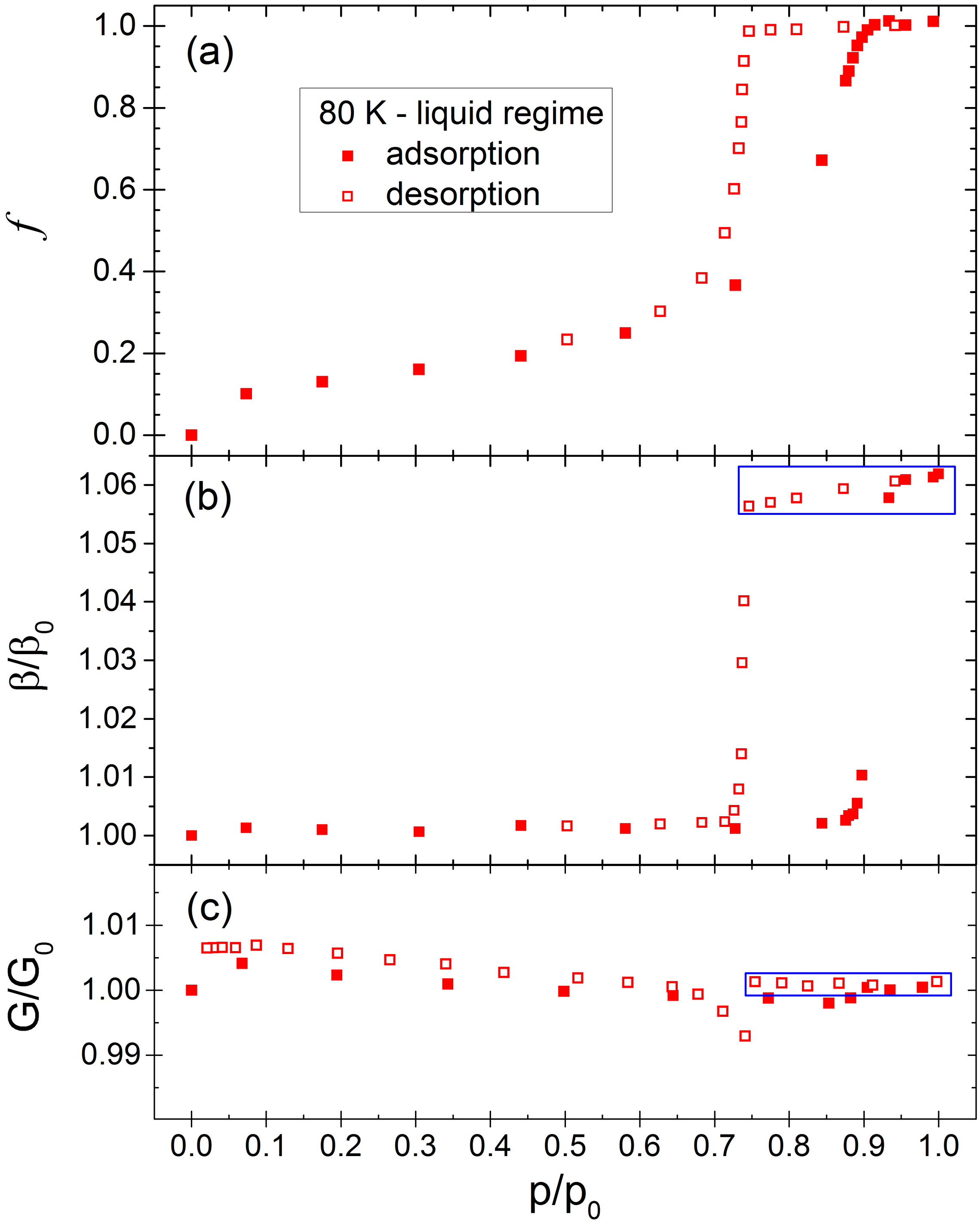

FIGURE 7.1 – *(a) Filling* f *of the sample with liquid argon as a function of the reduced pressure* p/p_0 *at a temperature of 80 K. (b) The effective longitudinal modulus* β *increases above the value for the empty sample* $\beta_0 = 16.88$ *GPa only when the pores are almost completely filled near* $p/p_0 \approx 0.9$*. During desorption the modulus is reduced to the initial value* β_0 *as soon as the pores start to empty and vapour voids appear (cp. section 6.1). (c) The effective shear modulus* G *is practically equal to the shear modulus of the empty sample* $G_0 = 6.86$ *GPa showing that the adsorbed liquid argon does not appreciably affect the solid Vycor*$^{®}$ *matrix.*

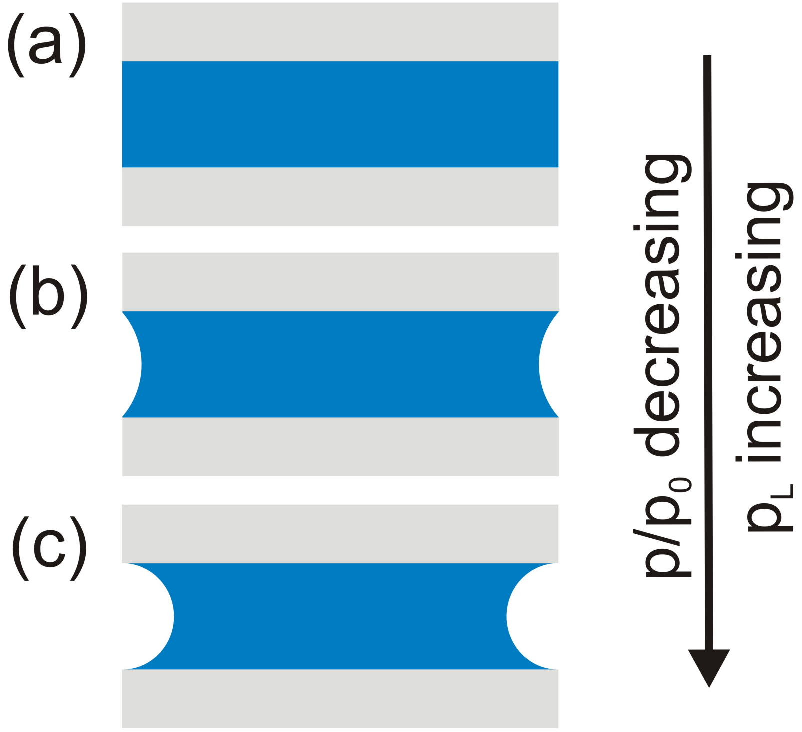

Figure 7.2 – *Schematic sketch of the influence of a reduction of the external pressure p below the bulk vapour pressure p_0 on the radius of curvature r_K of the hemispherical menisci at the pore ends. A decrease of the radius of curvature [from (a) to (c)] results in an increase of the negative Laplace pressure $p_L = 2\gamma_{lv}/r_K$.*

Laplace pressure $p_L = 2\gamma_{lv}/r_K$ during the initial desorption process and a considerable contraction of the sample [see figure 7.3(a)]. There is a linear dependence of the length change of the sample on the reduced pressure p/p_0. But besides the known influence of the concave menisci at the pore ends on the deformation of the sample, also an impact on the effective longitudinal modulus can be observed: There is a linear decrease of the effective longitudinal modulus for $0.74 \lesssim p/p_0 \leq 1$ (see figure 7.3(b)).

The clear decrease of the effective modulus β during desorption is just as the deformation provoked by the increase of the Laplace pressure as a result of the change of the curvature r_K of the concave menisci, $p_L = 2\gamma_{lv}/r_K$. With the aid of the Kelvin equation the Laplace pressure can be expressed as a function of the change of the external pressure p: $p_L = RT/V_m \ln(p/p_0)$ (see section 1.4) [114]. Thus, the Laplace pressure is increased from $p_L = 0$ at $p/p_0 = 1$ to a value of $p_L \approx -7.2$ MPa at $p/p_0 \approx 0.74$, where the curvature is approximately $|r_K| \approx 4.0$ nm ($\gamma_{lv} \approx 14.4$ mN/m [144], $V_m \approx 27.75$ cm^3/mol [141]; extrapolated values). Such a high negative pressure must have an impact on the elasticity of this argon. From bulk argon it is known that for pressures above the vapour pressure the elastic moduli are considerably increased [145, 146]. Indeed, an extrapolation of the behaviour of the elastic moduli for high pressures to negative pressures in the range of $p_L \approx -7$ MPa can explain a reduction of the elastic properties of argon by about $5-10$ %. The extraction of the longitudinal modulus of the adsorbed argon, $\beta_{Ar,ads}$,

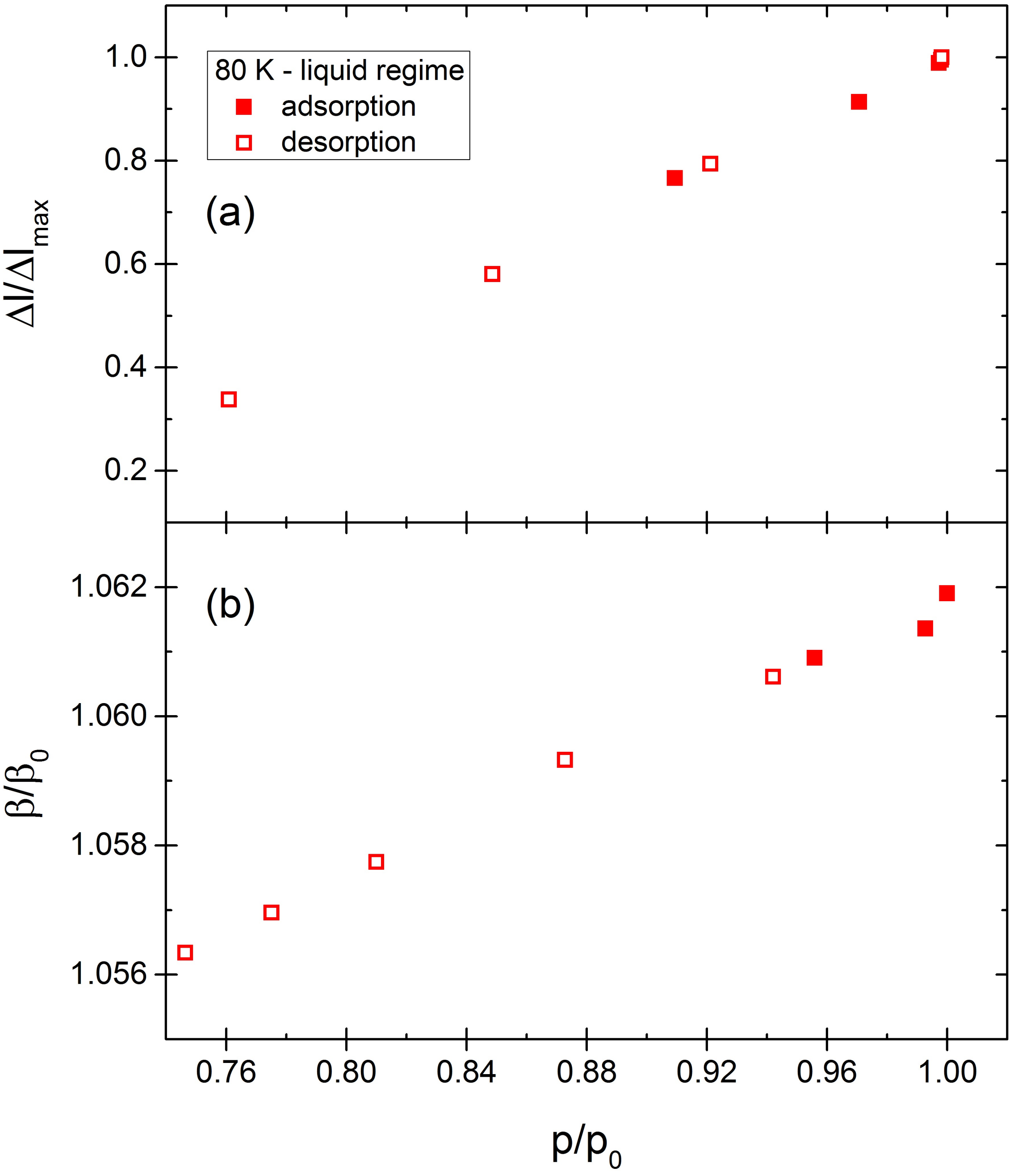

Figure 7.3 – *(a) Scaled length change* Δl *of the sample (*$\Delta l_{max} = 1.2$ μ*m: maximum length change at* $p/p_0 = 1$, $l_0 = 2.4$ *mm: length of the empty sample) and (b) scaled effective longitudinal modulus as a function of the reduced pressure for complete filling. Both the length and the effective longitudinal modulus decrease when the reduced pressure is decreased and consequently the negative Laplace pressure is increased; cp. figure 7.2.*

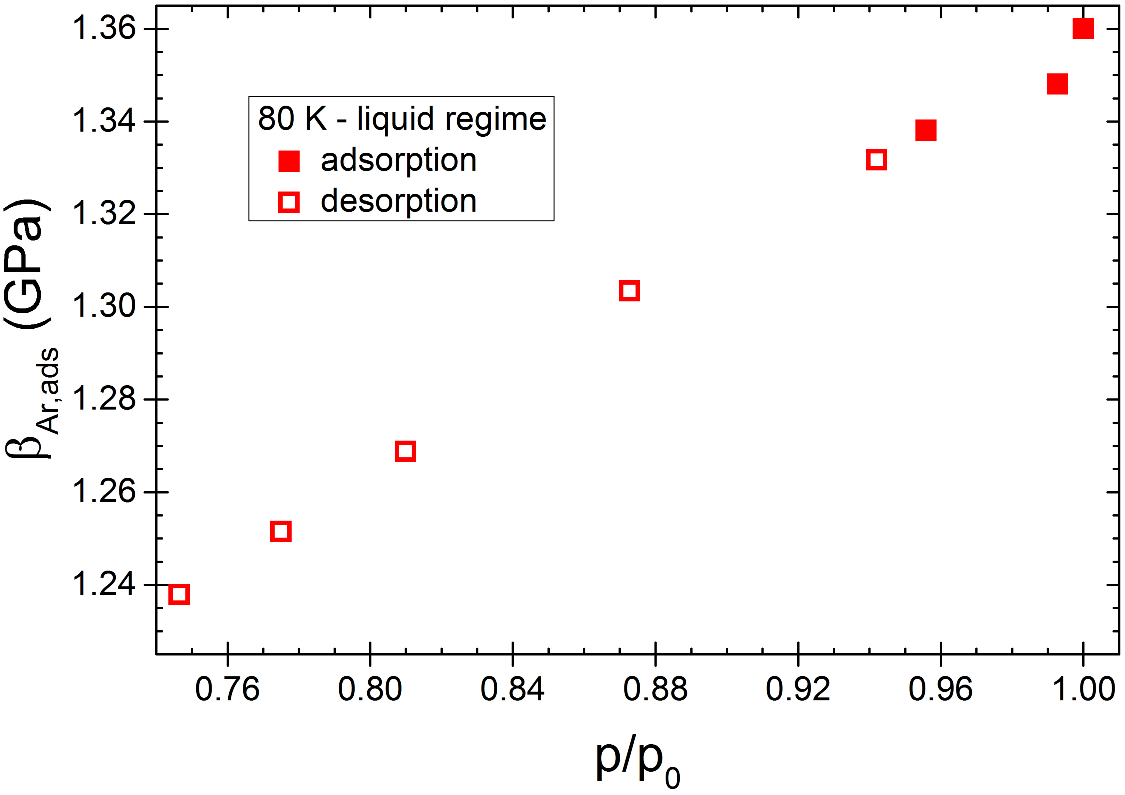

FIGURE 7.4 – *The increase of the Laplace pressure during the initial desorption process (at complete filling) causes a decrease of the longitudinal modulus of the adsorbed argon $\beta_{Ar,ads}$. The modulus $\beta_{Ar,ads}$ is calculated from the measured effective longitudinal modulus using equation 5.6 (from chapter 5).*

from the measurements of the effective modulus β at complete filling is possible via the effective medium analysis from chapter 5 (using equation 5.6 with $\beta_{pore} = \beta_{Ar,ads}$).

The analysis for the measurement at 80 K (see figure 7.4) shows that the elastic modulus of the adsorbed argon decreases when the pressure p/p_0 is reduced, i.e. when the absolute value of the Laplace pressure p_L is increased. The total decrease of about 9% is in the range that can be expected from the pressure behaviour known from bulk (see above). Thus, the Laplace pressure causes a deformation of the porous sample as well as a variation of the longitudinal modulus of the adsorbed argon.

The independence of the effective shear modulus G during the initial desorption process [$0.74 \lesssim p/p_0 \leq 1$, see marked values in figure 7.1(c)] evidences that the decrease of the effective longitudinal modulus in the same pressure range does not originate from a change of the elastic properties of the porous matrix. The shear modulus of a liquid is virtually zero and cannot really be reduced as a consequence of the Laplace pressure. If the effect would be caused by a change of the elasticity of the porous matrix, the effective shear modulus should also be influenced. Furthermore no influence on the effective longitudinal modulus during adsorption at pressures below $p/p_0 \approx 0.9$ (for adsorption) is observed. But it is known that also in this external pressure range a significant pressure is exerted on the

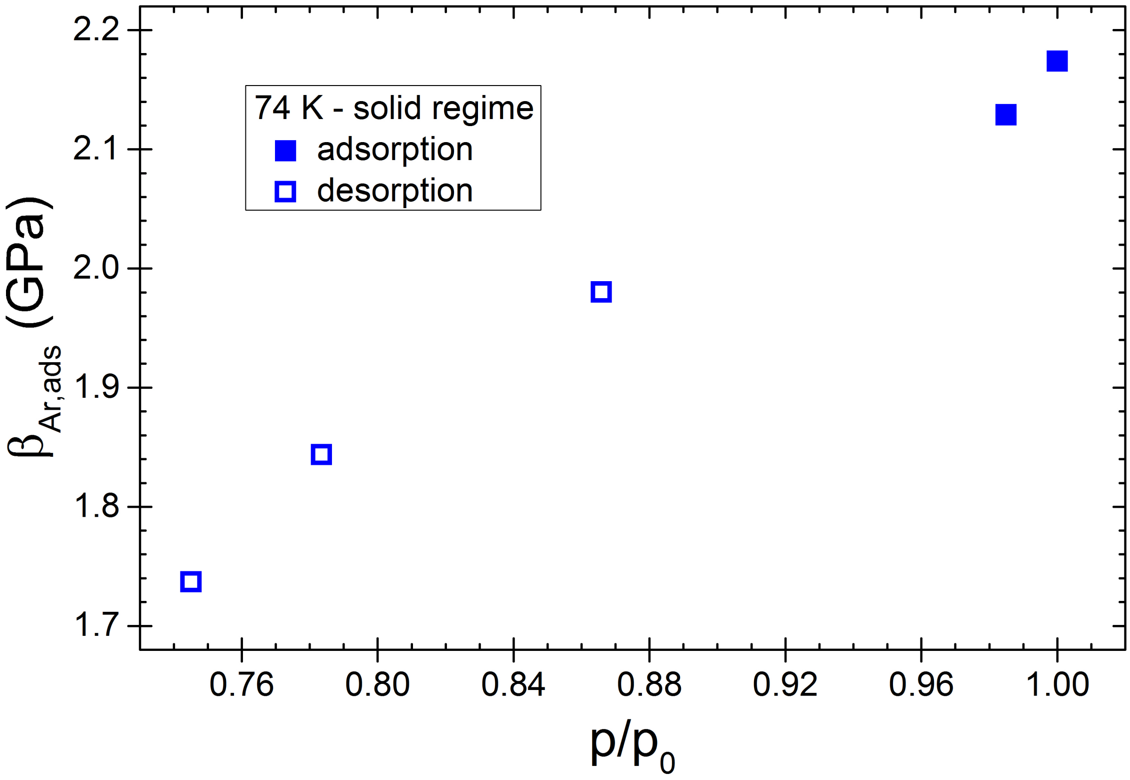

FIGURE 7.5 – *A reduction of the external pressure p at $T = 74$ K, i.e. a temperature below the onset of freezing at 75.8 K (see section 4), results in a considerable decrease of the modulus of the filling that consists of solid and liquid argon. This comparatively strong decrease might originate in a reduction of the fraction of solid argon.*

pore walls [44]. Therefore, and also because of the relative weakness of argon compared to quartz glass or to the effective longitudinal modulus ($\beta_{Ar,ads} \approx 1.36$ GPa, $\beta_Q \approx 72.85$ GPa, $\beta_0 \approx 16.88$ GPa), the pressure-induced change of the effective longitudinal modulus at complete filling is mainly due to a change of the longitudinal modulus of the adsorbed argon.

The measurement of the effective longitudinal modulus at a temperature of 74 K, i.e. below the onset of freezing [$T_{fr,Ar,pore} \approx 75.8$ K (see chapter 4)] reveals a further influence of the Laplace pressure. At 74 K only a fraction of the adsorbed argon is solid (see figure 2.4 in section 2.1). Thus, the longitudinal modulus (determined with the aid of equation 5.6) represents an average value for the whole pore filling of liquid and solid argon. At 74 K the influence of the Laplace pressure on the modulus of argon is much stronger; it changes by about 20% (see figure 7.5). As is generally known, the pressure influences phase transition temperatures. The stronger decrease of the longitudinal modulus of the pore filling in the solid regime might be related to a decrease of the fraction of solid argon in the pore filling ($\beta_{Ar,liquid} \approx 1/3\ \beta_{Ar,solid}$ [130]). Strains or distortions in the porous matrix because of solid adsorbate (capillary bridges) could be an additional factor for the strong dependence of $\beta_{Ar,ads}$ on p/p_0 (cp. section 6.2).

Conclusions

The Laplace pressure of concave menisci at the pore ends causes not only a deformation of the porous sample. The ultrasonic measurements show that the Laplace pressure also influences the effective longitudinal modulus; but in the liquid regime the Laplace pressure has no effect on the effective shear modulus. The analysis of the measurements proves that the changes in the effective longitudinal modulus originate in changes of the longitudinal modulus of the adsorbed argon as a consequence of the formation of concave menisci at the pore ends and the related negative Laplace pressure.

Chapter 8

The influence of the geometrical arrangement of adsorbate on the deformation of nanoporous glass

---

Sorption of adsorbates in pores generally results in a deformation of the porous matrix (see section 1.4). The measurements discussed in chapter 7 showed amongst others that the Laplace pressure generated by the concave menisci of adsorbed argon causes a deformation of the nanoporous glass sample at virtually complete filling. Here the macroscopic deformation of nanoporous glass is studied during sorption of different amounts of argon. The deformation behaviour differs significantly for adsorption and desorption. In the hysteretic region adsorbed surface layers and capillary bridges coexist. In particular, during desorption the formation of vapour voids results in a strong contraction of the porous sample. The investigation of the influence of different structures of the adsorbate on the pressure exerted on the porous sample shows that the deformation behaviour reveals differences in the thickness of the adsorbed film in the hysteretic region and it allows statements about the stability of these surface layers.

8.1 Deformation during sorption of argon and the effective longitudinal modulus

Sorption of argon results in a complex deformation behaviour of the nanoporous Vycor® glass sample. The change of the sample's length Δl depends significantly on whether the sample is filled or emptied. Equal amounts of adsorbate can result in both an expansion or contraction of the pores and the sample [cp. figures 8.1(a)+(b)]. The observed deformation mainly resembles what is known from literature, except the observed very pronounced contraction and re-expansion at a specific p/p_0-value during desorption [see figure 8.1(b) at $p/p_0 \approx 0.72$] that will be amongst others discussed in this chapter.

After adding some liquid argon at a temperature of 86 K, the sample considerably expands up to a reduced pressure in the range of $p/p_0 \approx 0.8$ [see figure 8.1(b)]. This pressure corresponds to the steep part of the adsorption branch [see figure 8.1(a)]. It can be

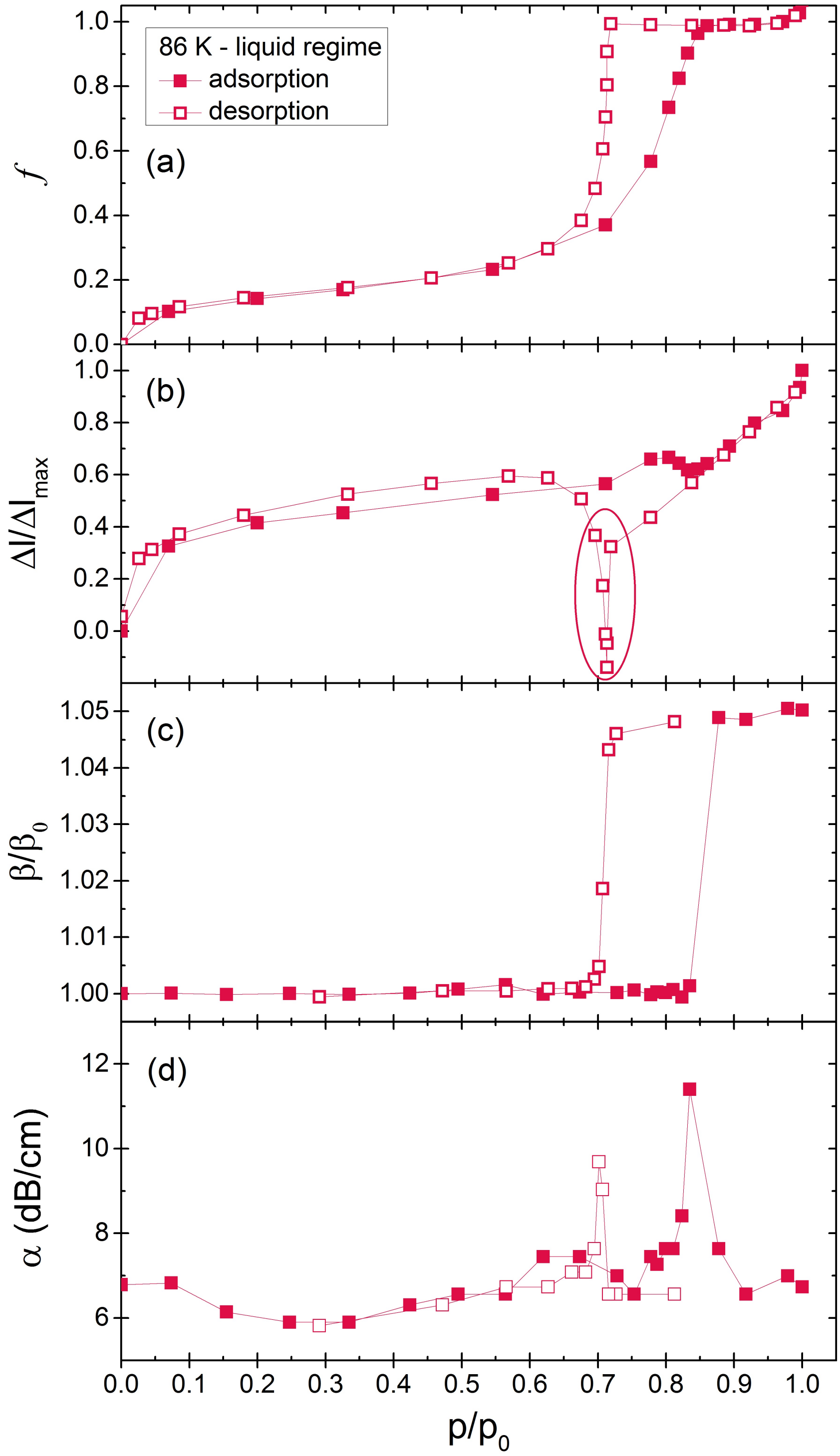

FIGURE 8.1 – *(a) Filling f of the porous glass with liquid argon (86 K) as a function of the reduced vapour pressure p/p_0. At low pressure (below $p/p_0 \approx 0.8$) the adsorbate forms surface layers on the pore wall. At higher pressure in the region of the steep part of the isotherm ($p/p_0 \approx 0.8$) capillary bridges are formed. (b) The adsorbed argon results in a deformation Δl of the sample (scaled to $\Delta l_{max} \approx 1.0$ μm at $p/p_0 = 1$). The circle marks an unusual contraction and re-expansion that has not been predicted theoretically. (c) The effective longitudinal modulus increases stepwise when the pores are completely filled. (d) The increase of the attenuation of the ultrasonic signal shows the appearance of vapour voids in the range of the formation and vanishing of capillary bridges.*

assumed that roughly up to this value the adsorbate forms surface layers on the pore walls. The measured expansion is mainly caused by the reduction of the surface free energy and the related pressure [44, 113] that is exerted by the liquid layer on the pore walls. The Laplace pressure $-\gamma_{lv}/\left(r_P - t\right)$ of the adsorbed film of thickness t counteracts this expansion [44]. Its contribution is, however, comparatively small for thin films [44].

At higher external pressure p additional filling forms capillary bridges in the pores. These become energetically more favourable at first in smaller pores, while in bigger pores the thickness of the surface layer still increases. Thus there are two coexistent configurations of the adsorbate in the pores. Now the negative Laplace pressure in both capillary bridges with concave hemispherical menisci and adsorbed surface layers seeks a reduction of the pore diameter and of the size of the sample. But the increasing thickness of the surface layer in regions without capillary bridges leads to a further reduction in the surface free energy (cp. reference [44]). Thus, there is once again an interplay between the two opposite deformation effects. But above $p/p_0 \approx 0.8$ the contracting effect of the Laplace pressure predominates and a slight relative contraction is observed up to $p/p_0 \approx 0.85$, where $f \approx 1$ holds and the pores are completely filled with capillary bridges [see figures 8.1(a+b)]. There only remain concave menisci at the pore ends. A subsequent increase of the pressure [cp. figure 8.1(a)] leads to a flattening of those menisci and no perceptible increase of the filling; thus the negative pressure in the adsorbate is reduced and the sample expands.

During desorption mainly the described behaviour is reversed [see figure 8.1(b)]. A reduction of the pressure in the sample cell yields to an increasing curvature of the menisci at the pore ends and hence a contraction of the sample is observed. In the steep desorption branch of the isotherm [see figure 8.1(a)] the number of capillary bridges diminishs which should lead to a continuous expansion of the sample until only surface layers exist. But, initially a sharp contraction of the sample is observed at $p/p_0 \approx 0.72$. All measurements with the globular argon show the contraction peak, however, it has not previously been observed in other systems, e.g. for water in porous glass (see reference [50]).[1] At this point it can be stated that this contraction cannot simply be explained by the disappearance of capillary bridges.

At lower values of the reduced pressure the disappearance of capillary bridges becomes noticable by an expansion of the sample until only surface layers remain, just as it is expected ($p/p_0 \approx 0.65$). When the thickness of the surface layer, respectivley the number of adsorbed argon layers, is reduced in the further desorption process, the length reduces continuously to the value for the empty sample because of the related change of the surface free energy (cp. above). The measurements at 80 K and 74 K show essentially the same deformation behaviour [see figure 8.2(a+c)].

The comparison of the measured deformation with the effective longitudinal modulus and

---

[1] Haines and McIntosh [110] observed for activated carbon a reduction of the length of the porous sample below its initial length during desorption. A comparison with the sorption isotherm (filling fraction as a function of the reduced pressure) shows, however, that the minimum of the contraction is observed just before the steep part of the desorption branch.

the attenuation of the ultrasonic pulses [see figure 8.1(c+d)] shows that local minima of both deformation curves (adsorption and desorption) correspond to stepwise changes of the effective longitudinal modulus. Above a reduced pressure of $p/p_0 \approx 0.8$ during adsorption the attenuation of the ultrasonic signal increases because of the appearance of capillary bridges and vapour voids, which has also been observed for hexane in Vycor® [62, 63]. Just before the complete filling of the pores, when all pores are filled with capillary bridges, the effective modulus is increased in comparison to the empty sample. Adsorbed liquid surface layers do not result in a change of the effective modulus due to existance of argon vapour in the pore centre and the unrestricted mobility of the adsorbed atoms (cp. section 6.1).

At high reduced pressures ($p/p_0 \geq 0.85$ during adsorption and $p/p_0 \geq 0.72$ during desorption) both the effective longitudinal modulus β and the length change Δl are approximately linear functions of the reduced pressure. The formation of concave menisci with decreasing radius r_P at the pore ends during desorption leads to an increase of the negative Laplace pressure $p_L = 2\gamma_{lv}/r_P$ and thus both to a considerable contraction of the sample and to a pressure-induced change of the adsorbate's intrinsic elastic properties (see chapter 7).

The relationship between the deformation behaviour and the effective longitudinal modulus is basically the same for all measured temperatures, i.e. in the liquid regime for 86 K and 80 K and in the solid regime for 74 K (see figure 8.2). The sharp contraction peak during desorption is differently strong [cp. figure 8.1(b) at $p/p_0 \approx 0.72$, figure 8.2(a) at $p/p_0 \approx 0.74$, and figure 8.2(c) at $p/p_0 \approx 0.75$]. The inset in figure 8.2(c) shows that the extent of the sharp contraction can vary for measurements with different samples at one and the same temperature. These differences are mainly related to differences in the geometrical structure of the pore filling during desorption. A different geometric arrangement of the adsorbate can first appear because of differences in the pore structure of different samples and second because of differences in the size of individual desorption steps i (with Δp_i, respectively Δf_i) for one and the same sample. The influence of the geometrical structure of the filling will be thoroughly studied in section 8.3.

At a temperature of 74 K only a fraction of the filling is solid; the first layers near the pore wall remain liquid-like and only at fillings above $f \approx 0.66$, i.e. for $p/p_0 \approx 0.95$, solid argon exists (see section 2.1). Therefore, the deformation behaviour up to $p/p_0 \approx 0.95$ should mainly not differ from the liquid regime. But also above $p/p_0 \approx 0.95$, when solid adsorbate exists no major differences in the deformation behaviour are observed.

From the comparison of the sharp contraction of the sample during desorption at $p/p_0 \approx 0.72$ (at 86 K) to the effective longitudinal modulus one might conclude that the sharp contraction is related to the observed weakening of the effective longitudinal modulus [see figure 8.1(c)] as a result of the appearance of vapour voids which becomes noticable in an increase of the attenuation of the ultrasonic signal [see figure 8.1(d)]. In contrast, during adsorption at the steep increase of the longitudinal modulus near $p/p_0 \approx 0.85$ no real peak in the deformation is observed. At this higher reduced pressure the Laplace pressure is of course lower, but only by a factor of two in comparison to desorption. Consequently,

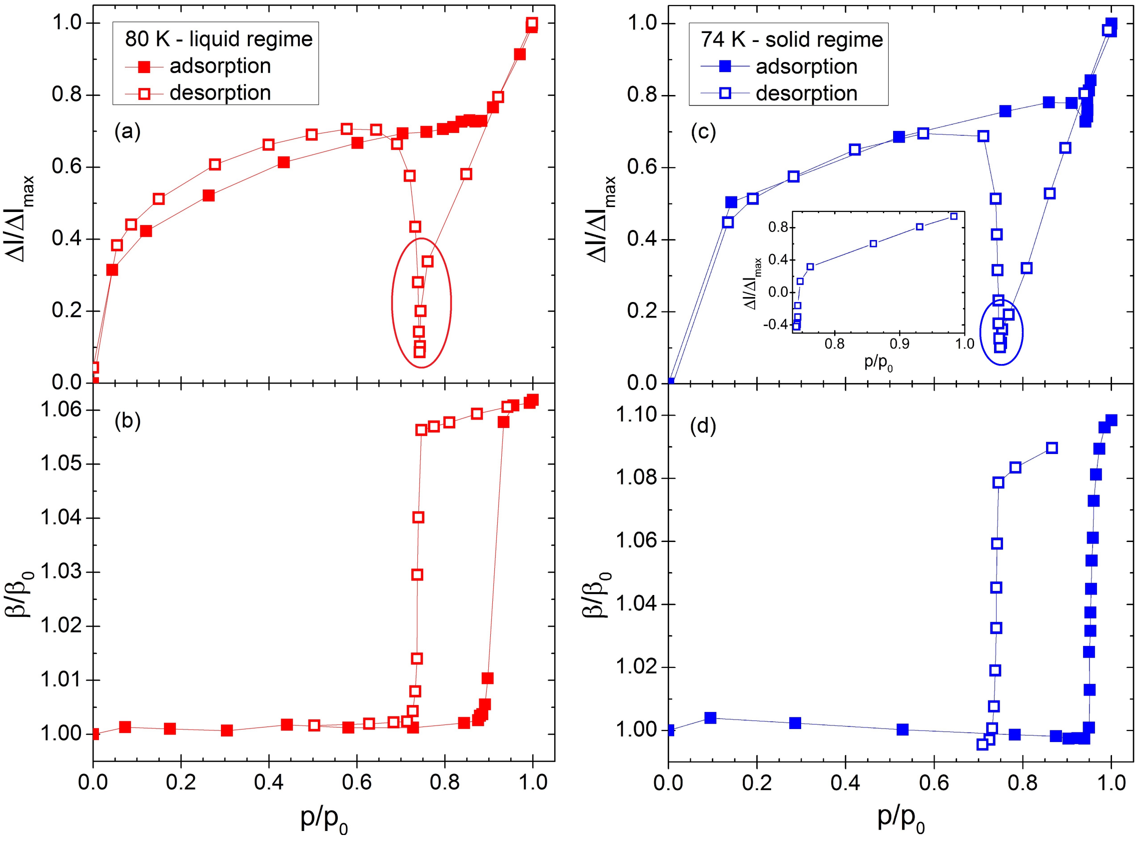

FIGURE 8.2 – *Scaled length change of the nanoporous Vycor$^{\circledR}$ glass as a function of the reduced vapour pressure p/p_0 during sorption of argon at (a) 80 K, i.e. in the liquid regime (with $\Delta l_{max} = 1.2\ \mu$m) and (c) 74 K, i.e. in the solid regime (with $\Delta l_{max} = 0.9\ \mu$m). The circles mark a contraction peak that has not been predicted theoretically. The longitudinal modulus increases at complete filling of the sample [(b) at 80 K (with $\beta_0 = 16.88$ GPa) and (d) at 74 K (with $\beta_0 = 16.96$ GPa)]. Because of the higher longitudinal modulus of solid argon, the step is bigger at 74 K. As a result of the increase of the Laplace pressure during the initial desorption process at complete filling, the modulus decreases with decreasing external pressure p (cp. chapter 7). The inset in (c) shows a desorption measurement for a different sample at 74 K.*

the almost non-existance of a contraction peak during adsorption seems to contradict the impression of the relation between the steep change of the longitudinal modulus and the contraction peak; at least as the sole origin of the contraction peak.

For the further investigation of the origin of the strong contraction peak during desorption the model by Gor and Neimark [44] for the theoretical description of the deformation behaviour is discussed. Finally, their idealized model is amended to include the coexistance of adsorbed films and capillary bridges, a condition that is typically present in porous samples over a certain pressure range. Thereby, the steep contraction peak can be related to the geometric configuration of the adsorbate argon.

8.2 Model by Gor and Neimark

Gor and Neimark [44] used a thermodynamical model to describe the deformation at different reduced pressures for pores without any variation of the radius. In this model the deformation behaviour is described as a result of the so-called solvation pressure p_s that consists of pressure contributions for different fillings. The extend of the deformation $\varepsilon = \Delta V/V_0$ (with V_0 being the volume of the empty sample and ΔV its change that is equal to the change of the pore volume)[2] depends on the difference between the mechanical stress σ_s induced by the adsorbate and the external pressure p, the later being usually negligible small [44]. Assuming the validity of the Hook law, the solvation pressure is related to the deformation ε via an effective elastic modulus M of the pore system [44]:

$$p_s = \sigma_s - p = M \cdot \varepsilon + \sigma_0 \tag{8.1}$$

Equation 8.1 also includes the existance of a prestress σ_0 of the empty sample. The modulus M is an "elastic modulus of the pore system" [56], but the meaning of the modulus M in terms of the moduli of the heterogeneous system of porous sample and pore filling is not obvious.

The models for the description of the deformation behaviour regard the elastic properties of the sample usually as independent of the filling of the pores [56], which contrasts to the experimental observations (see figure 8.1 and e.g. section 2.1). Discrepances between the theoretical predictions and the measured deformation resulted in the assumption of a possible influence of the effective elastic properties on the deformation behaviour [56]. But the independence of the modulus M in equation 8.1 on the pore filling corresponds to observations for porous silicon [48] (see section 1.4).

For completely filled pores with only concave menisci at the pore ends, the solvation pressure, i.e. the pressure exerted by the pore filling on the pore walls, is usually equalized with the Laplace pressure [48]. The relation of the radius of curvature at different external pressures p can be calculated with the Kelvin equation, thus that the solvation pressure p_s^c for pores filled with capillary bridges is given by [44]

$$p_s^c(p) = -\frac{\gamma_{wl}}{r_P} + (p_0 - p) + \frac{RT}{V_m}\ \ln(p/p_0), \tag{8.2}$$

with the pore wall-liquid surface tension γ_{wl}. The first summand is a constant and the changes in the second are comparatively small ($\Delta p \lesssim 1$ kPa).

If there is solely an adsorbed film on the pore walls the Laplace pressure of the adsorbed film with the thickness t has to be considered as well as the altered surface energy and the following relation holds for the solvation pressure p_s^f for adsorbed surface layers [44]:

$$p_s^f(t) = -\frac{\gamma_{wl}}{r_P} - p - \frac{\gamma_{lv}}{r_P - t} - \frac{t}{r_P}\Pi(t) - \frac{1}{r_P}\int_t^\infty \Pi(t')dt' \tag{8.3}$$

---

[2] Note that in experiments the total volume change of the porous sample is measured.

where γ_{lv} is the liquid-vapour surface tension and $\Pi(t)$ is the disjoining pressure which is for argon usually approximated with the Frenkel-Halsey-Hill (FHH) equation [44]:

$$\Pi(t) = \frac{RT}{V_m} \frac{k}{(t/\tilde{t})^m} \tag{8.4}$$

with the constants $\tilde{t} = 0.1$ nm, $k = 73.17$ and $m = 2.665$ for argon (at $T = 87.3$ K) [113].

The first term on the right hand side of equation 8.3 is the same constant as in equation 8.2 and the contribution of the pressure p is again very small. The contracting Laplace pressure $-\gamma_{lv}/(r_P - t)$ of the adsorbed film increases with increasing thickness t. The last two terms with the disjoining pressure account for changes in the surface free energy in consequence of the adorption of molecules on the pore walls. The absolute value of this "free energy" contribution decreases with increasing film thickness (cp. reference [44]). Thus there are mainly two competing deformation pressures for adsorbed films.

The model developed by Gor and Neimark [44] (on the basis of the Derjaguin-Broekhoff-de Boer theory) allows to calculate the deformation behaviour during sorption with the above equations.[3] The model presumes that at a certain pressure the pores fill abruptly and completely with capillary bridges, i.e. it does not describe the coexistance of both adsorbate states, which is usually present in porous systems with a certain pore size distribution. The calculated solvation pressure during adsorption and desorption of argon in pores with a pore radius of $r_P = 4$ nm is shown in figure 8.3 for reduced pressures above $p/p_0 = 0.05$ (for low pressures the FHH equation is not valid).[4] Assuming a constant modulus M during sorption (see equation 8.1), the form of the solvation pressure should be identic with the deformation $\varepsilon = \Delta V/V_0 \approx 3\Delta l/l_0$ (the latter equality sign is valid for typical volume changes with $\Delta V << V_0$).

Considering the presence of a certain pore size distribution of the porous Vycor® glass sample, the measured deformation [see figure 8.1(b)] is in good agreement with the theoretical curve for the solvation pressure apart from the sharp dip during desorption at $p/p_0 \approx 0.72$. The discussion in the next section will show that it is necessary to take the coexistance of adsorbed surface layers and capillary bridges into account as well as certain requirements regarding the thickness of the adsorbed surface layers, in order to explain the observed sharp contraction and re-expansion peak.

---

[3] Equation 8.3 gives the solvation pressure as a function of the thickness t of the adsorbed film. For the calculation of the solvation pressure at a specific external pressure the knowledge of the relation between the film thickness t and the external pressure p is necessary. For this the Derjaguin equation for the chemical potential μ has been used [44]:

$$\mu = RT \ln(p/p_0) = -\left(\Pi(t) + \frac{\gamma_{lv}}{r_P - t}\right) V_m \tag{8.5}$$

With the aid of equation 8.5 also the external pressure p at which the pores fill abruptly with capillary bridges can be determined (maximum of the chemical potential) [44].

[4] Calculated with the following values for bulk argon at $T = 86$ K: $\gamma_{lv} = 12.9$ mN/m [144] (interpolated) and $V_m = m_M/\rho_{ads} = 28.5$ cm^3/mol [141] (extrapolated)

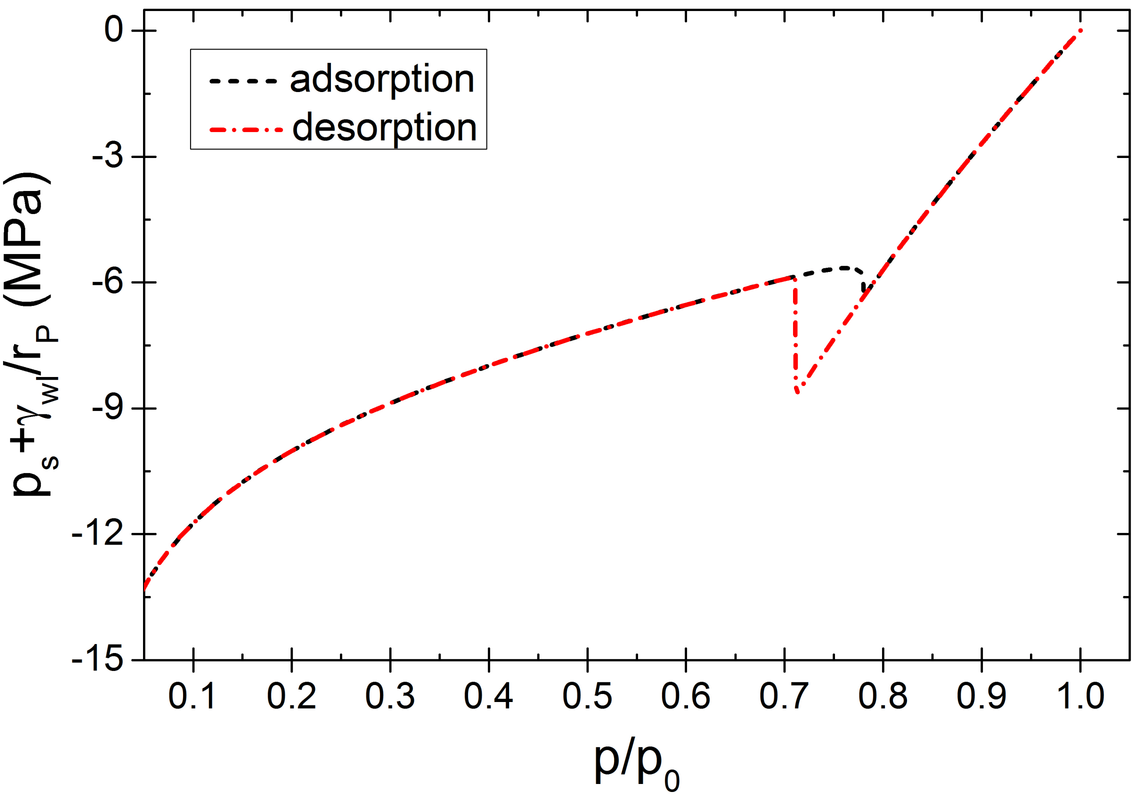

FIGURE 8.3 – *Calculated solvation pressure p_s (shifted by γ_{wl}/r_P) during adsorption and desorption of liquid argon in pores with a radius of $r_P = 4$ nm. In a small pressure range a hysteresis is observed; otherwise both branches are identic. The behaviour of the solvation pressure closely resembles the measured deformation behaviour $\Delta l/\Delta l_{max}$. The main difference is the sharp contraction at $p/p_0 \approx 0.72$ which is not present in the theoretical curve.*

8.3 Modification of the Gor-Neimark model for the coexistance of adsorbed layers and capillary bridges

For the explanation of the measured sharp contraction peak, the coexistance of adsorbed surface layers and capillary bridges will be included in the model by Gor and Neimark. Therefore the individual equations for the solvation pressure (equations 8.2 and 8.3) have to be combined. The simplest assumption is an additive composition of the solvation pressure of a fraction ξ of pores with capillary bridges and a fraction $1-\xi$ of pores with only adsorbed surface layers:

$$p_s^{f+c} = \xi \cdot p_s^c + (1-\xi) \cdot p_s^f \tag{8.6}$$

At the onset of the formation of capillary bridges at f_c the fraction ξ starts to increase until it reachs $\xi = 1$ at complete filling ($f = 1$). The problem now consists in determining the fraction ξ of pores with capillary bridges at a certain filling f of the pores, respectively at a given external pressure p. Also the filling-dependent fraction ξ must be connected to a thickness t of the adsorbed film. Before the formation of capillary bridges at f_c, the thickness t of the adsorbed layers increases with increasing filling f according to (cp. equation 2.1)

$$t = r_P \left(1 - \sqrt{1 - f}\right) \tag{8.7}$$

(assuming cylindrical pores).

The formation of capillary bridges changes this behaviour at high fillings. At the onset of the formation of capillary bridges at f_c it can be assumed that either the thickness of the existing surface layer remains constant or that the top layers become instable, form capillary bridges, and consequently the thickness of the surface layer is reduced [see figures 8.4(a)+(c)]. In the latter case, the fraction ξ jumps at f_c abruptly to a certain value $\xi > 0$. If it is assumed that in both cases the thickness of the adsorbed layer remains at a constant value t_0 above f_c [see figures 8.4(a)+(c)], this thickness t_0 corresponds to a filling $f_0 = \left(r_P^2 - (r_P - t_0)^2\right)/r_P^2$. Then the pore filling is $f = f_0 \cdot (1 - \xi) + 1 \cdot \xi$ and thus

$$\xi = \frac{f - f_0}{1 - f_0} \qquad (\text{for } f \geq f_c). \tag{8.8}$$

Equation 8.8 permits accordingly the determination of the fraction ξ of pores filled with capillary bridges above f_c. In figure 8.4(b)+(d) the fraction ξ of capillary bridges is shown for the two thickness dependences from figure 8.4(a)+(c). Here, it is assumed that during desorption almost all capillary bridges have disappeared at $p/p_0 \approx 0.69$ and $f_c^{des} \approx 0.47$ (corresponding to three surface layers). For the determination of the reduced pressure at a certain filling f the isothermal sorption measurements can be used [see figure 8.1(a)]. Consequently, the solvation pressure p_s^{f+c} of a porous sample filled with both surface layers and capillary bridges can be calculated assuming certain configurations of the adsorbate, e.g. those shown in figure 8.4(a)+(c) for the desorption branch.

The results of the calculations (according to equation 8.6) for three thickness dependences [including those from figure 8.4(a)+(c)] are shown in figure 8.5. Assuming that t does not change abruptly at f_c [cp. figure 8.4(a)], the behaviour of the solvation pressure p_s^{f+c} is basically the same as in the simplified case without the coexistance of surface layers and capillary bridges (cp. figures 8.3 and 8.5 for $t_0 = 1.08$ nm, i.e. three surface layers). The major difference being only a broadening around f_c^{des}. But for a thickness of the surface layers of $t_0 = 0.36$ nm (one surface layer) above f_c^{des} [cp. figure 8.4(c)], the solvation pressure shows a relatively sharp contraction peak and thus closely resembles the measured deformation during desorption [see figures 8.1(b) and 8.2(a)]. Thus, for thickness dependences that are similar to those shown in figure 8.4(c), the theoretical curve corresponds well to the measurements. The behaviour of the solvation pressure in figure 8.5 evidences that a thickness of $t_0 = 0.72$ nm (two monolayers) above f_c^{des} is impossible because this thickness does not result in a contraction peak. Theoretically it is possible that there is no film on the pore walls above f_c^{des}, i.e. $t_0 = 0$ nm. This would

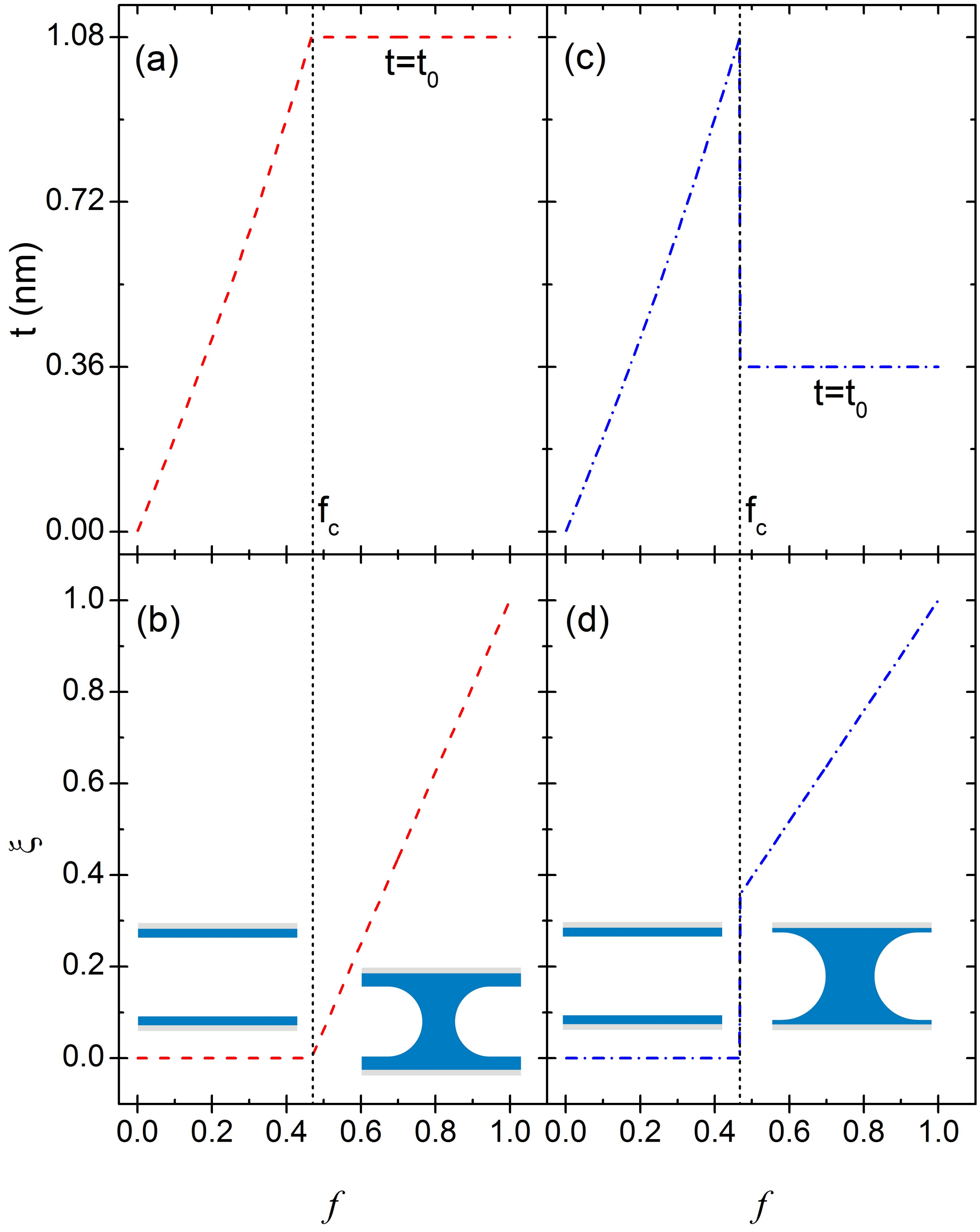

FIGURE 8.4 – (a)+(c) Thickness t of an adsorbed surface layer and (b)+(d) appropriate fraction ξ of capillary bridges as a function of the filling during desorption. It is assumed that above a critical filling $f_c \approx 0.47$ ($p/p_0 \approx 0.69$) capillary bridges and surface layers coexist; below f_c there are (almost) no capillary bridges. In (a)+(b) it is presumed that the thickness of the layer does not change abruptly at f_c. The case of a rearrangement of the adsorbate and the sudden change of the thickness of the layer is shown in (c)+(d) [capillary bridges become unstable and form surface layers at f_c]. Here the thickness of the surface layer above f_c is taken to be approximately the thickness of one surface layer $u \approx 0.36$ nm.

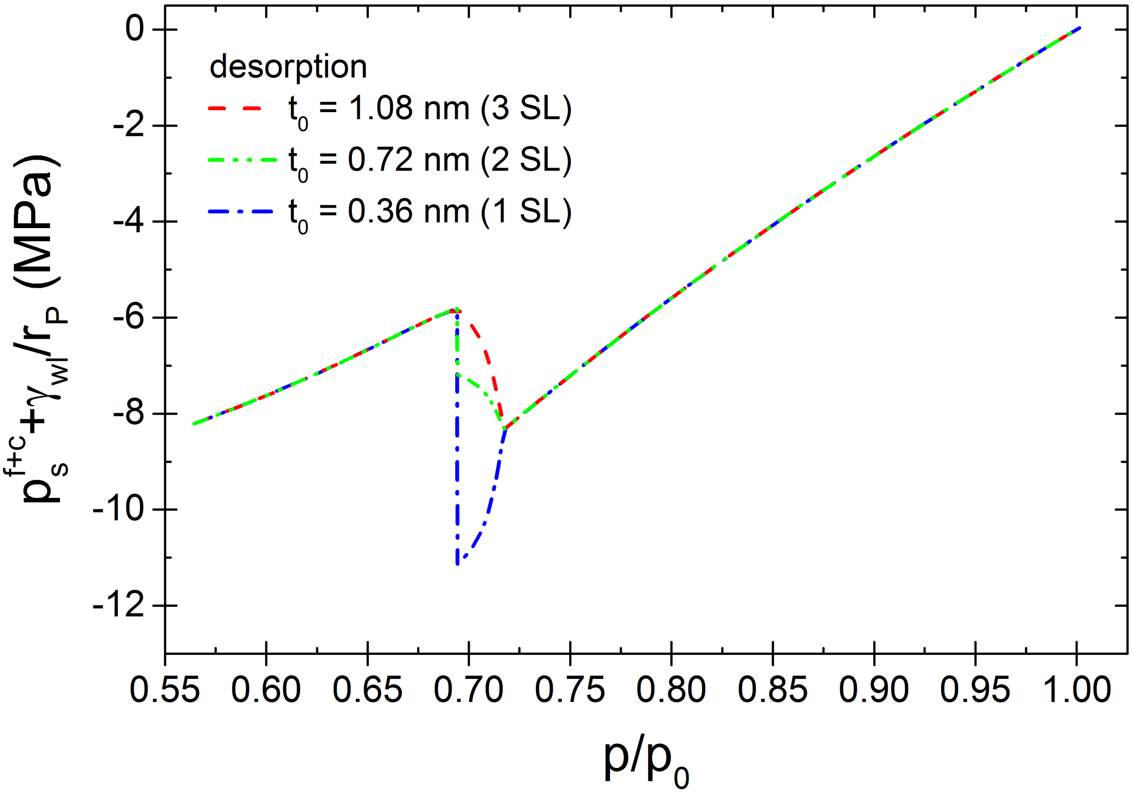

FIGURE 8.5 – *The solvation pressure during desorption assuming the coexistance of adsorbed layers and capillary bridges for three different thickness dependences. Only for a thickness of the adsorbed layer corresponding to one surface layer ($t_0 = 0.36$ nm) above f_c^{des}, the theoretical curve shows a sharp contraction peak similar to the measured deformation.*

result in an even stronger peak than the one shown in figure 8.5 for $t_0 = 0.36$ nm, however, such a configuration appears not to be very likely.[5]

During adsorption the onset of capillary condensation can be at relatively high fillings (above $p/p_0 \approx 0.76$) [cp. figure 8.1(b)]. Therefore, during adsorption a higher filling fraction, e.g. $f_c^{ads} \approx 0.59$ (four monolayers), must be used for the calculation of the solvation pressure. The reduced pressure that corresponds to f_c^{ads} is consequently also higher than during desorption. This shift of f_c influences also the solvation pressure which is shown in figure 8.6 for four different thicknesses t_0 above f_c^{ads}.

In contrast to the desorption branch, the best agreement with the measurements is achieved if there is no step in the thickness of the adsorbed layer (and the thickness remains constant at the onset of capillary condensation) or if the thickness t jumps to $t_0 = 1.08$ nm (three monolayers) at f_c^{ads} [cp. figures 8.1(b) and 8.6]. Also $t_0 = 0.72$ nm still seems to be possible because this thickness results in only a very small contraction near f_c^{ads}. But clearly at least the first two surface layers remain stable when capillary bridges form.

---

[5] The solvation pressure for a film tickness of $t_0 = 0$ nm cannot be calculated with equation 8.3, it tends to negative infinity.

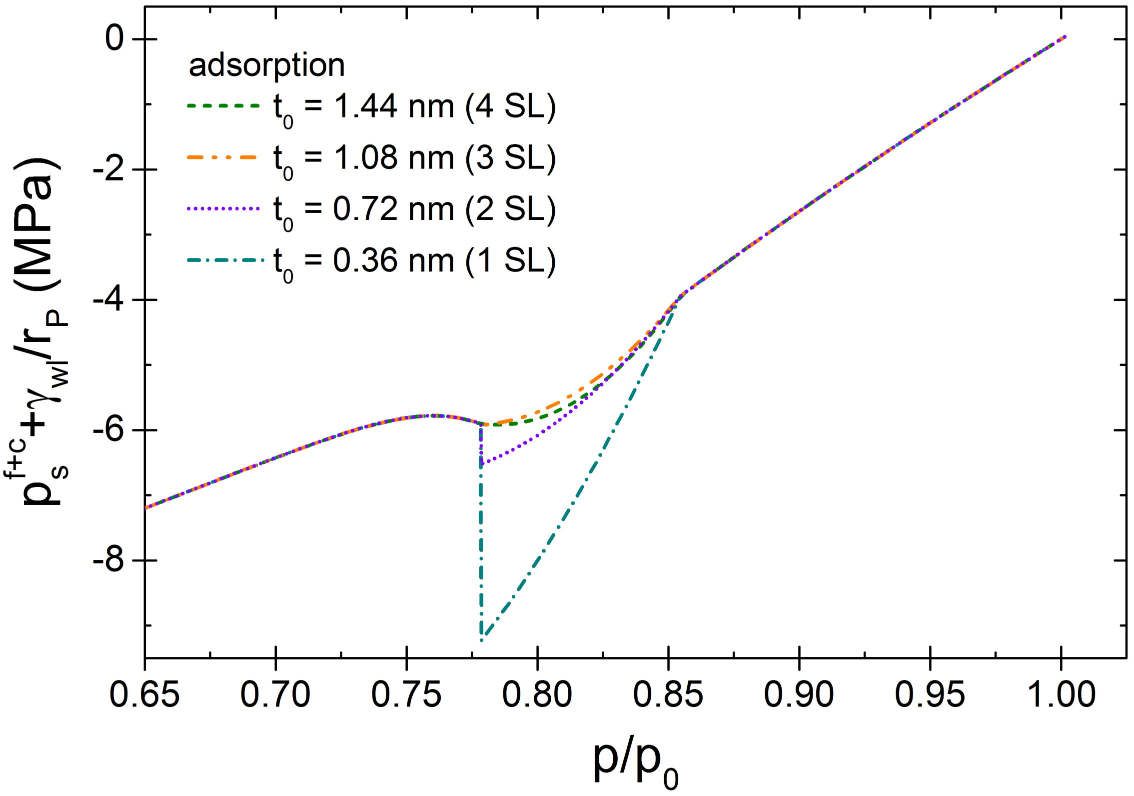

FIGURE 8.6 – *During adsorption the solvation pressure* p_s^{f+c} *fits best to the measured deformation curve if there is no step in the thickness of the adsorbed layer or if the thickness* t *jumps to* $t_0 = 1.08$ *nm at* f_c^{ads} *[cp. figures 8.1(b) and 8.7]. At least the first two surface layers remain stable when capillary bridges form.*

With the expanded model (equation 8.6) it is thus possible to determine the geometrical arrangement during sorption of the adsorbate using deformation measurements. The comparison between the measured deformation and the theoretical behaviour during adsorption reveals that both a rearrangement of the fourth and also the third adsorbed layer in favour of the formation of capillary bridges as well as the stability of the film consisting of four monolayers at f_c^{ads} are possible (cp. figure 8.7). From theoretical considerations it is known that there is a “stability limit for the thickness of” adsorbed films and consequently during adsorption the adsorbate forms capillary bridges above a metastable limit for the film [67, 147]. This is also shown in the sketched behaviour for the film thickness (cp. possible plateau values in figure 8.7). The calculations shown in figure 8.6 show that the third and fourth layer can be in a metastable state, but clearly at least the first two surface layers of argon are stable. In contrast, during desorption at maximum one monolayer remains absorbed on the pore walls above f_c^{des}.[6] Apparently, it is easier to remove argon atoms from the (second and higher) surface layers than from the concave

---

[6] The finding of such a small surface layer during the desorption process may lead to the necessity to correct pore radii determined with the aid of the Halsey equation because the pore radius r_P should be calculated as the sum of the Kelvin radius and the thickness of this layer only (cp. section A.2).

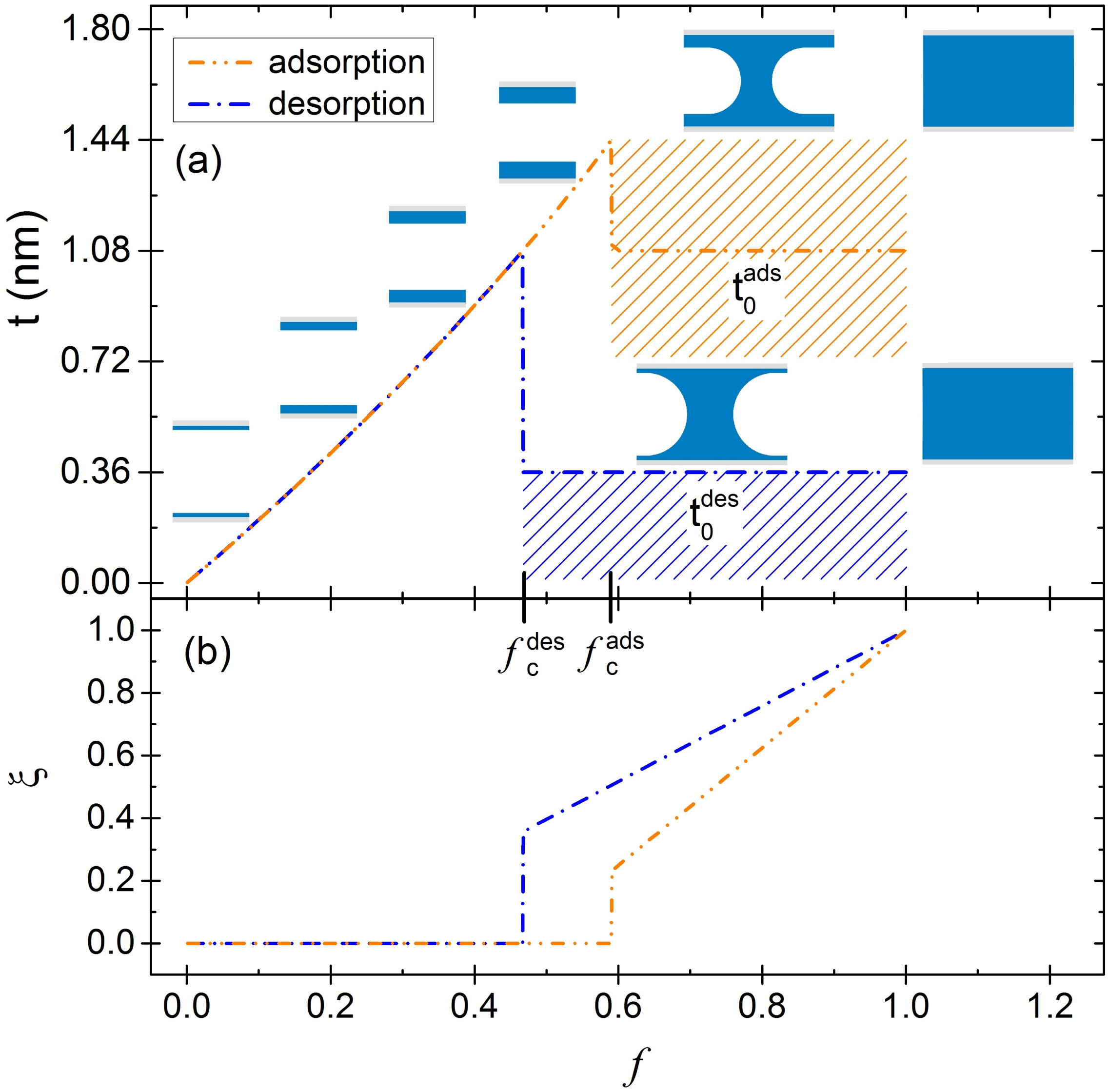

Figure 8.7 – *(a) The thickness of the adsorbed film during sorption of argon as a function of the filling fraction f. For the filling range with coexistent capillary bridges and adsorbed surface layers, the thickness of these layers differs between adsorption and desorption. During adsorption the thickness of the layers, t_0^{ads}, can correspond to values in the shaded area between 0.72 nm and 1.44 nm (two to four monolayers). During desorption only a thinner layer of at maximum one monolayer is possible above f_c^{des} (shaded area 0 nm $\leq t_0^{ads} \leq 0.36$ nm). (b) Also the fraction of capillary bridges ξ differs between adsorption and desorption. The lines are for a thickness $t_0^{ads} = 1.08$ nm (three monolayers) during adsorption above f_c^{ads} and $t_0^{des} = 0.36$ nm (one monolayer) during desorption above f_c^{des}.*

hemispherical menisci. The analysis of the measurements suggests that during desorption capillary bridges vanish in favour of thicker surface layers at f_c^{des} (see schematic sketch in figure 8.7).

Conclusions

In this chapter the model by Gor and Neimark describing adsorption-induced deformation was expanded to account for the coexistance of capillary bridges and adsorbed layers. This makes it possible to explain the measured deformation behaviour of porous Vycor® glass during sorption of argon. The comparison between theory and experiment shows that during adsorption at least the first two layers are stable. During desorption only a thin surface layer (at maximum one monolayer) is present as long as there are capillary bridges. When these capillary bridges disappear, however, a thicker layer is formed, which indicates that then surface layers are more stable up to a certain thickness (2-3 monolayers). An inclusion of the actual pore size distribution of the porous sample can yield an even better agreement between theory and experiment as it naturally leads to a smoothening of the thickness dependence (in figures 8.4 and 8.7) and of the contraction peak (in figure 8.5). The ultrasonic measurements show that the elastic properties change significantly during filling [$5-10\%$, see figures 8.1(c) and 8.2(b)+(d)]. But the observed change of the elastic properties during sorption is at least not the major reason for the strong contraction peak during desorption.

The fact that the sharp contraction peak during desorption has not been observed for other systems raises the question for the reason of this difference. Different interaction between adsorbate and the porous sample (cp. section 9) as well as the very long times spend to reach equilibrium after each filling step might account for this different behaviour. The analysis method presented in this chapter can together with further measurements help to resolve the correlations between the configuration of the adsorbate, the interaction between adsorbate and porous sample, and the deformation behaviour.

Chapter 9

Strongly enhanced elastic modulus of solid nitrogen in nanopores

The chapters 2-7 addressed the phase behaviour of argon and the possibility to extract the intrinsic elastic properties of adsorbate in nanoporous glass from ultrasonic measurements of the effective elastic moduli. The confined argon exhibits a shear modulus that corresponds to the modulus of bulk argon, however, this behaviour cannot necessarily be generalized to substances other than argon. The noble gas argon has a spherical structure, which limits the interactions of the adsorbate mainly to the van der Waals forces. For diatomic molecules, even for such a simple one like nitrogen, the interations are complicated due to the presence of electrical moments. In this chapter the previously developed analysis method (see section 2.2.2 and chapter 5) is applied to ultrasonic measurements on nitrogen in nanoporous glass. Solid nitrogen has considerably enhanced elastic properties in the nanopores of the porous glass sample. Particularly, the first adsorbed molecular layer near the pore wall possesses a shear modulus more than twice as high as the modulus of bulk nitrogen. The interaction between pore surface and pore filling provides a mean for the enhancement of elastic properties. This discovery shows that nanoconfinement in porous samples can be used to influence the mechanical properties of substances.

During cooling of a sample filled with approximately one surface layer of nitrogen [virtually constant volume filling fraction $f \approx 0.12$,[1] cp. figure 9.1(b)] or completely filled pores [cp. figure 9.1(c)], the effective shear modulus of the (partially) filled sample starts to increase below a temperature of $T \approx 55$ K (see figure 9.2); bulk nitrogen freezes at 65 K [148]. This is a clear sign that the adsorbed nitrogen starts to freeze (and crystallize) on cooling. As expected the increase is considerably higher for the completely filled sample as more nitrogen can crystallize. A close look reveals, however, a peculiarity: One surface layer of nitrogen, i.e only $\approx 12\%$ of the amount necessary for complete filling, causes an increase of the effective shear modulus that corresponds to about 20% of the increase observed for complete filling. This contrasts with the observance for argon, where surface layers contributed proportional to their filling fraction with the shear modulus of bulk argon

---

[1] The filling fraction f can be regarded as constant over the whole temperature range. The amount of nitrogen vapour in the sample cell is negligible due to the low vapour pressure of nitrogen below 60 K and the small volume of the sample cell. A similar statement holds for argon (see figure 3.1 in section 3.1).

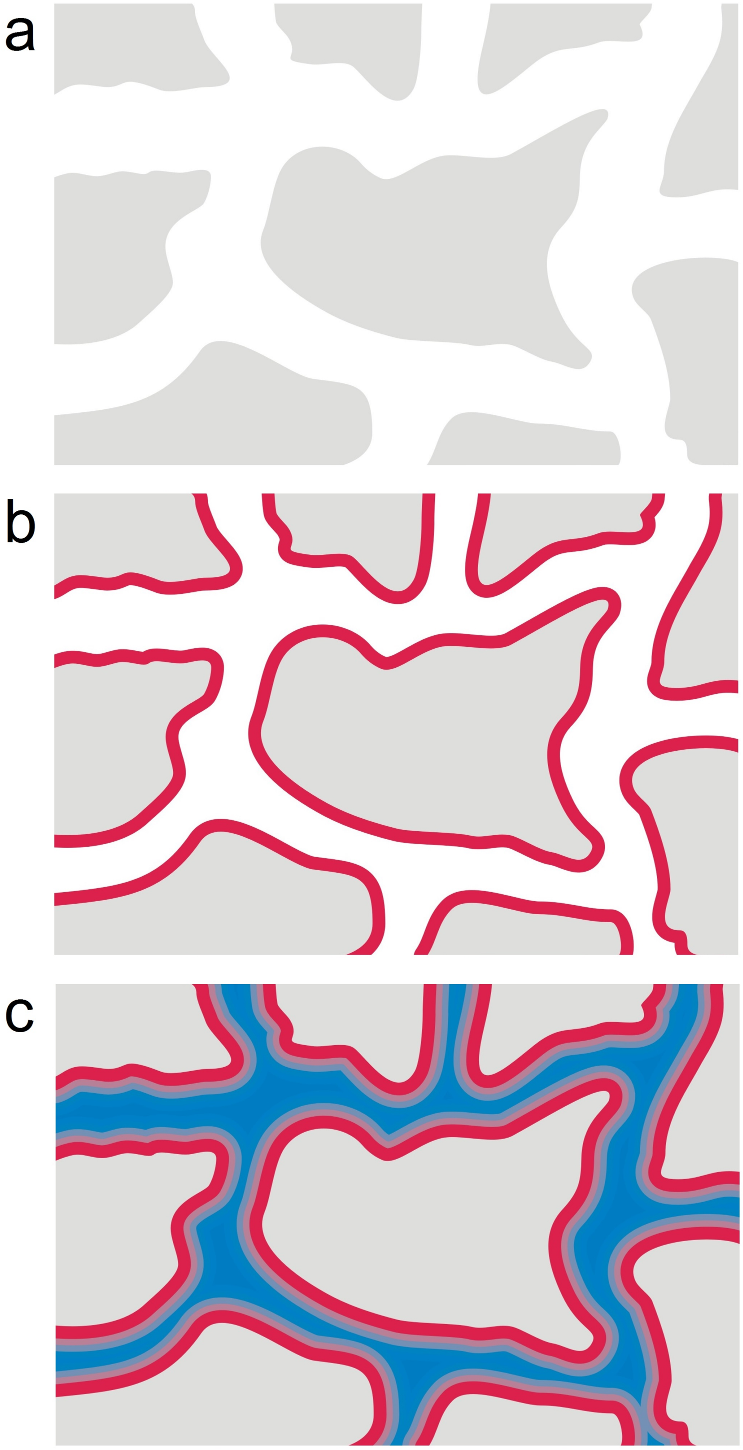

FIGURE 9.1 – *Schematic sketch of nanoporous Vycor® glass for different fillings. (a) Structure of the empty sample. (b) At low fillings with nitrogen the adsorbate forms a surface layer (red) with enhanced elastic properties on the pore walls. (c) The completely filled sample. The influence of the pore wall on the filling decreases gradually with increasing distance from the wall. The analysis shows that in the pore centre bulk properties (marked in blue) are reached. Figure from [6] (Copyright © 2013 by the American Physical Society).*

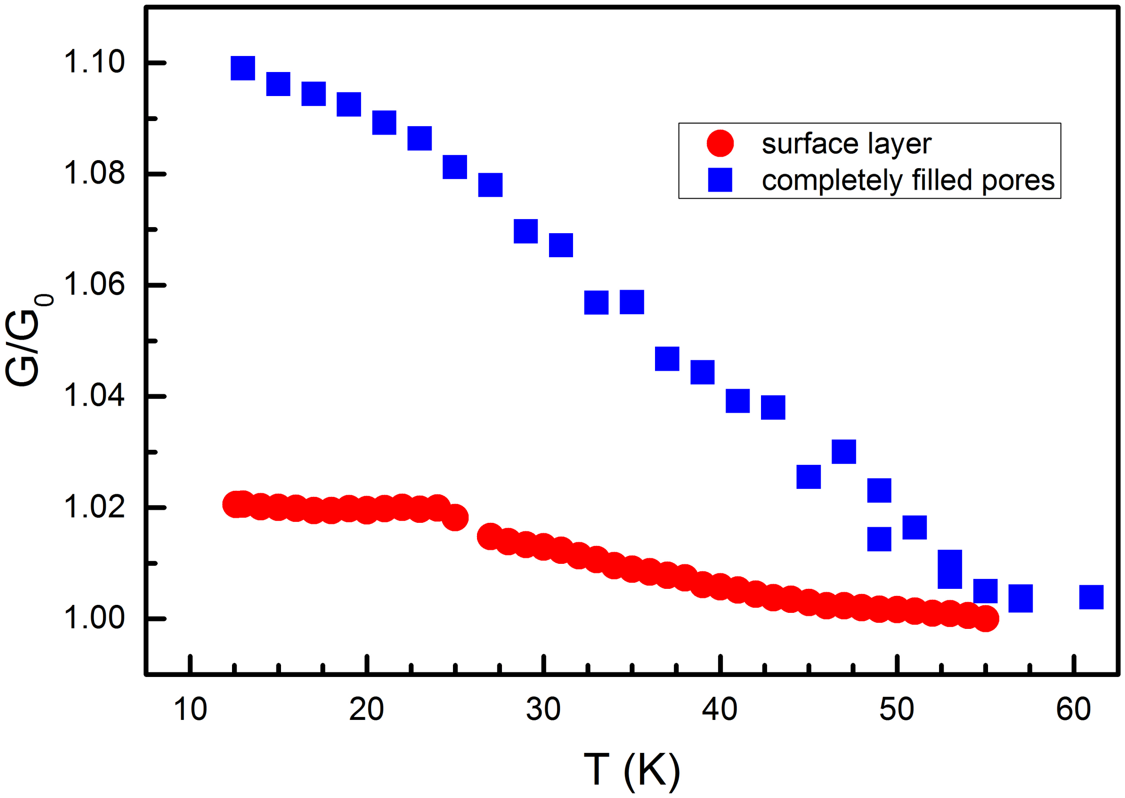

FIGURE 9.2 – *Effective shear modulus of the sample scaled with the modulus of the empty sample at two different fillings: During cooling the effective modulus starts to increase below a temperature of about 55 K. The increase is considerably higher for complete filling ($f = 1$) than for one surface layer ($f \approx 0.12$). At the lowest temperature, however, the increase for the surface layer corresponds to about 20% of the increase for the completely filled sample. Figure from [6] (Copyright © 2013 by the American Physical Society).*

(cp. section 3.1).

The unusual behaviour of the effective shear modulus at different fillings of nitrogen shown in figure 9.2 signifies already different elastic properties of the pore filling. Obviously, the first adsorbed surface layer near the pore wall possesses a higher shear modulus than the rest of the adsorbate or the whole pore filling in the case of complete filling.

With the effective medium analysis for the determination of the intrinsic shear modulus of pore fillings $G_{filling}$ (cp. equations 2.7 or 5.4 for $M = G$ and $G_{pore} = fG_{filling}$) it is possible to quantify the differences between the shear modulus of different fillings. The average of the modulus of the pore filling for both measurements is shown in figure 9.3(a). For both fillings the average shear modulus increases over a broad range with decreasing temperature. This confirms that the adsorbed nitrogen in the nanopores freezes continuously; a reduction of temperature increases the fraction of solid nitrogen. Below $T \approx 25\ K$ the shear modulus of one surface layer remains almost constant and the nitrogen layer seems to be completely frozen.

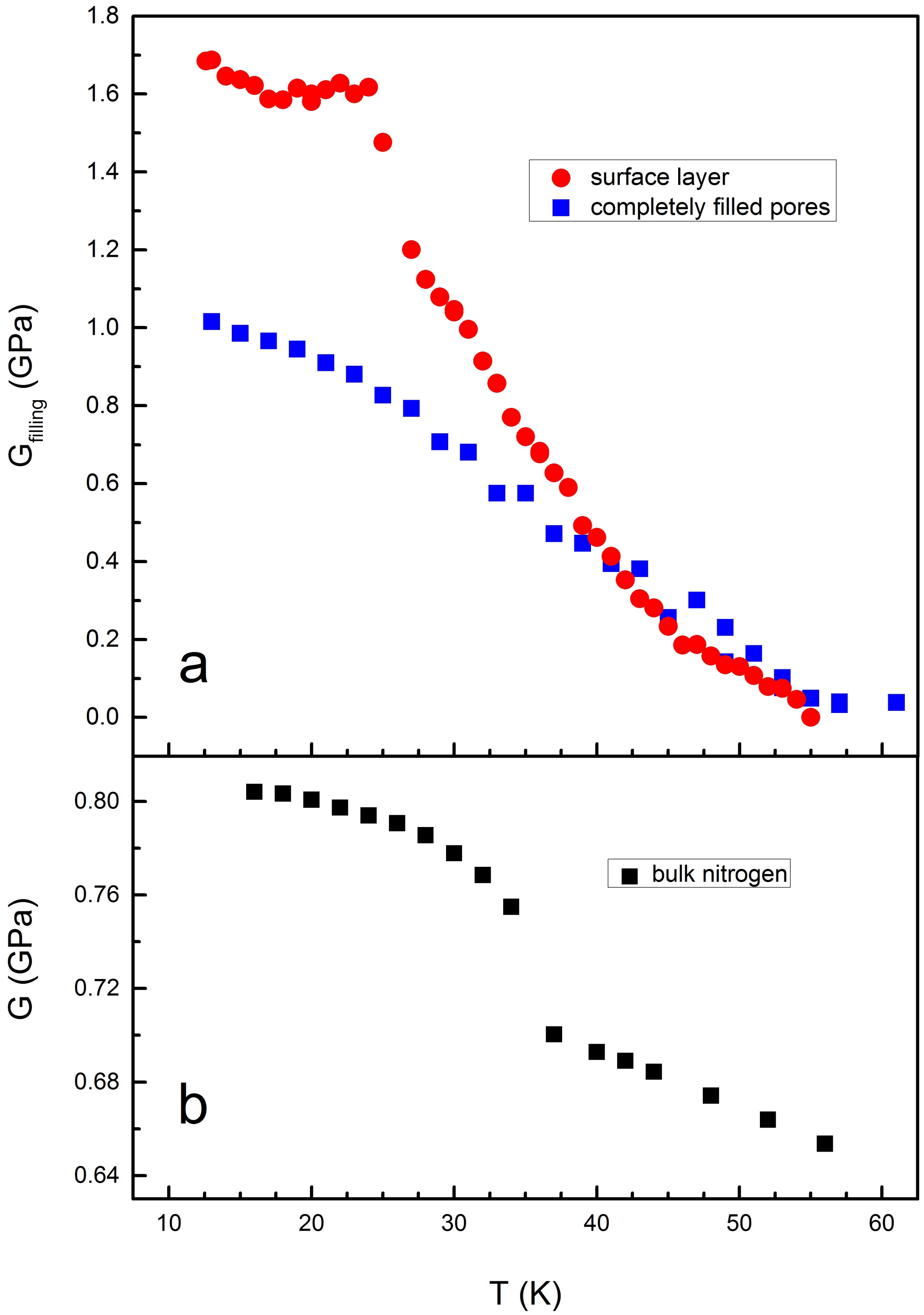

FIGURE 9.3 – *Shear modulus of one surface layer, of the adsorbate for completely filled pores, and of bulk nitrogen as a function of temperature. (a) Below* ≈ 40 *K the modulus of the surface layer deviates considerably from the modulus of the complete pore filling, reaching a value of* ≈ 1.7 *GPa at low temperatures. In comparison, the complete pore filling has a modulus of only* ≈ 1.0 *GPa. (b) At low temperatures the shear modulus of bulk nitrogen (calculated from ultrasonic measurements [149]) corresponds to less than* 50% *of the value for one surface layer. Figure from [6] (Copyright © 2013 by the American Physical Society).*

The conclusions drawn from the increase of the effective shear modulus (see above and figure 9.2) are further confirmed by the moduli of one surface layer and the complete pore filling [see figure 9.3(a)]: Whereas the modulus of the complete filling is in the range of 1.0 GPa at low temperatures, the first layer exhibits an unusual high modulus around 1.7 GPa. For comparison the elastic properties known for bulk nitrogen are shown in figure 9.3(b) [149]. Solid bulk nitrogen changes its crystalline structure from hexagonally closed packed (β-phase) to face centred cubic (α-phase) during cooling ($T \approx 35$ K) [149]. This structural transformation is accompanied by an increase of the shear modulus [cp. figure 9.3(b)]. At low temperatures the shear modulus of bulk nitrogen is only 0.8 GPa [see figure 9.3(b)].

There is no step in the average shear modulus that would hint to a structural transformation of the crystal structure of the adsorbate, which clearly suggests that the α-phase is supressed in the nanopores. This is in accordance with x-ray measurements of two similar types of completely filled porous glass samples: the confinement in nanopores prevents the transition of the crystalline structure from the β-phase to the α-phase [150]. At low temperature a quasi-hcp structure (with lattice defects) is maintained in the pore centre [150]. This absence of a reorientation during cooling shows an influence of nanoconfinement on nitrogen. The impact of confinement in pores on the structure of the pore filling is known for different porous systems and can result in strains, different crystalline structure or induce disorder in the first few surface layers near the pore wall [24, 150–152]. The structure of a thin nitrogen layer adsorbed on pore walls of porous glasses has sometimes been described as amorphous or liquid-like [150, 152]. But the x-ray diffraction patterns can also be interpreted as resulting from a two-dimensional triangular lattice [152].

The observance that the average shear modulus of the completely filled pore ($G_{filling} \approx 1.0$ GPa at ≈ 12.5 K) is only $\approx 25 - 30\%$ higher than the bulk modulus reveals that the greatest part of the filling possesses the elastic modulus of bulk nitrogen. Indeed, the deviation can be explained by a simple superposition of approximately two surface layers ($f_{2SL} \approx 0.25$) with an enhanced modulus and the remaining pore filling with bulk properties: $G_{filling} \approx f_{2SL} G_{surface} + (1 - f_{2SL}) G^{\beta}_{bulk}$, where $G_{surface} \approx 1.7$ GPa and $G^{\beta}_{bulk} \approx 0.76$ GPa [taken from a linear extrapolation of the shear modulus of the β-phase of bulk nitrogen at ≈ 12.5 K, cp. figure 9.3(b)]. Of course, also a continuous transition from the high surface values to bulk properties in the pore centre is possible.

The high shear modulus of the surface layer must be related to the pore wall, i.e. to the structure of the surface, its chemical properties and possibly also the high curvature. The influence of the pore wall is reduced with increasing distance to the wall and the pore centre may exhibit “normal” (bulk) properties [cp. figure 9.1(c)]. The interaction between the pore surface and the nitrogen molecules thus provides a mean for considerably enhanced elastic properties of the adsorbed surface layer. But the observance of bulk elastic properties for argon (cp. sections 2.2.2 and 3.1) confined in the same porous sample poses a question: Why does nitrogen show enhanced elastic properties and argon does not?

Both substances have bulk shear moduli of the same order. Argon has a spherical structure, whereas nitrogen is a diatomic molecule with a quadrupole moment. It appears important to consider how the electrical and chemical properties influence or even determine the elastic properties of the surface layer. Previously, an infrared spectroscopy study had shown that the pore wall influences the nitrogen molecules in the first two surface layers; whereas pore condensate in the pore centre remains bulk-like, i.e. infrared inactive [148]. The porous glass has a polar pore surface with silanol OH-groups [148]. It is known that the interaction of hydroxyl groups with nitrogen is much stronger than for argon [153]. This stronger hydrogen bonding is certainly the crucial factor that gives rise to the high elastic modulus of the adsorbed nitrogen layer. It is also well-known, that the interaction of the quadrupole moment of nitrogen with hydroxyl groups results in an orientation of the adsorbed nitrogen molecules and a higher density of molecules per surface area [61]. Taking such a higher density into account would result in even higher values for the shear modulus of the surface layer compared to those displayed in figure 9.3(a).[2] So in any case the surface layer exhibits a considerably enhanced modulus compared to bulk nitrogen.

The above interaction and possibly also the influence of the amorphous (and heterogeneous) pore wall of the porous glass sample can impose a certain structure and a different crystalline structure on the first few nitrogen layers. Therewith, the basis is formed for the observed enhanced elastic properties of nitrogen near the wall. In addition, the diatomic structure of nitrogen possibly causes more difficulties for the pore filling to accomodate to the pore surface and higher strains are induced.

Conclusions

The discovery of considerably enhanced elastic properties of nitrogen confined in nanopores shows that nanoporosity can be used to change elastic properties of substances. The surface of pore walls is of particular importance and determines the degree of influence on the elastic behaviour of adsorbed substances. Besides the amorphous or cyrstalline structure of the pore walls, also the polarizability and existing electrical moments of pore surface and adsorbed substances can have an effect on the elastic properties of adsorbed layers. The differences between the strength of the binding of argon and nitrogen to OH-groups can explain the observed differences in the elastic properties of both adsorbates. Thus the increase of the shear modulus of adsorbed layers in comparison to the bulk shear modulus should be particularly high for systems with a strong binding between the adsorbed molecules and the pore surface. The further investigation of the fundamental correlations

---

[2] For the determination of the intrinsic shear modulus with the aid of equation 5.4 (for $M = G$ and $G_{pore} = fG_{filling}$) the volume filling fraction f must be known. The number of adsorbed molecules, n, scaled to the number necessary for complete filling, n_0, was determined experimentally. The density of the adsorbed nitrogen was regarded as independent of the filling, i.e. $f = V_{ads}/V_{pore} = n/n_0$. If the density of the first surface layer, ρ_{SL}, differed from the average density of the pore filling, ρ_{avg}, the filling fraction $f = 0.12$ would have to be replaced by $f' = \rho_{avg}/\rho_{SL} \cdot f$. According to Eq. 5.4 (for $M = G$ and $G_{pore} = fG_{filling}$) a possibly higher density of the first nitrogen layer [61] would thus correspond to a value of the shear modulus of this layer that is even higher than the calculated modulus. For completely filled pores always $f = f' = 1$ holds, so that $G_{filling}$ is determined correctly (even without knowing the exact density).

between the mechanical and electrical properties of nanoporous systems and adsorbed substances and its influence on the elastic properties in nanopores will help to provide tools for the tuning of mechanical properties.

Conclusions and Outlook

Ultrasonic measurements have proven as a particular good method to study liquid-solid phase transitions and the elastic properties in the nanopores of porous Vycor® glass. Together with the simultaneous measurement of the filling fraction of the pores, the effective elastic moduli (shear modulus and longitudinal modulus) can be determined. These effective elastic moduli supply some first information on the phase state of the adsorbate: The measurements of sorption isotherms at varying temperatures between 75 K and 50 K evidenced that some liquid argon (up to a filling fraction f_1) remains in the pores even $\approx$ 26 K below the onset of freezing (at $\approx$ 76 K). A reduction of the temperature within this range results in a continuous decrease of f_1, however, near 50 K no appreciable change can be observed. From these isothermal measurements information on the geometrical arrangement of the adsorbate during filling arise via an effective medium analysis: Below a temperature $T \approx 76$ K solid surface layers of argon form on top of liquid-like layers above the temperature-dependent filling fraction f_1 (corresponding to the linear increase of G/G_0 in region II, cp. figure 2.4). Only at a considerably higher filling fraction f_2 solid capillary bridges form.

The effective medium analysis offers further findings on grounds of its capability to determine from the measured effective moduli the elastic properties of the adsorbate itself. Both the shear modulus and the longitudinal modulus of nanoconfined solid argon are about equal to the corresponding moduli of bulk argon, i.e the nanoconfinement has no notable effect on the elasticity of the solid argon. For pores that are completely filled with liquid argon, also the longitudinal modulus of this liquid is about equal to the longitudinal modulus of liquid argon. The formation of concave menisci at the pore ends during the initial desorption process at virtual complete filling of the pores results, however, in a slight influence on the longitudinal modulus of the adsorbed argon: The decrease of the radius of curvature of the concave hemispherical menisci is related to an increase of the negative Laplace pressure and a decrease of the longitudinal modulus of the pore filling by a few per cent. In addition, at partial fillings adsorbed liquid argon layers contribute to the longitudinal modulus of the pore filling only in consequence of the formation of solid layers on top of these layers and the related loss of the liquid layers' mobility.

The confinement in the nanopores results in considerable changes of the phase behaviour of argon as the above mentioned sorption isotherms at different temperatures foreshadowed. Temperature cycles with one and two adsorbed surface layers of argon on the pores walls reveal a continuous freezing and melting of these two layers over a very broad temperature range of at least 40 K. Thus it could be shown that at very low temperatures (around 20 K) also these layers solidify completely in contrast to previous assumptions [29]. Argon in completely filled pores shows also a pronounced confinement effect in terms of a continuous phase transition over about 45 K. These observed phase transitions are related to the effect of premelting and interfacial melting (on flat substrates) that is particular well-known for ice [91, 94]. But for argon in nanopores there are significant deviations from this known behaviour, notably the temperature-dependence differs. These differences certainly originate in the strong curvature and the heterogeneous structure of the pore walls (cp. e.g. also reference [35]). The presence of solid argon in the pore centre influences the phase behaviour of the first two surface layers insofar as this solid argon impresses its structure on the first two layers near the pore wall. This results in an increase of the freezing temperature of the first layers by about 10 K in comparison to fillings with solely one or two adsorbed layers.

The Laplace pressure of concave menisci at the pore ends causes both a change of the longitudinal modulus of the pore filling as well as a deformation of the porous sample. The latter behaviour is a phenomenon that is particularly known for liquids in porous systems (see e.g. reference [97]). Not only the Laplace pressure but also changes of the surface free energy as a consequence of adsorption lead to the so-called effect of sorption-induced deformation [44]. The analysis of deformation measurements during sorption of argon showed that for the explanation of the deformation behaviour the coexistance of capillary bridges and adsorbed surface layers has to be considered. The comparison between theory and experiment shows that at least the first two monolayers forming during adsorption are stable when capillary bridges form. During desorption a thin surface layer with a maximum thickness of one monolayer is present as long as there are capillary bridges. When these capillary bridges disappear, however, a thicker layer is formed, indicating that surface layers of argon are more stable up to a certain thickness ($\approx 2-3$ monolayers).

All deformation measurements with the adsorbate argon exhibit the sharp contraction peak during desorption that is associated with the stability of surface layers. This contrasts to other earlier measurements, e.g. for water in Vycor® glass [50]. The interaction between the pore walls and the adsorbate argon differs from the interaction with water and might constitute a factor influencing the stability of adsorbed surface layers. But possibly also a deviation from the equilibrium state [if the system is not given enough time after a filling (or emptying) step] may account for an absence of the contraction peak.

The ultrasonic measurements with adsorbed nitrogen distinctively showed that the preservation of the elastic bulk properties in confinement is not a general phenomenon. Indeed, the discovery of a considerably enhanced shear modulus of nitrogen confined in nanopores shows that nanoporosity can be used to change elastic properties of substances.

The discussed findings can have some impact on forthcoming studies of phase transitions and elastic properties in nanopores as well as the adsorption-induced deformation. Together with further measurements the methods will help to resolve the correlations between the configuration of the adsorbate, the interaction between adsorbate and porous sample, the elastic properties, and the deformation behaviour. The analysis of ultrasonic measurements allows to determine the state of the phase and the elastic properties of adsorbate in pores filled with surface layers and in completely filled pores, which is a very common phenomenon in nature, e.g. also for water in porous rocks. The measurements with the adsorbate nitrogen instead of argon evidenced already what a unusual elastic behaviour can be found in nanopores. The transfer of the ultrasonic technique presented in this dissertation from the model system to other more complex adsorbates and different porous samples will contribute to a further enlightenment of the complex confinement effects in nanopores. For this, in particular a variation of the structure of the pore walls (e.g. crystallinity, polarizability) and of the adsorbate (with different electrical and mechanical properties in its bulk state) seems a promising direction for further studies and for the research of possibilities to tune mechanical properties.

Appendix A

Experimental setups and details

For the studies of the liquid-solid phase transition, the elastic properties and the adsorption-induced deformation presented in this dissertation different sample cells were constructed. In the following sections the measurement methods and the experimental setups are described.

All sample cells are mounted on the cold head of a cryostat and are surrounded by an insulation vacuum ($p \lesssim 5 \cdot 10^{-6}$ mbar) for the measurements at the required low temperatures (cp. schematic sketch in figure A.1). For the regulation of the temperature each sample cell includes a temperature sensor (silicon diode) and a heating resistor that are connected to a temperature controller. This makes it possible to stabilize the temperature to the required value (fluctuations smaller than ±10 mK). The absolute accuracy of the measured temperature is ±0.25 K.

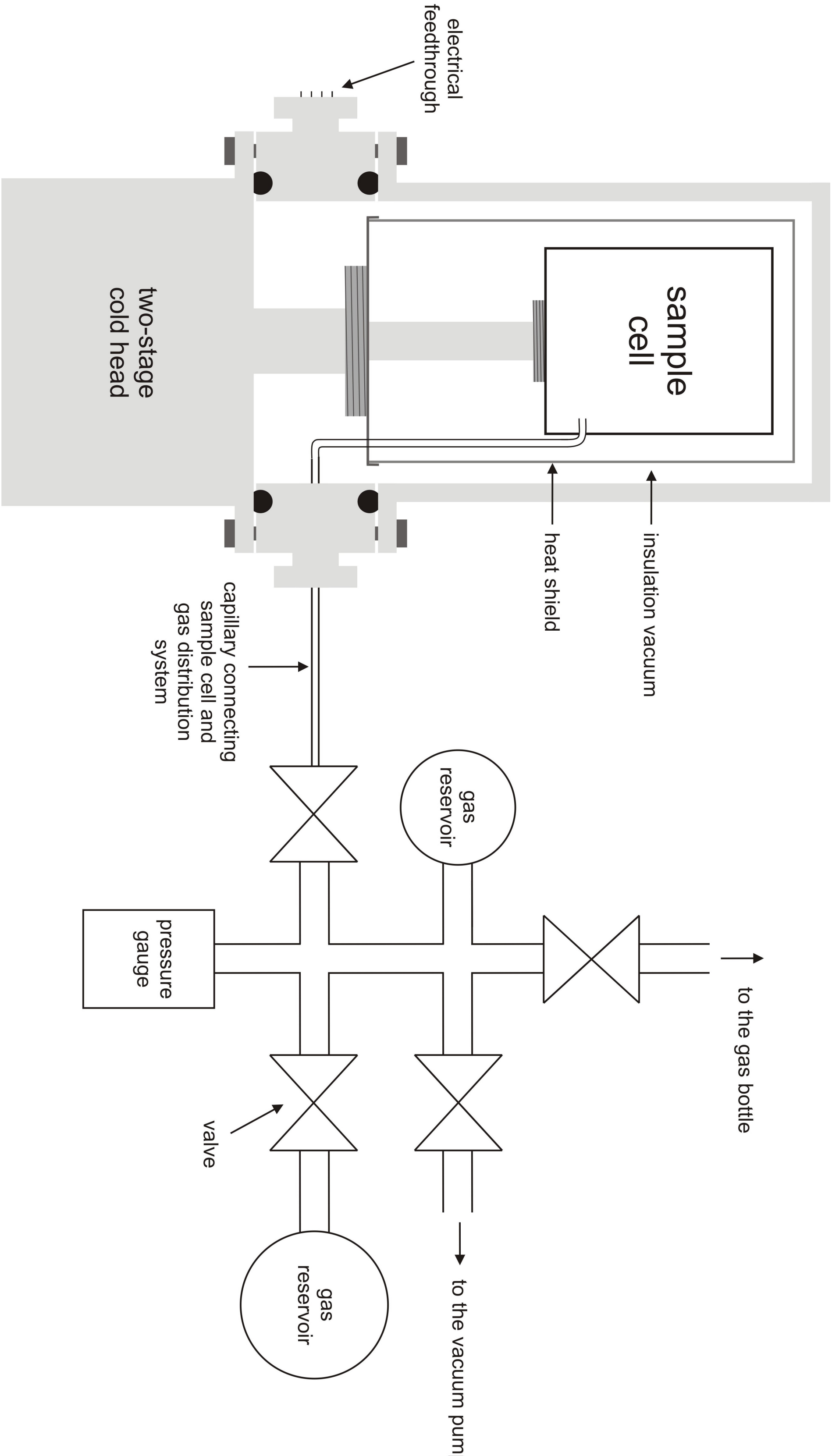

Figure A.1 – *Sketch of an experimental setup with cold head and gas distribution system.*

A.1 Filling of the samples

During the measurement of a sorption isotherm, the nanporous Vycor® glass sample (Corning, Inc.) must be filled with exactly determined quantities of argon. Also for the measurements of temperature cycles with constant fillings, it is necessary to know the amount of adsorbate in the porous sample. Therefore each sample cell is connected via a metallic capillary (diameter ≈ 1 mm) to a gas distribution system with several valves, one or two pressure gauges, and metallic containers (see schematic sketch in figure A.1). With the gas distribution system defined quantities of argon (or also nitrogen) gas can be given into the sample cell. The quantity can be calculated with the ideal gas equation from the pressure before and after each filling step using the temperature of the sample cell, the temperature of the gas distribution system and the volumina of the gas distribution system (including capillary). Consequently, the molar amount of added adsorbate, Δn^i, and the filling fraction of the sample after a series of filling steps, $f = \left(\sum_i \Delta n^i\right)/n_0$ (with n_0 being the molar amount of adsorbate necessary for complete filling), can be determined.[1] For all measurements the density of the adsorbate, ρ_{ads}, is considered to be independent of the position of the adsorbate in the pores, thus that the filling fraction f is identic with the volume of the adsorbed substance scaled to the total volume of the pores, i.e. $f = n/n_0 = V_{ads}/V_{pore}$.

Small fluctuations of the temperature in the laboratory that are present in spite of an air-conditioner influence to a minor degree the measured pressure in the gas distribution system and hence the calculated filling fraction f. For a damping of the oscillations of the room temperature with an interval of ≈ 40 minutes caused by the air-conditioner, the gas distribution systems were isolated (amongst others with styrofoam). The remaining fluctuations (typically $\Delta T \lesssim \pm 0.5$ K) were insignificant (as they resulted in pressure

---

[1] Before a filling step the gas distribution system (with the volume V_{GDS} at the temperature T_{GDS}) is filled with a certain pressure of gas, p^i_{GDS} (the valve to the sample cell is closed). In addition, there is some vapour (pressure $p^{i-1'}_{SC}$) in the sample cell (with the volume V_{SC} at the temperature T_{SC}) and some adsorbate Δn^{i-1} in the pores of the sample (if it is not the first filling step). Thus, for the total molar amount of the molecules in the experimental setup before the opening of the valve the ideal gas equation yields:

$$n_{total} = \frac{p^i_{GDS} V_{GDS}}{RT_{GDS}} + \frac{p^{i-1'}_{SC} V_{SC}}{RT_{SC}} + \Delta n^{i-1}, \tag{A.1}$$

with the gas constant R. After the opening of the valve a new equilibrium pressure $p^{i'}_{GDS} = p^{i'}_{SC}$ is reached and some additional adsorbate Δn^i has formed:

$$n_{total} = \frac{p^{i'}_{GDS} V_{GDS}}{RT_{GDS}} + \frac{p^{i'}_{SC} V_{SC}}{RT_{SC}} + \Delta n^{i-1} + \Delta n^i \tag{A.2}$$

Consequently, the amount of adsorbate, Δn^i, added in one filling step can be calculated according to

$$\Delta n^i = \frac{V_{GDS}}{RT_{GDS}} \left(p^i_{GDS} - p^{i'}_{GDS}\right) + \frac{V_{SC}}{RT_{SC}} \left(p^{i-1'}_{SC} - p^{i'}_{SC}\right). \tag{A.3}$$

For the consideration of the molecules in the capillary (with the volume V_C at the temperature T_C) the additional term $V_C/\left(RT_C\right)\left(p^{i-1'}_{SC} - p^{i'}_{SC}\right)$ has to be added on the right hand side of equation A.3.

variations near the range of the resolution limit of the pressure gauges, see figure A.7 in section A.4).

Sorption dynamics are rather complex [63, 154]. Because of a spatial rearrangement of the adsorbate after each filling step very long waiting times were necessary to reach the equilibrium pressure after each change of the filling during the measurement of a sorption isotherm. Therefore the measurement of a complete sorption isotherm needs a long time: Already in the liquid regime of the adsorbate typically about a month is necessary. The lower the temperature, the longer the waiting times to reach a constant pressure after a filling step. At a temperature of 50 K the measurement of an incomplete adsorption isotherm required already 4 months. (At a filling of $f \approx 0.7$ the measurement was stopped because of a defect of the cold head.)

A.2 Characterization of the porous samples

For the characterization of the porous Vycor® glass samples, i.e. the determination of the average pore radius, the pore size distribution and the porosity, sorption isotherms with liquid argon (usually at $T = 86$ K) were used. The porosity ϕ of the sample is easily calculated from the ratio of the volume $V_{ads,0}$ of the molar amount of adsorbate necessary for complete filling, n_0, and the volume of the porous sample, V_{sample}:

$$\phi = \frac{V_{ads,0}}{V_{sample}} = \frac{n_0 m_M}{\rho_{ads} V_{sample}}, \tag{A.4}$$

with the molar mass m_M and the density of the adsorbate, ρ_{ads}.

The pore size distribution was determined from the desorption branch of sorption isotherms. Following the usual assumption of cylindrical pores [155], the radius of withdrawing menisci in the steep part of the desorption branch (cp. figure 1.3) was determined with the Kelvin equation [59, 60] (assuming complete wetting):

$$r_K = -\frac{2\,\gamma_{lv}\,V_m}{R\,T\,\ln\left(p/p_0\right)} \tag{A.5}$$

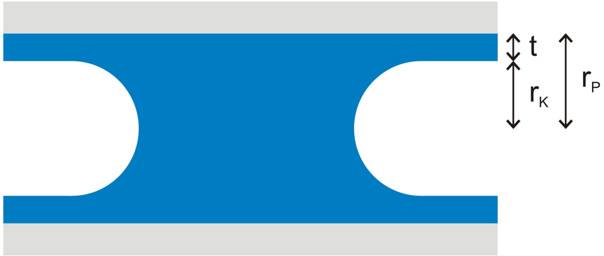

FIGURE A.2 – *The pore radius r_P is estimated as the sum of the radius of curvature r_K determined from the Kelvin equation and the thickness t of the film remaining on the pore walls.*

The Halsey equation [61] was used to estimate the thickness t of the remaining surface layer (see figure A.2):

$$t = u \cdot \sqrt[3]{-5/\ln(p/p_0)}, \tag{A.6}$$

with the thickness u of one monolayer of the adsorbate.

The sum of both quantities forms the pore radius r_P:

$$r_P = r_K + t \tag{A.7}$$

The pore radius with the highest occurance (determined from the steepest point of the desorption isotherm) is denoted the average pore radius. For most samples this average pore radius is 4.0 nm. The pore size distributions determined from the desorption branch of an isotherm are rather sharp (cp. figure 1.2), which corresponds to previous studies (see e. g. reference [155]). But as mentioned in section 1.1 (see footnote 1 on page 3) draining mechanisms, in particular the pore-blocking effect (cp. section 1.2), may result in a distorted picture of the actual distribution.

A.3 Ultrasonic measurements

In order to investigate the liquid-solid phase transition during temperature cycles ultrasonic shear waves and longitudinal waves were used. Shear waves are a particular good indicator for liquid-solid phase transitions [85–87] as liquids cannot sustain shear stress; the shear modulus is only increased if there is solid adsorbate. But also longitudinal waves can provide significant information on the elastic properties (see chapter 6).

The effective elastic moduli of the samples were determined via the pulse-echo-method. Short ultrasonic pulses ($\Delta t_{pulse} \approx 2 - 2.5\ \mu s$) are generated by appling voltage pulses to a piezo-crystal (both sides are coated with a thin gold film) that is glued with an silver epoxy composite on the sample (see figure A.3 for a sketch of one of the two sample cells for ultrasonic measurements). The used piezo-crystals are always $LiNbO_3$: 36°Y-cut for the generation of longitudinal waves and 41°X-cut for shear waves [142]. The carrier frequency of the ultrasonic pulses varies for the different measurements between $\approx$ 6 MHz and $\approx$ 13 MHz. The wavelength λ is in the range between one hundred and a few hundred micrometres, i.e. it is much larger than the pore size ($\lambda \gg r_P$).

The generated ultrasonic pulse propagates through the sample with a length l, is reflected at the end of the sample and returns to the piezo-crystal. Thus the transit time Δt necessary for the propagation of the ultrasonic pulse through the sample can be determined using a (digital) oscilloscope. The accuracy of the measured transit time of typically $\Delta t \approx 2 - 5\ \mu s$ is better than 1 ns. Subsequent reflections of the ultrasonic pulse results in a series of attenuated echos (see figure A.4). For the ultrasonic velocity c

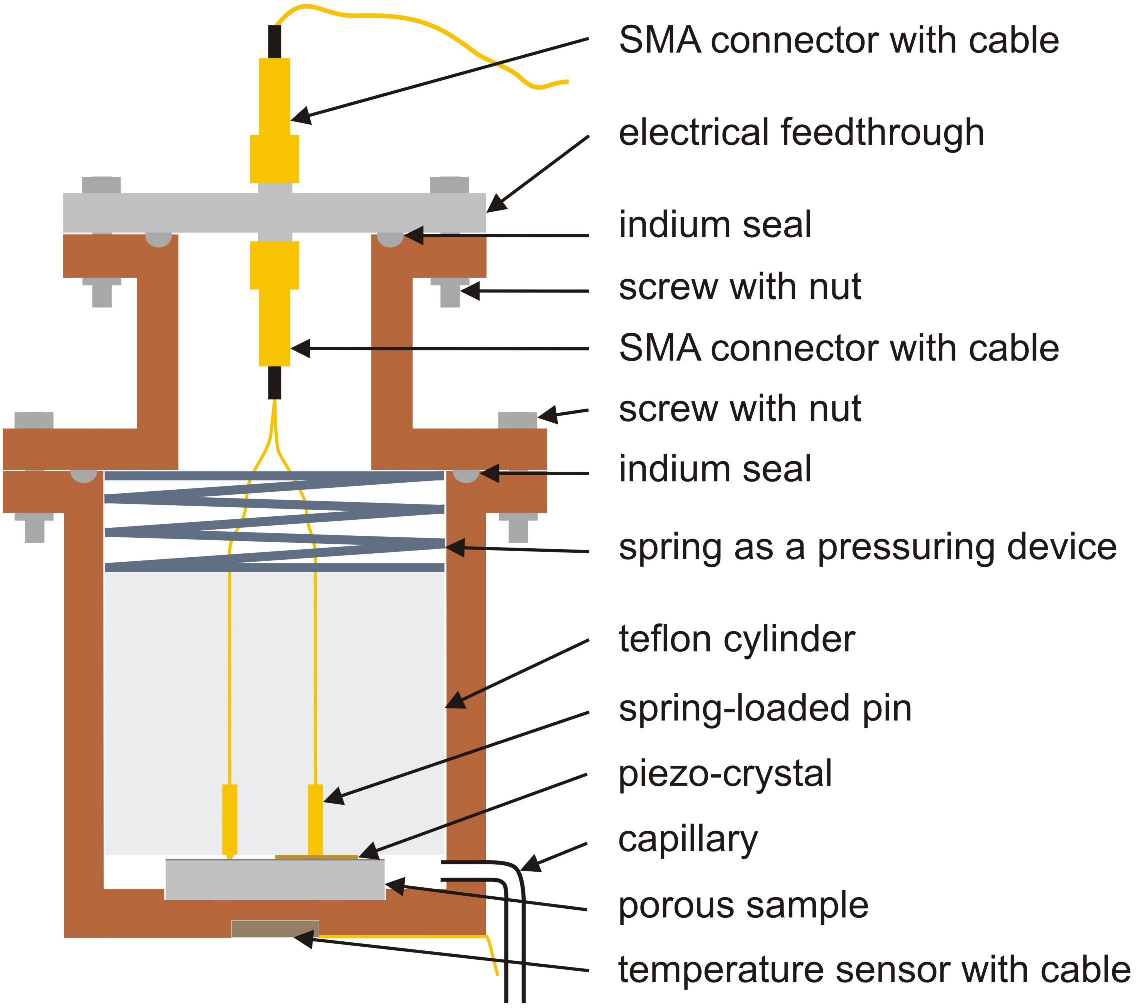

FIGURE A.3 – *Schematic sketch of a sample cell for the ultrasonic measurements. The copper sample cell is mounted on the cold head of a cryostat (cp. figure A.1).*

$$c = \frac{2l}{\Delta t} \tag{A.8}$$

holds. The effective shear modulus G and the effective longitudinal modulus β was calculated from the experimentally determined velocity of ultrasonic shear waves, c_s, or of longitudinal waves, c_l, propagating through the sample:

$$G = c_s^2 \rho \tag{A.9}$$

$$\beta = c_l^2 \rho \tag{A.10}$$

with the effective density of the sample [142],

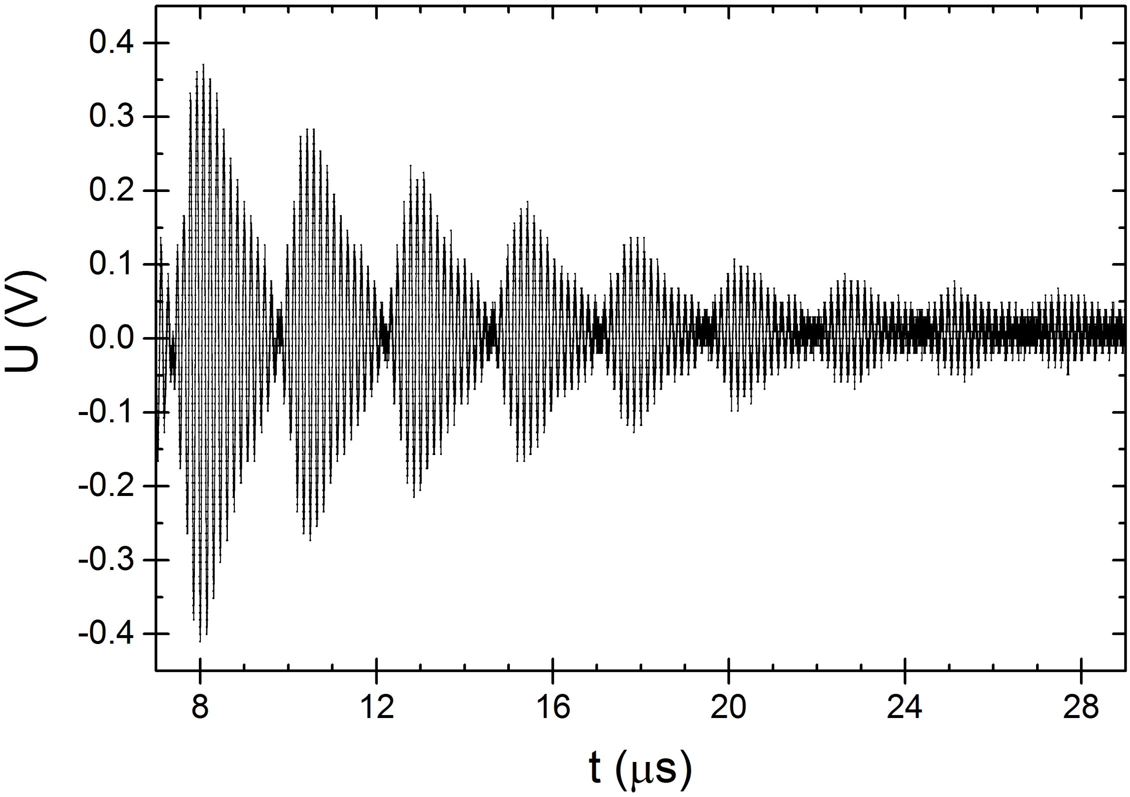

FIGURE A.4 – *Exemplary series of attenuated ultrasonic echos. The ultrasonic velocity is determined from the time difference Δt between consecutive echos and the length l of the sample.*

$$\rho = \rho_0 \left(1 + \frac{n m_M}{m_0}\right), \tag{A.11}$$

for a filling with n moles of an adsorbate with the molar mass m_M, with the mass of the empty sample, m_0, and its density ρ_0. The filling is determined volumetrically according to the procedure described in section A.1 simultaneously with the ultrasonic measurements.

The adsorption-induced deformation can be neglegted for the determination of the ultrasonic velocity and the effective density because the maximum length changes Δl_{max} are very small compared to the length of the empty sample l_0 (cp. section A.4):

$$\frac{\Delta l_{max}}{l_0} \lesssim 5 \cdot 10^{-4} \tag{A.12}$$

The samples for the ultrasonic measurements have a length l_0 between $\approx$ 2.5 mm and $\approx$ 5 mm. The base of these samples is at maximum 20 x 20 mm^2 and not smaller than 10 x 10 mm^2. The piezo-crystals have a diameter of 4 mm or 10 mm.

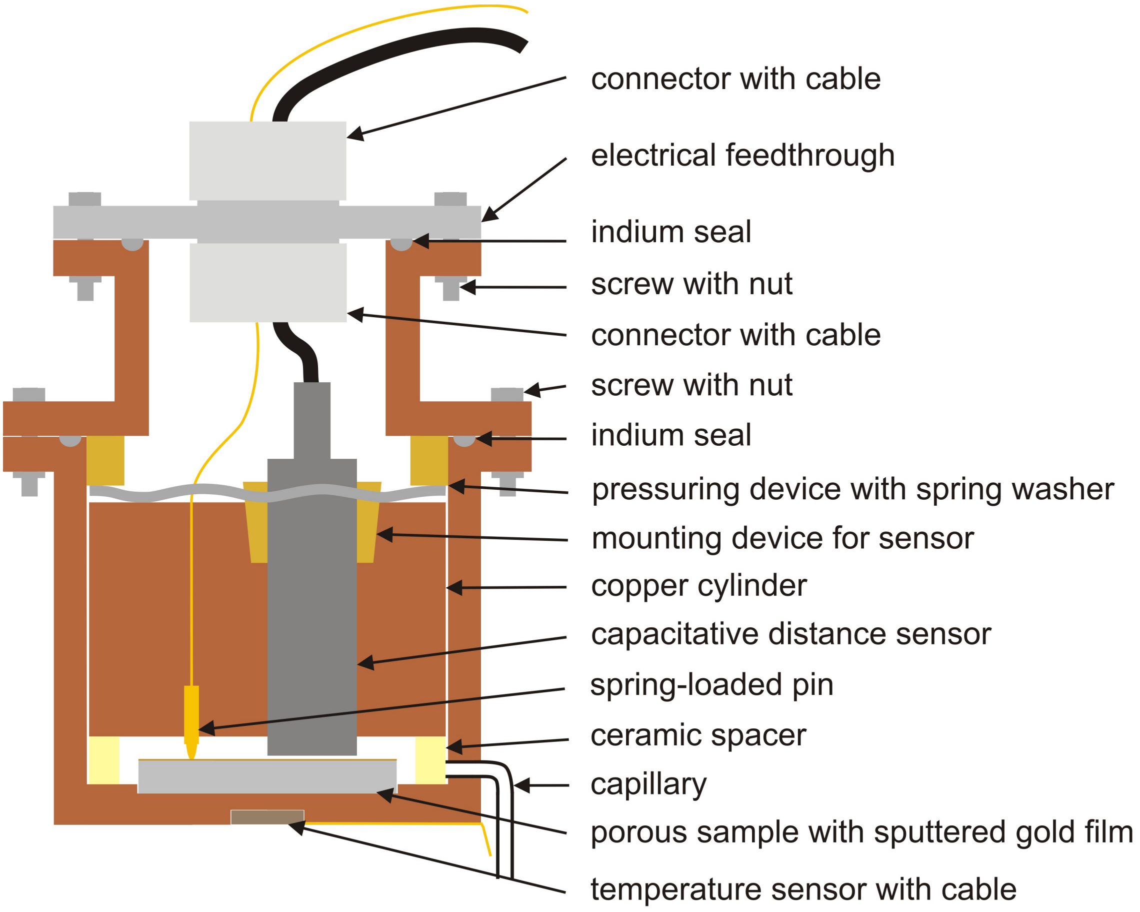

FIGURE A.5 – *Schematic sketch of the sample cell for the deformation measurements. The copper sample cell is mounted on the cold head of a cryostat (cp. figure A.1).*

A.4 Deformation measurements

The adsorption-induced deformation of the porous Vycor® glass sample is determined with a capacitative distance sensor. The sensor forms one plate of a capacitor and is mounted a few micrometres (typically $10 - 20$ μm) above the upper surface of the porous sample (see schematic sketch in figure A.5). On the upper surface a thin gold film is sputtered. Thus this surface of the sample can serve as the second plate of the capacitor. A change of the length of the sample reflects directly in a change of the distance between the two plates of the capacitor and its capacity C. The capacity must be converted into the distance between the two plates. The evaluation unit of the sensor supplies for the standard cable (between the sensor and the unit) a voltage signal between -10 V and $+10$ V corresponding to 10 μm and 30 μm. The linear relation between the voltage and the distance is, however, lost if another cable is used. The location of the sensor within a closed metallic container on a cold head requires electrical feedthroughs and also a change of the cable length. Therefore, the sensor was calibrated with spacers (e.g. Kapton) of

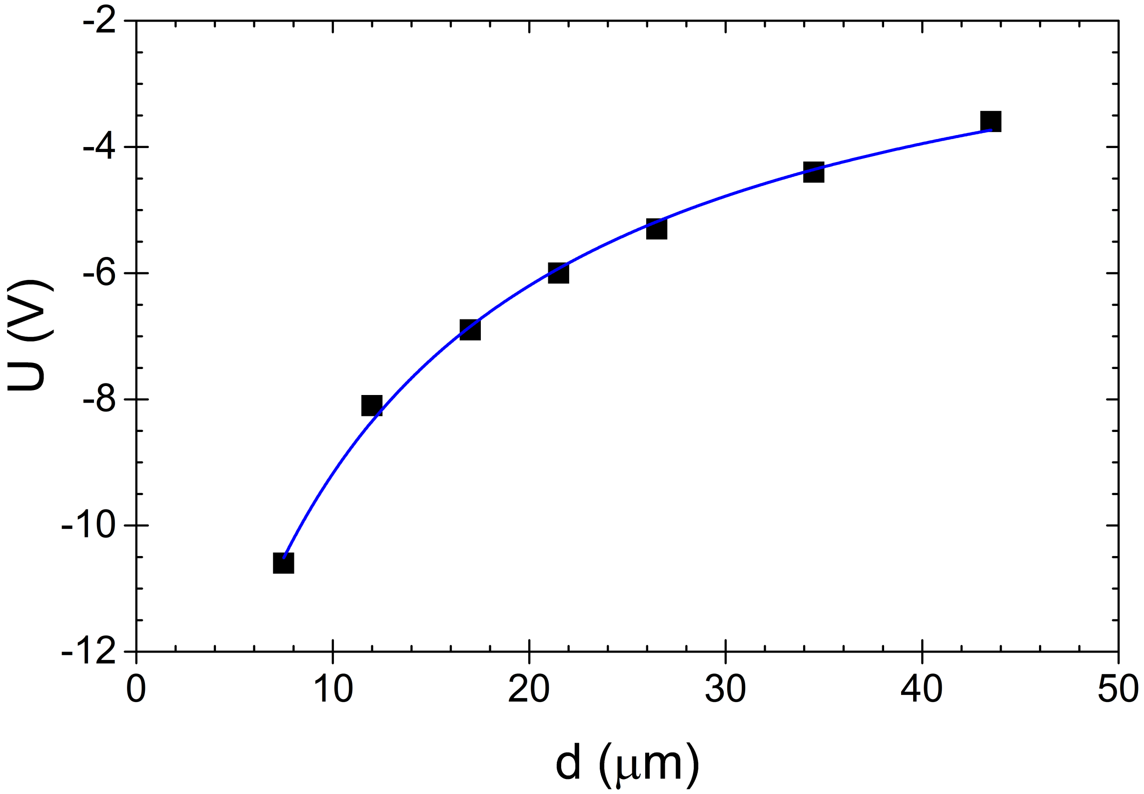

FIGURE A.6 – *Calibration curve for the distance sensor. The measured values are fitted with equation A.14*

different thicknesses before the start of the measurements.[2]

A typical calibration curve is shown in figure A.6. The measured values are fitted with the theoretically expected curve. For this the total capacity C_{total} is regarded as the sum of the capacity related to the distance d between the two plates with surface A and the capacity of the triax-cable (including feedthroughs):

$$C_{total} = C_{cable} + \varepsilon_0 \frac{A}{d}, \tag{A.13}$$

with the permittivity of vacuum ε_0. Assuming an inverse proportionality between the voltage supplied by the evaluation unit and the total capacity it follows:

$$U = U_0 + \frac{\alpha d / (\varepsilon_0 A)}{1 + C_{cable} d / (\varepsilon_0 A)} = U_0 + \frac{a_c d}{1 + d/k}, \tag{A.14}$$

with the offset voltage U_0 for a distance of $d = 0$, the proportionality constant α, $a_c := \alpha / (\varepsilon_0 A)$, and $k := \varepsilon_0 A / C_{cable}$.

The measurement of the length changes during isothermal sorption was a challenging

---

[2] After any reconstruction of the experimental setup a new calibration was necessary.

task. In particular, the location of the sample cell with the sensor on a vibrating cold head required a firm fixing of the sensor to prevent shifts of the sensor during the long measurements. For the electrical vacuum feedthroughs special plug connectors were necessary.

The laboratory with the experimental setup was air-conditioned, however, often a small change of the room temperature was still present [with approximately a 40 minutes interval, see figure A.7(a)]. This change of the room temperature resulted in changes of the capacity of the cable and consequently in a small inaccuracy of the measured distance between sensor and sample [see figure A.7(c) for the influence of the room temperature on the distance signal]. It may also be possible that the adsorption or desorption of a very small number of molecules because of the displayed change of the temperature partly causes the fluctuations shown in figure A.7(c). These fluctuations limited the relative accuracy of the measured length changes to $\approx \pm 5$ nm. But with a maximum deformation of typically several hundred nanometers (at $p/p_0 = 1$) this resolution limit is far better than necessary for the measured sorption isotherms and these fluctuations are not visible on the graphs (cp. e.g. figure 1.6). The accuracy of the absolute values of the measured length changes are, however, limited by the accuracy of the calibration of the sensor.

All samples for the deformation measurements have a base of 20 x 20 mm^2 and a length of typically $2.4 - 2.7$ mm. The filling of the sample is determind according to the procedure described in section A.1 simultaneously with the deformation measurement.

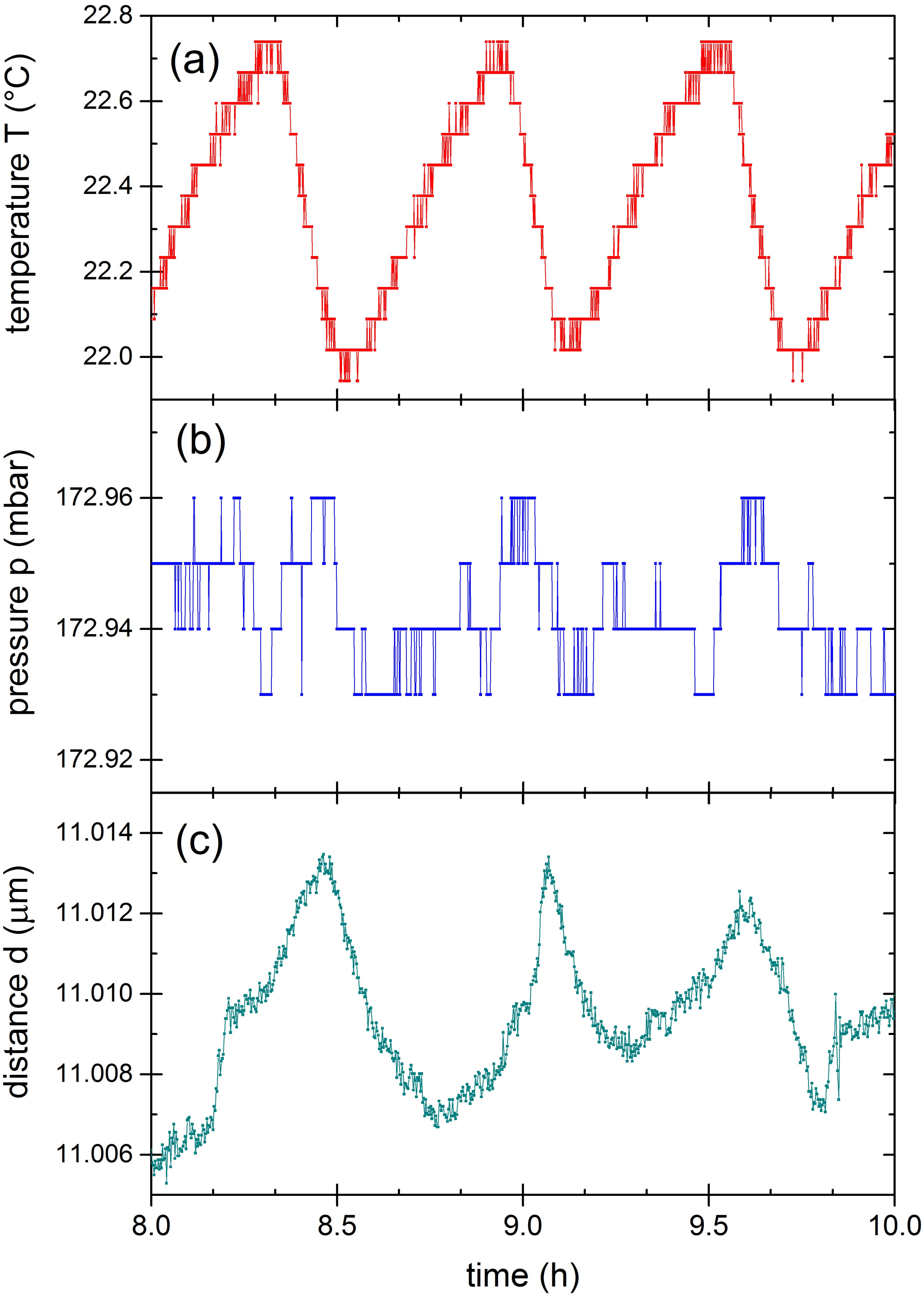

FIGURE A.7 – *(a) Fluctuation of the room temperature caused by the air-conditioner. (b) The measured pressure and (c) the determined distance between the distance sensor and the sample vary in consequence of these temperature changes, even though the gas distribution system was isolated (see section A.1). The time shift between the oscillations may be related to differences between the measured temperature and the actual temperature of the gas distribution system and the cables of the sensor.*

Bibliography

[1] Klaus Schappert and Rolf Pelster. Elastic properties and freezing of argon confined in mesoporous glass. *Phys. Rev. B*, 78:174108, 2008.

[2] Klaus Schappert and Rolf Pelster. Freezing behavior of argon layers confined in mesopores. *Phys. Rev. B*, 83:184110, 2011.

[3] Klaus Schappert and Rolf Pelster. Continuous freezing of argon in completely filled mesopores. *Phys. Rev. Lett.*, 110:135701, 2013.

[4] Klaus Schappert and Rolf Pelster. Elastic properties of liquid and solid argon in nanopores. *J. Phys.: Condens. Matter*, 25:415302, 2013.

[5] Klaus Schappert and Rolf Pelster. Influence of the Laplace pressure on the elasticity of argon in nanopores. *EPL*, 105:56001, 2014.

[6] Klaus Schappert and Rolf Pelster. Strongly enhanced elastic modulus of solid nitrogen in nanopores. *Phys. Rev. B*, 88:245443, 2013.

[7] Jacob Klein and Eugenia Kumacheva. Confinement-induced phase transitions in simple liquids. *Science*, 269:816–819, 1995.

[8] Sinan Keten, Zhiping Xu, Britni Ihle, and Markus J. Buehler. Nanoconfinement controls stiffness, strength and mechanical toughness of β-sheet crystals in silk. *Nature Materials*, 9:359–367, 2010.

[9] Bin Wu, Andreas Heidelberg, and John J. Boland. Mechanical properties of ultrahigh-strength gold nanowires. *Nature Materials*, 4:525–529, 2005.

[10] Juergen Biener, Andrea M. Hodge, Joel R. Hayes, Cynthia A. Volkert, Luis A. Zepeda-Ruiz, Alex V. Hamza, and Farid F. Abraham. Size effects on the mechanical behavior of nanoporous Au. *Nano Lett.*, 6:2379–2382, 2006.

[11] Yannick Champion, Cyril Langlois, Sandrine Guérin-Mailly, Patrick Langlois, Jean-Louis Bonnentien, and Martin J. Hÿtch. Near-perfect elastoplasticity in pure nanocrystalline copper. *Science*, 300:310–311, 2003.

[12] Jakob Schiøtz and Karsten W. Jacobsen. A maximum in the strength of nanocrystalline copper. *Science*, 301:1357–1359, 2003.

[13] C. Q. Chen, Y. Shi, Y. S. Zhang, J. Zhu, and Y. J. Yan. Size dependence of Young's modulus in ZnO nanowires. *Phys. Rev. Lett.*, 96:075505, 2006.

[14] Christopher M. Stafford, Bryan D. Vogt, Christopher Harrison, Duangrut Julthongpiput, and Rui Huang. Elastic moduli of ultrathin amorphous polymer films. *Macro-*

molecules, 39:5095–5099, 2006.

[15] C. T. Sun and Haitao Zhang. Size-dependent elastic moduli of platelike nanomaterials. *J. Appl. Phys.*, 93:1212–1218, 2003.

[16] Alexander I. Fedorchenko, An-Bang Wang, and Henry H. Cheng. Thickness dependence of nanofilm elastic modulus. *Appl. Phys. Lett.*, 94:152111, 2009.

[17] L. G. Zhou and Hanchen Huang. Are surfaces elastically softer or stiffer? *Appl. Phys. Lett.*, 84:1940–1942, 2004.

[18] H. L. Duan, J. Wang, Z. P. Huang, and B. L. Karihaloo. Size-dependent effective elastic constants of solids containing nano-inhomogeneities with interface stress. *J. Mech. Phys. Solids*, 53:1574–1596, 2005.

[19] Stéphane Cuenot, Christian Frétigny, Sophie Demoustier-Champagne, and Bernard Nysten. Surface tension effect on the mechanical properties of nanomaterials measured by atomic force microscopy. *Phys. Rev. B*, 69:165410, 2004.

[20] Xi-Qiao Feng, Re Xia, Xide Li, and Bo Li. Surface effects on the elastic modulus of nanoporous materials. *Appl. Phys. Lett.*, 94:011916, 2009.

[21] Xiao-Yu Sun, Guang-Kui Xu, Xiaoyan Li, Xi-Qiao Feng, and Huajian Gao. Mechanical properties and scaling laws of nanoporous gold. *J. Appl. Phys.*, 113:023505, 2013.

[22] H. L. Duan, J. Wang, B. L. Karihaloo, and Z. P. Huang. Nanoporous materials can be made stiffer than non-porous counterparts by surface modification. *Acta Mater.*, 54:2983–2990, 2006.

[23] Hai-Jun Jin and Jörg Weissmüller. A material with electrically tunable strength and flow stress. *Science*, 332:1179–1182, 2011.

[24] T. Hofmann, P. Kumar, M. Enderle, and D. Wallacher. Growth of highly oriented deuterium crystals in silicon nanochannels. *Phys. Rev. Lett.*, 110:065505, 2013.

[25] F. G. Alabarse, J. Haines, O. Cambon, C. Levelut, D. Bourgogne, A. Haidoux, D. Granier, and B. Coasne. Freezing of water confined at the nanoscale. *Phys. Rev. Lett.*, 109:035701, 2012.

[26] Bharat Bhushan, Jacob N. Israelachvili, and Uzi Landman. Nanotribology: friction, wear and lubrication at the atomic scale. *Nature*, 374:607-616, 1995.

[27] M. Heuberger, M. Zäch, and N. D. Spencer. Density fluctuations under confinement: When is a fluid not a fluid? *Science*, 292:905–908, 2001.

[28] Hugo K. Christenson. Confinement effects on freezing and melting. *J. Phys.: Condens. Matter*, 13:R95–R133, 2001.

[29] D. Wallacher and K. Knorr. Melting and freezing of Ar in nanopores. *Phys. Rev. B*, 63:104202, 2001.

[30] Kunimitsu Morishige and Keiji Kawano. Freezing and melting of water in a single cylindrical pore: The pore-size dependence of freezing and melting behavior. *J.*

Chem. Phys., 110:4867–4872, 1999.

[31] Kunimitsu Morishige. Freezing and melting of Kr in hexagonally shaped pores of turbostratic carbon: Lack of hysteresis between freezing and melting. *J. Phys. Chem. C*, 115:2720–2726, 2011.

[32] Kunimitsu Morishige and Kouji Mikawa. Pore size dependence of melting point for Kr confined in crystalline carbon pores. *J. Phys. Chem. C*, 116:14979–14985, 2012.

[33] P. Huber and K. Knorr. Adsorption-desorption isotherms and x-ray diffraction of ar condensed into a porous glass matrix. *Phys. Rev. B*, 60:12657–12665, 1999.

[34] Hendrik Hansen-Goos and J. S. Wettlaufer. Theory of ice premelting in porous media. *Phys. Rev. E*, 81:031604, 2010.

[35] T. Ishizaki, M. Maruyama, Y. Furukawa, and J. G. Dash. Premelting of ice in porous silica glass. *J. Cryst. Growth*, 163:455–460, 1996.

[36] R. Berwanger, A. Henschel, K. Knorr, P. Huber, and R. Pelster. Phase transitions and molecular dynamics of n-hexadecanol confined in silicon nanochannels. *Phys. Rev. B*, 79:125442, 2009.

[37] Oleg V. Petrov, Dulce Vargas-Florencia, and István Furó. Surface melting of octamethylcyclotetrasiloxane confined in controlled pore glasses: Curvature effects observed by ^{1}H NMR. *J. Phys. Chem. B*, 111:1574–1581, 2007.

[38] Andreas Schreiber, Ingke Ketelsen, and Gerhard H. Findenegg. Melting and freezing of water in ordered mesoporous silica materials. *Phys. Chem. Chem. Phys.*, 3:1185–1195, 2001.

[39] R. Berwanger, Ch. Schumacher, P. Huber, and R. Pelster. Size-dependent freezing of n-alcohols in silicon nanochannels. *Eur. Phys. J. Special Topics*, 189:239–249, 2010.

[40] Estefanía González Solveyra, Ezequiel de la Llave, Damián A. Scherlis, and Valeria Molinero. Melting and crystallization of ice in partially filled nanopores. *J. Phys. Chem. B*, 115:14196–14204, 2011.

[41] Emily B. Moore, James T. Allen, and Valeria Molinero. Liquid-ice coexistence below the melting temperature for water confined in hydrophilic and hydrophobic nanopores. *J. Phys. Chem. C*, 116:7507–7514, 2012.

[42] Sungho Han, M. Y. Choi, Pradeep Kumar, and H. Eugene Stanley. Phase transitions in confined water nanofilms. *Nature Physics*, 6:685–689, 2010.

[43] Hans Riegler and Ralf Köhler. How pre-melting on surrounding interfaces broadens solid-liquid phase transitions. *Nature Physics*, 3:890–894, 2007.

[44] Gennady Yu. Gor and Alexander V. Neimark. Adsorption-induced deformation of mesoporous solids. *Langmuir*, 26:13021–13027, 2010.

[45] Curt M. White, Duane H. Smith, Kenneth L. Jones, Angela L. Goodman, Sinisha A. Jikich, Robert B. LaCount, Stephen B. DuBose, Ekrem Ozdemir, Badie I. Morsi,

and Karl T. Schroeder. Sequestration of carbon dioxide in coal with enhanced coalbed methane recoverys - a review. *Energy Fuels*, 19:659–724, 2005.

[46] Laurent Brochard, Matthieu Vandamme, Roland J.-M. Pellenq, and Teddy Fen-Chong. Adsorption-induced deformation of microporous materials: Coal swelling induced by CO_2CH_4 competitive adsorption. *Langmuir*, 28:2659–2670, 2012.

[47] Kan Yang, Xiancai Lu, Yangzheng Lin, and Alexander V. Neimark. Deformation of coal induced by methane adsorption at geological conditions. *Energy Fuels*, 24:5955–5964, 2010.

[48] Johannes Prass, Dirk Müter, Peter Fratzl, and Oskar Paris. Capillary-driven deformation of ordered nanoporous silica. *Appl. Phys. Lett.*, 95:083121, 2009.

[49] Christian Balzer, Timo Wildhage, Stephan Braxmeier, Gudrun Reichenauer, and James P. Olivier. Deformation of porous carbons upon adsorption. *Langmuir*, 27:2553–2560, 2011.

[50] C. H. Amberg and R. McIntosh. A study of adsorption hysteresis by means of length changes of a rod of porous glass. *Can. J. Chem.*, 30:1012–1032, 1952.

[51] Martin Schoen, Oskar Paris, Gerrit Günther, Dirk Müter, Johannes Prass, and Peter Fratzl. Pore-lattice deformation on ordered mesoporous matrices: experimental studies and theoretical analysis. *Phys. Chem. Chem. Phys.*, 12:11267–11269, 2010.

[52] D. H. Bangham and F. A. P. Maggs. The strength and elastic constants of coals in relation to their ultra-fine structure. In *Proceedings of a Conference on the Ultra-fine Structure of Coals & Cokes*. The British Coal Utilisation Research Association, 1944.

[53] D. J. C. Yates. The expansion of porous glass on the adsorption of non-polar gases. *Proc. Roy. Soc. A*, 224:526–544, 1954.

[54] George W. Scherer. Dilatation of porous glass. *J. Am. Ceram. Soc.*, 69:473–480, 1986.

[55] Gerald A. Zickler, Susanne Jähnert, Sérgio S. Funari, Gerhard H. Findenegg, and Oskar Paris. Pore lattice deformation in ordered mesoporous silica studied by in situ small-angle x-ray diffraction. *J. Appl. Cryst.*, 40:s522–s526, 2007.

[56] Gennady Yu. Gor, Oskar Paris, Johannes Prass, Patrícia A. Russo, M. Manuela L. Ribeiro Carrott, and Alexander V. Neimark. Adsorption of n-pentane on mesoporous silica and adsorbent deformation. *Langmuir*, 29:8601–8608, 2013.

[57] Data sheet for porous Vycor® 7930, Corning, Inc.

[58] Ferdi Schüth, Kenneth S. W. Sing, and Jens Weitkamp, editors. *Handbook of Porous Solids*, volume 3. WILEY-VCH Verlag, Weinheim, 2002.

[59] S. J. Gregg and K. S. W. Sing. *Adsorption, Surface Area, and Porosity.* Academic Press, London, 1982.

[60] F. Rouquerol, Jean Rouquerol, and K. S. W. Sing. *Adsorption by Powders and*

Porous Solids. Academic Press, London, 1999.

[61] S. Lowell, J. E. Shields, M. A. Thomas, and M. Thommes. *Characterization of Porous Solids and Powders: Surface Area, Pore Size and Density.* Kluwer Academic Publishers, Dordrecht, 2004.

[62] J. H. Page, J. Liu, B. Abeles, H. W. Deckman, and D. A. Weitz. Pore-space correlations in capillary condensation in Vycor. *Phys. Rev. Lett.*, 71:1216–1219, 1993.

[63] J. H. Page, J. Liu, B. Abeles, E. Herbolzheimer, H. W. Deckman, and D. A. Weitz. Adsorption and desorption of a wetting fluid in Vycor studied by acoustic and optical techniques. *Phys. Rev. E*, 52:2763–2777, 1995.

[64] Victor P. Soprunyuk, Dirk Wallacher, Patrick Huber, Klaus Knorr, and Andriy V. Kityk. Freezing and melting of Ar in mesopores studied by optical transmission. *Phys. Rev. B*, 67:144105, 2003.

[65] Dirk Wallacher, Viktor P. Soprunyuk, Andriy V. Kityk, Patrick Huber, and Klaus Knorr. Capillary sublimation of Ar in mesoporous glass. *Phys. Rev. B*, 71:052101, 2005.

[66] F. Bonnet, M. Melich, L. Puech, and P. E. Wolf. Light scattering study of collective effects during evaporation and condensation in a disordered porous material. *EPL*, 101:16010, 2013.

[67] W. F. Saam and Milton W. Cole. Excitations and thermodynamics for liquid-helium films. *Phys. Rev. B*, 11:1086–1105, 1975.

[68] Annie Grosman and Camille Ortega. Influence of elastic deformation of porous materials in adsorption-desorption process: A thermodynamic approach. *Phys. Rev. B*, 78:085433, 2008.

[69] P. A. Monson. Understanding adsorption/desorption hysteresis for fluids in mesoporous materials using simple molecular models and classical density functional theory. *Microporous Mesoporous Mater.*, 160:47–66, 2012.

[70] Christopher J. Rasmussen, Aleksey Vishnyakov, Matthias Thommes, Bernd M. Smarsly, Freddy Kleitz, and Alexander V. Neimark. Cavitation in metastable liquid nitrogen confined to nanoscale pores. *Langmuir*, 26:10147–10157, 2010.

[71] Phuong T. M. Nguyen, Chunyan Fan, D. D. Do, and D. Nicholson. On the cavitation-like pore blocking in ink-bottle pore: Evolution of hysteresis loop with neck size. *J. Phys. Chem. C*, 117:5475–5484, 2013.

[72] Oleg Petrov and István Furó. A study of freezing-melting hysteresis of water in different porous materials. Part I: Porous silica glasses. *Microporous Mesoporous Mater.*, 138:221–227, 2011.

[73] Sebastian T. Moerz, Klaus Knorr, and Patrick Huber. Capillary condensation, freezing, and melting in silica nanopores: A sorption isotherm and scanning calorimetry study on nitrogen in mesoporous SBA-15. *Phys. Rev. B*, 85:075403, 2012.

[74] Christof Schaefer, Tommy Hofmann, Dirk Wallacher, Patrick Huber, and Klaus Knorr. Melting and freezing of argon in a granular packing of linear mesopore arrays. *Phys. Rev. Lett.*, 100:175701, 2008.

[75] J. J. Hoyt. Effect of stress on melting and freezing in nanopores. *Phys. Rev. Lett.*, 96:045702, 2006.

[76] Gerhard H. Findenegg, Susanne Jähnert, Dilek Akcakayiran, and Andreas Schreiber. Freezing and melting of water confined in silica nanopores. *ChemPhysChem*, 9:2651–2659, 2008.

[77] B. Kuchta, L. Firlej, R. Denoyel, S. Rols, M. R. Johnson, and B. Coasne. Melting mechanism of monolayers adsorbed in cylindrical pores: The influence of the pore wall roughness. *J. Chem. Phys.*, 128:184703, 2008.

[78] M. Sliwinska-Bartkowiak, M. Jazdzewska, and K. E. Gubbins. Melting behavior of water in cylindrical pores: carbon nanotubes and silica glasses. *Phys. Chem. Chem. Phys.*, 10:4909–4919, 2008.

[79] Malgorzata Sliwinska-Bartkowiak, Grazyna Dudziak, Roman Gras, Roman Sikorski, Ravi Radhakrishnan, and Keith E. Gubbins. Freezing behavior in porous glasses and MCM-41. *Colloids Surf., A*, 187-188:523–529, 2001.

[80] J.C. van Miltenburg and J.P. van der Eerden. Very large melting point depression of water in silica. *J. Cryst. Growth*, 128:1143–1149, 1993.

[81] J.W. Cahn, J.G. Dash, and Haiying Fu. Theory of ice premelting in monosized powders. *J. Cryst. Growth*, 123:101–108, 1992.

[82] D. Wallacher, V.P. Soprunyuk, K. Knorr, and A.V. Kityk. Dielectric response of acetonitrile condensed into mesoporous glass. *Phys. Rev. B*, 69:134207, 2004.

[83] Ralf Schmidt, Eddy Walther Hansen, Michael Stöcker, Duncan Akporiaye, and Ole Henrik Ellestad. Pore size determination of MCM-41 mesoporous materials by means of ^{1}H NMR spectroscopy, N_2 adsorption, and HREM. A preliminary study. *J. Am. Chem. Soc.*, 117:4049–4056, 1995.

[84] Kunimitsu Morishige. Layer-by-layer freezing of Kr confined in hexagonal pores with crystalline carbon walls. *J. Phys. Chem. C*, 115:12158–12162, 2011.

[85] Eric Molz, Apollo P. Y. Wong, M. H. W. Chan, and J. R. Beamish. Freezing and melting of fluids in porous glasses. *Phys. Rev. B*, 48:5741–5750, 1993.

[86] Eric B. Molz and John R. Beamish. Freezing and melting of helium in different porous media. *J. Low Temp. Phys.*, 101:1055–1077, 1995.

[87] J. R. Beamish, A. Hikata, L. Tell, and C. Elbaum. Solidification and superfluidity of ^{4}He in porous Vycor glass. *Phys. Rev. Lett.*, 50:425–428, 1983.

[88] Martin Schoen and Gerrit Günther. Phase transitions in nanoconfined fluids: Synergistic coupling between soft and hard matter. *Soft Matter*, 6:5832–5838, 2010.

[89] Maxim Erko, Dirk Wallacher, and Oskar Paris. Deformation mechanism of

nanoporous materials upon water freezing and melting. *Appl. Phys. Lett.*, 101:181905, 2012.

[90] A. R. Ubbelohde. *Melting and Crystal Structure.* Clarendon Press, Oxford, 1965.

[91] J. G. Dash, A. W. Rempel, and J. S. Wettlaufer. The physics of premelted ice and its geophysical consequences. *Rev. Mod. Phys.*, 78:695–741, 2006.

[92] J. S. Wettlaufer, J. G. Dash, and N. Untersteiner, editors. *Ice Physics and the Natural Environment.* NATO Advance Studies Institute, Series I: Global Environmental Change. Springer, Berlin/Heidelberg/New York, 1999.

[93] J. G. Dash, Haiying Fu, and J. S. Wettlaufer. The premelting of ice and its environmental consequences. *Rep. Prog. Phys.*, 58:115–167, 1995.

[94] Da-Ming Zhu and J. G. Dash. Surface melting and roughening of adsorbed argon films. *Phys. Rev. Lett.*, 57:2959–2962, 1986.

[95] J. S. Wettlaufer and M. Grae Worster. Premelting dynamics. *Annu. Rev. Fluid Mech.*, 38:427–452, 2006.

[96] S. Engemann, H. Reichert, H. Dosch, J. Bilgram, V. Honkimäki, and A. Snigirev. Interfacial melting of ice in contact with SiO_2. *Phys. Rev. Lett.*, 92:205701, 2004.

[97] P. J. Sereda and R. F. Feldman. *The Solid-Gas Interface*, volume 2, chapter Mechanical Properties and the Solid-Gas Interface, pages 729–764. Edward Arnold Ltd., London, and Marcel Dekker Inc., New York, 1967.

[98] F. T. Meehan. The expansion of charcoal on sorption of carbon dioxide. *Proc. Roy Soc. A*, 115:199–207, 1927.

[99] D. H. Bangham and Nazim Fakhoury. The expansion of charcoal accompanying sorption of gases and vapours. *Nature*, 122:681–682, 1928.

[100] D. H. Bangham and Nazim Fakhoury. The swelling of charcoal. Part I.–Preliminary experiments with water vapour, carbon dioxide, ammonia, and sulphur dioxide. *Proc. Roy Soc. A*, 130:81–89, 1930.

[101] Donald Hugh Bangham and Nazim Fakhoury. The translational motion of molecules in the adsorbed phase on solids. *J. Chem. Soc.*, 1324–1333, 1931.

[102] D. H. Bangham, N. Fakhoury, and A. F. Mohamed. The swelling of charcoal. Part II.–Some factors controlling the expansion caused by water, benzene and pyridine vapours. *Proc. Roy Soc. A*, 138:162–183, 1932.

[103] D. H. Bangham, N. Fakhoury, and A. F. Mohamed. The swelling of charcoal. Part III.–Experiments with the lower alcohols. *Proc. Roy Soc. A*, 147:152–175, 1934.

[104] D. H. Bangham. The swelling of charcoal. Part IV.–Stoichiometric relations for the films of the alcohols. *Proc. Roy Soc. A*, 147:175–188, 1934.

[105] D. H. Bangham and R. I. Razouk. The swelling of charcoal. Part V.– The saturation and immersion expansions and the heat of wetting. *Proc. Roy Soc. A*, 166:572–586, 1938.

[106] M. Folman and D. J. C. Yates. Expansion-contraction effects in rigid adsorbents at low coverages. *Trans. Faraday Soc.*, 54:429–440, 1958.

[107] D. H. Bangham. The Gibbs adsorption equation and adsorption on solids. *Trans. Faraday Soc.*, 33:805–811, 1937.

[108] D. J. C. Yates. A note on some proposed equations of state for the expansion of rigid porous solids on the adsorption of gases and vapours. *Proc. Phys. Soc. B*, 65:80–81, 1952.

[109] R. Shuttleworth. The surface tension of solids. *Proc. Phys. Soc. A*, 63:444–457, 1950.

[110] R. S. Haines and R. McIntosh. Length changes of activated carbon rods caused by adsorption of vapors. *J. Chem. Phys.*, 15:28–38, 1947.

[111] G. E. Boyd and H. K. Livingston. Adsorption and energy changes at crystalline solid surfaces. *J. Am. Chem. Soc.*, 64:2383–2388, 1942.

[112] George Jura and William D. Harkins. Surfaces of solids. XI. Determination of the decrease (Π) of free surface energy of a solid by an adsorbed film. *J. Am. Chem. Soc.*, 66:1356–1362, 1944.

[113] Gennady Yu. Gor and Alexander V. Neimark. Adsorption-induced deformation of mesoporous solids: Macroscopic approach and density functional theory. *Langmuir*, 27:6926–6931, 2011.

[114] Arthur W. Adamson and Alice P. Gast. *Physical Chemistry of Surfaces.* John Wiley & Sons, Inc., 1997.

[115] S. Dourdain, D. T. Britton, H. Reichert, and A. Gibaud. Determination of the elastic modulus of mesoporous silica thin films by x-ray reflectivity via capillary condensation of water. *Appl. Phys. Lett.*, 93:183108, 2008.

[116] G. Reichenauer and G. W. Scherer. Nitrogen adsorption in compliant materials. *J. Non-Cryst. Solids*, 277:162–172, 2000.

[117] G. Dolino, D. Bellet, and C. Faivre. Adsorption strains in porous silicon. *Phys. Rev. B*, 54:17919–17929, 1996.

[118] Gerhard H. Findenegg, Susanne Jähnert, Dirk Müter, Johannes Prass, and Oskar Paris. Fluid adsorptionin ordered mesoporous solids determined by in situ small-angle x-ray scattering. *Phys. Chem. Chem. Phys.*, 12:7211–7220, 2010.

[119] Gerrit Günther, Johannes Prass, Oskar Paris, and Martin Schoen. Novel insights into nanopore deformation caused by capillary condensation. *Phys. Rev. Lett.*, 101:086104, 2008.

[120] Gerrit Günther and Martin Schoen. Sorption strains and their consequences for capillary condensation in nanoconfinement. *Mol. Simul.*, 35:138–150, 2009.

[121] Stuart G. Ash, Douglas H. Everett, and Clay Radke. Thermodynamics of the effects of adsorption on interparticle forces. *J. Chem. Soc., Faraday Trans. 2*, 69:1256–1277,

1973.

[122] D. J. C. Yates. The influence of the polar nature of the adsorbate on adsorption expansion. *J. Phys. Chem.*, 60:543–549, 1956.

[123] D. J. C. Yates. Volume changes in porous glass produced by the physical adsorption of gases. In Adalbert Farkas, editor, *Proceedings of the International Congress on Catalysis. Philadelphia, Pennsylvania, 1956*, Advances in Catalysis and Related Subjects, pages 481–487, New York, N. Y., 1957. Academic Press Inc.

[124] M. Folman and D. J. C. Yates. Perturbation effects due to hydrogen bonding in physical adsorption studied by length-change and infra-red techniques. *Proc. Roy Soc. A*, 246:32–51, 1958.

[125] Y. Kozirovski and M. Folman. Surface hydrogen bonds and the elastic properties of a solid adsorbent. *Trans. Faraday Soc.*, 58:2228–2238, 1962.

[126] Klaus Schappert. Ultraschall-Untersuchungen an Argon in nanoporösem Glas. Diploma thesis, Universität des Saarlandes, 2007.

[127] E. R. Dobbs, B. F. Figgins, G. O. Jones, D. C. Piercey, and D. P. Riley. Density and expansivity of solid argon. *Nature*, 178:483, 1956.

[128] B. Paul. Prediction of elastic constants of multiphase materials. *Trans. Metall. Soc. AIME*, 218:36–41, 1960.

[129] Data sheet for base Vycor® 7913, Corning, Inc.

[130] G. J. Keeler and D. N. Bachelder. Measurement of the elastic constants of argon from 3 to 77 K. *J. Phys. C*, 3:510–522, 1970.

[131] J. R. Barker and E. R. Dobbs. Measurement of the elasticity of solid argon with an ultrasonic interferometer. *Philos. Mag.*, 46:1069–1080, 1955.

[132] Y. Fujii, N. A. Lurie, R. Pynn, and G. Shirane. Inelastic neutron scattering from solid ^{3}6Ar *Phys. Rev. B*, 10:3647–3659, 1974.

[133] C. T. Herakovich and S. C. Baxter. Influence of pore geometry on the effective response of porous media. *J. Mater. Sci.*, 34:1595–1609, 1999.

[134] J. P. Panakkal, H. Willems, and W. Arnold. Nondestructive evaluation of elastic parameters of sintered iron powder compacts. *J. Mater. Sci.*, 25:1397–1402, 1990.

[135] Kenichiro Koga, G. T. Gao, Hideki Tanaka, and X. C. Zeng. Formation of ordered ice nanotubes inside carbon nanotubes. *Nature*, 412:802–805, 2001.

[136] A. V. Kityk and K. Knorr. Calorimetric study of co condensed into mesoporous silica. *Phys. Rev. B*, 78:033401, 2008.

[137] James Day, Tobias Herman, and John Beamish. Freezing and pressure-driven flow of solid helium in Vycor. *Phys. Rev. Lett.*, 95:035301, 2005.

[138] D. Kondrashova, C. Reichenbach, and R. Valiullin. Probing pore connectivity in random porous materials by scanning freezing and melting experiments. *Langmuir*,

26:6380–6385, 2010.

[139] Kunimitsu Morishige, Hiroaki Yasunaga, and Yuki Matsutani. Effect of pore shape on freezing and melting temperatures of water. *J. Phys. Chem. C*, 114:4028–4035, 2010.

[140] W. van Dael, A. van Itterbeek, A. Cops, and J. Thoen. Sound velocity measurements in liquid argon, oxygen and nitrogen. *Physica*, 32:611–620, 1966.

[141] A. van Itterbeek and O. Verbeke. Density of liquid nitrogen and argon as a function of pressure and temperature. *Physica*, 26:931–938, 1960.

[142] K. L. Warner and J. R. Beamish. Ultrasonic measurement of the surface area of porous materials. *J. Appl. Phys.*, 63:4372–4376, 1988.

[143] A. B. Wood. *A Textbook of Sound*. G. Bell and Sons Ltd, London, 1955.

[144] D. Stansfield. The surface tension of liquid argon and nitrogen. *Proc. Phys. Soc.*, 72:854–866, 1958.

[145] Hiroyasu Shimizu, Hideyuki Tashiro, Tetsuji Kume, and Shigeo Sasaki. High-pressure elastic properties of solid argon to 70 GPa. *Phys. Rev. Lett.*, 86:4568–4571, 2001.

[146] M. Grimsditch, P. Loubeyre, and A. Polian. Brillouin scattering and three-body forces in argon at high pressures. *Phys. Rev. B*, 33:7192–7200, 1986.

[147] Milton W. Cole and W. F. Saam. Excitation spectrum and thermodynamic properties of liquid films in cylindrical pores. *Phys. Rev. Lett.*, 32:985–988, 1974.

[148] D. Wallacher, P. Huber, and K. Knorr. Adsorption isotherms and infrared spectroscopy study of nitrogen condensed in porous glasses. *J. Low Temp. Phys.*, 113:19–29, 1998.

[149] T. A. Scott. Solid and liquid nitrogen. *Physics Reports*, 27:89–157, 1976.

[150] P. Huber, D. Wallacher, and K. Knorr. Solid N_2 and CO in nanoporous glasses. *Phys. Rev. B*, 60:12666–12674, 1999.

[151] B. S. Schirato, M. P. Fang, P. E. Sokol, and S. Komarneni. The structure of confined oxygen in silica xerogels. *Science*, 267:369–371, 1995.

[152] D. Wallacher, P. Huber, and K. Knorr. Solid Ar, N_2, CO, and O_2 in nanopores. *J. Low Temp. Phys.*, 122:313–322, 2001.

[153] R. S. McDonald. Study of the interaction between hydroxyl groups of aerosil silica and adsorbed non-polar molecules by infrared spectrometry. *J. Am. Chem. Soc.*, 79:850–854, 1957.

[154] Rustem Valiullin, Sergej Naumov, Petrik Galvosas, Jörg Kärger, Hyung-June Woo, Fabien Porcheron, and Peter A. Monson. Exploration of molecular dynamics during transient sorption of fluids in mesoporous materials. *Nature*, 443:965–968, 2006.

[155] P. Levitz, G. Ehret, S. K. Sinha, and J. M. Drake. Porous Vycor glass: The mi-

crostructure as probed by electron microscopy, direct energy transfer, small-angle scattering, and molecular adsorption. *J. Chem. Phys.*, 95:6151–6161, 1991.

List of figures

Danksagung

Mein besonderer Dank geht an Herrn Prof. Dr. Rolf Pelster, der mir die Forschung in seiner Arbeitsgruppe ermöglichte, meine Arbeit mit interessanten Diskussionen und Anregungen begleitete und mich auch nach Strom- und Kühlwasserausfällen während meiner Langzeitmessungen ermutigte.

Ich danke allen ehemaligen und momentanen Mitarbeitern der Arbeitsgruppe für die angenehme Zusammenarbeit und das freundliche Miteinander: insbesondere Frau Christina Werle für ihre Mühe beim Beseitigen kleiner und großer Probleme, Béatrice Hallouet für ihre Hilfsbereitschaft und freundschaftliche Zusammenarbeit, Sebastian Kiepsch, Michael Konter, Daniel Rau, Nicolas Reiplinger; meinen Zimmerkollegen Dr. René Berwanger, Matthias Jacob, Thomas Geber, Olivier Gauthier, Christian Lamberti und Dr. Serguei Nessis.

Herrn Prof. Dr. Klaus Knorr, Herrn Prof. Dr. Patrick Huber und Herrn Dr. Heinz Schmitt danke ich für interessante Anregungen.

Dank geht auch an die Elektroniker Herrn Stefan Loew und Herrn Jürgen Hoppe für die Durchführung von diversen Reparaturen und Konstruktionen elektrischer Bauteile, an die Feinmechaniker-Werkstatt unter Leitung von Herrn Michael Schmidt für den Aufbau verschiedener Probenzellen sowie an Frau Karin Kretsch und Frau Eva Zaszlos.

Meinen Eltern Birgit und Bernhard Schappert danke ich für ihre ständige Unterstützung.

Prof. Dr. Bert Hornback danke ich für die unzähligen Diskussionen über Charles Dickens und die Welt.